Control and Prediction of Eliminative Cyclisation

Dinga Wonanke

A thesis presented for the degree of

Doctor of Philosophy in Chemistry

School of Physical and Chemical Sciences University of

Canterbury

August, 2018

Abstract

Eliminative cyclisation is a class of intramolecular reactions that provide a versatile synthetic route to functionalised and substituted polyaromatic and heteroaromatic compounds, which form the building blocks of molecular electronic devices such as organic photovoltaics and organic light-emitting diodes.

These reactions may be either thermally or photochemically driven, and proceed via two steps: 1) planarisation to form a stable proto-aromatic intermediate, and 2) elimination of the groups or atoms adjacent to the forming bond to yield the final fully aromatic product. Although experimental studies have been performed on a wide range of starting materials to characterise reaction mechanisms and product distributions, there remains no predictive model for determining whether or not any given reactant will yield a product under specified reaction conditions.

This thesis investigated the factors that control both the thermodynamics and kinetics of these reactions by explicitly mapping out reaction coordinate profiles

and analysing induced atomic forces upon photo-excitation for a diverse range of molecules. Results showed that the kinetics and thermodynamics of both planarisation and elimination in thermal cyclisation are highly sensitive to the reaction conditions, which include the presence and position of the heteroatoms as well as the oxidation potential of the reactants. In photocyclisation, the planarisation step is a photo-activated excited-state process that is in contrast less sensitive to reaction condition; elimination is proposed to proceed in the ground state. The magnitude of the projected force along the bond vectors of the putative forming ring is shown to be a good predictor for the outcome of the photoplanarisation step.

Dedication

I dedicate this work to the Almighty God.

Ps 127:1-3

Declaration

I declare that the work presented in this thesis is mine except otherwise stated. This study was undertaken under the supervision of Deborah Crittenden in the School of Physical and Chemical Sciences, University of Canterbury. A part of this thesis has been incorporated into a previously published research paper:

1. Chapter 3: Wonanke A. D. Dinga, Crittenden Deborah L. (2018) Beyond the Woodward-Hoffman Rules: What Controls Reactivity in Eliminative Aromatic Ring-Forming Reactions?. Australian Journal of Chemistry 71, 249-256.

Acknowledgements

My most profound gratitude and thanks go to my supervisor, Deborah Crittenden, who has been an incredibly amazing, supporting, encouraging go-to person who makes even stressful moments still worth experiencing. Thanks so much for guiding and assisting me throughout this period. It has been a fantastic journey tapping your wealth of knowledge

Special thanks go to my wonderful mother, who has been a continuous source of support and inspiration and who made it a duty to call me every morning and evening to ensure that I was keeping well. Mummy, you are special and one of the best gifts from God.

I would like to thank all of the university lecturers and staff who are so friendly and approachable. Sincere thanks go especially to Sally Gaw, Sarah Masters, Bryce Williamson, Jan Wikaira and Nathan Alexander for all their continuous support throughout this period.

I would like to thank my lovely sisters, Dorothy, Akazong and Mbiatedem for being such wonderful human beings who make life so enjoyable and sweet. Big thanks to my one-and-only big brother Frank and my amazing mentor Terence A. Thank you all for making these years of studies enjoyable, regardless of the distance that separated us all.

Many thanks as well to my office and group mates and especially to Ali, Nate and Mr Flanagan for their continual support and motivation.

I would also like to thank my friends who have been so supportive during these last years. Vijay and Rachel, Biplang, Jess and Eion, Sam, Carissa, Richie, Chad, Nneka, Surin, Hans, Luis, Jake, Ryan, Lisa, Anna, Rob, Dave Jardin.

Furthermore, I would like to thank my future wife. If you ever get to read this thesis, know that I was thinking of you.

Finally, I would like to acknowledge the Marsden Fund Council from New Zealand Government funding, managed by the Royal Society, Te Apārangi for sponsoring this research.

Contents

CHAPTER 1

Introduction

1.1 Optoelectronic technologies

The aim of every human civilisation from one generation to another is to devise new methods and means that can be used to meet the needs of humanity cost-effectively. The industrial revolution in the 19th century was a very significant human invention that brought a remarkable improvement in the living conditions and social wellbeing of humanity. [1–3] Impetus from this has led to an increased in the desire to develope new techniques and devices to accelerate production processes but with little or no human accountability for sustainability. [4,5] The direct consequence of this is the present day electronic revolution, which is the driving force of a vast majority of modern day technology. [6, 7]

Today, our world can be referred to as an electronic world. Electronic technol-

ogy has led to a remarkable improvement and growth in information technology, economic development, health, agriculture, energy, and national security. [8] For this reason, a great deal of scientific and technical research has focused on developing electronically active materials and devices such as transistors, integrated circuits, lasers, optical fibres and solar cells. The primary raw materials responsible for the electronic properties of these devices are inorganic semiconductors such as silicon, germanium, and compounds obtained from combining group III and group V elements. [9] However, the resources and methodologies used in processing these semiconductors, as well as their use and disposal, raises urgent questions about their adverse environmental impacts and cost-effectiveness. Further, the purity of these compounds is crucial to their semiconducting ability, and their rigidity limits their range of application in flexible devices. [10]

1.1.1 Organic semiconductors

In recent years, organic semiconductors have attracted significant interest as a potential replacement of inorganic semiconductors. One reason for this is that they promise a more sustainable technology that extends across the entire lifecycle of the device, beginning with synthesise rather than mining and ending with potentially biodegradable or recyclable devices. Furthermore, organic semiconductors can be flexible, stretchable and soft materials that can be be used to fabricate devices with shapes that are difficult or almost impossible to obtain with inorganic semiconductors. [11, 12] Despite their advantages, the field of organic electronics is reasonably in its infancy when assessed by the number and range of devices in the market. [13–15] The most common commercial applications are organic light emitting diodes (OLED), [16–22] organic field effect transistors (OFET), [23–27] organic solar cells (OSC), [28–32] liquid crystals and sensors.

Organic semiconductors contain conjugated systems that allow delocalisation of π-electrons across aligned π-orbitals. This results in a smaller energy gap between the highest occupied molecular orbital (HOMO) and the lowest unoccupied molecular orbital (LUMO) giving rise to semiconducting properties. [33–35] Current commercial organic semiconductors are mostly composed of linked aromatic units, and can be classified under two broad categories: polymer organic semiconductors and small organic molecule semiconductors.

- Polymer organic semiconductors are complex long chains of aromatic units linked together via σ-bonds. [36] They usually form amorphous films with virtually no long-range structural order and short π-conjugated length, consequently resulting in low charge-carrier mobility. The most common commercially applied polymer organic semiconductor is polythiophene, represented in Fig. 1.1a.

- Small organic molecule semiconductors are less complex monodisperse molecular species with well-defined chemical structures. They are typically polyaromatic compounds that can self-assemble into a well-ordered polycrystalline framework. [37] This long-range order is important because it provides an excellent overlap of frontier molecular orbitals, which leads to better charge-carrier mobility. The most commercially applied small organic molecule semiconductor is rubrene, represented in Fig. 1.1b. Rubrene is currently the organic semiconductor possessing the highest carrier mobility, with carrier mobility of 40 $cm^2\ V^{-1}\ s^{-1}$ for holes. [22]

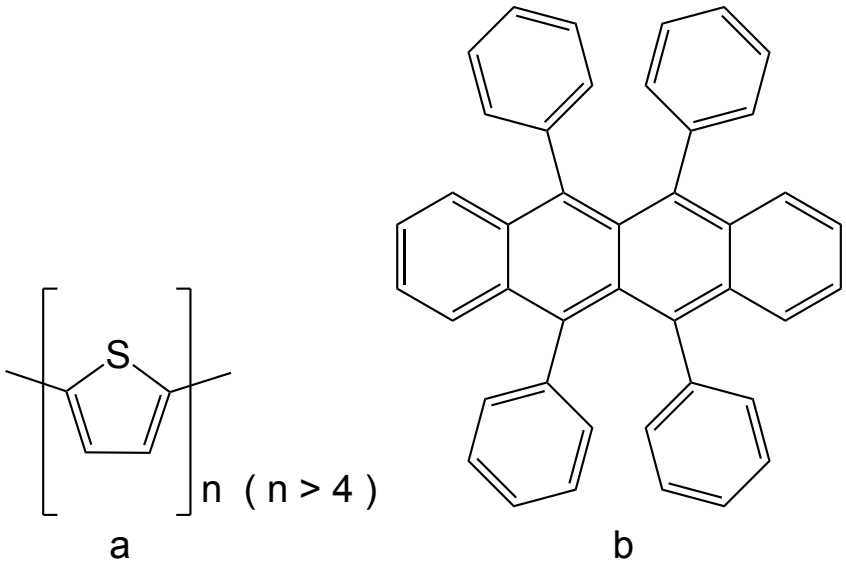

Fig. 1.1 Illustration of representatives of two broad types of organic semiconductors. (a) Polythiophene, the most common polymer organic semiconductor and (b) rubrene, the most common small organic molecule semiconductor.

Because of the better charge-carrier mobility of small organic molecule semiconductors, they are an important class of organic semiconductors that should be investigated further. Consequently, understanding and controlling the synthesis of these compounds will help to expedite the development of novel compounds with improved semiconducting ability. It is important to understand what these compounds are, how they are synthesised and how their synthesis can be improved.

1.2 Polycyclic aromatic compounds

Polyaromatic compounds (PACs) constitute an extraordinarily large and diverse class of organic molecules. Formally, they are defined by the International Union of Pure and Applied Chemistry (IUPAC) as systems with at least three fused aro-

matic rings. [38] The fusion of these rings can be angularly or linearly as illustrated in Fig. 1.2 . [39]

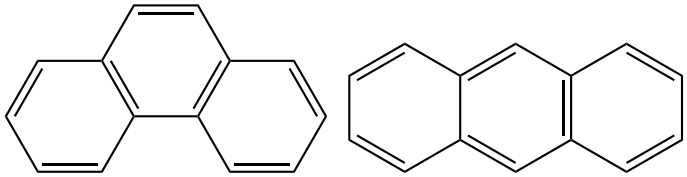

Fig. 1.2 Illustration of an angular (**left**) and a linear (**right**) PAC

Most PACs are planar. Examples of non-linear PACs are helicenes for which intramolecular crowding causes the system to twist into nonplanar helical structures with substantially lowered steric hindrance between the terminal rings Fig. 1.3. [40] This deviation from planarity leads to a disruption in the π-system, which prevents the π-surfaces from overlapping and consequently reducing their semiconducting ability. [41]

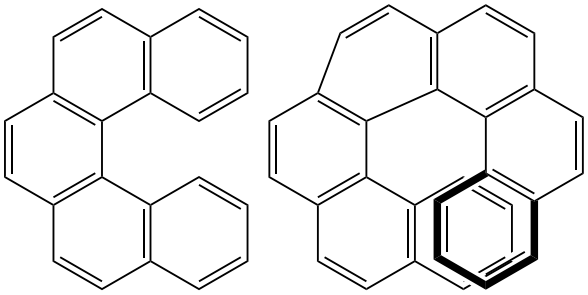

Fig. 1.3 Planar helicene (**left**) and non-planar helicene (**right**).

PACs can be divided into two classes, polyaromatic hydrocarbon (PAH) and polyheteroaromatic (PHC) compounds. PAHs are fused aromatic ring compounds, containing purely carbon and hydrogen. PHCs are analogues of the PAHs containing one or more heteroatom such as nitrogen, oxygen and sulfur. An example of each class is represented in Fig. 1.4.

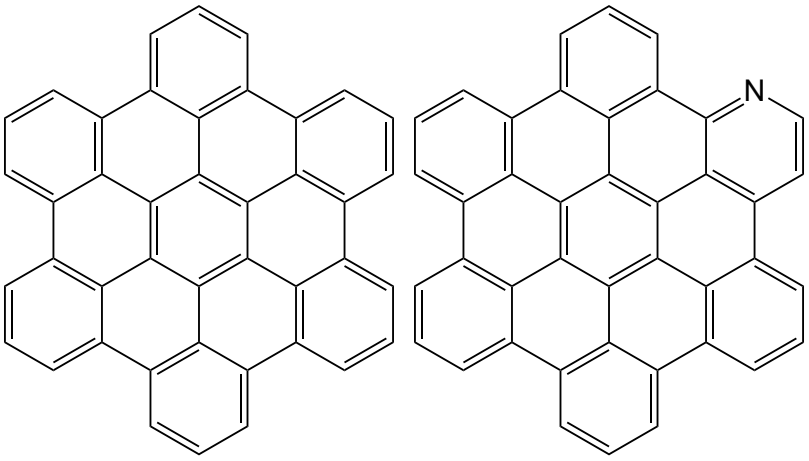

Fig. 1.4 Example of a PAH (1.1) and PHC (1.2)

PACs are ubiquitous in the environment. Naturally, they are present in fossil fuels such as crude oil, coal, and oil shales, and are often emitted into the environment during the refinery process of these fossils fuels. [42] They are widely produced during volcanic eruptions, forest fires or any form of incomplete combustion of organic matter. [43–46] They also enter the environment through several other natural or anthropogenic processes such as bacterial and algal synthesis, petroleum seeps, erosion of sedimentary rocks containing petroleum hydrocarbons, and decomposition of vegetative litter. [47, 48]

Scientific interest in PACs was instilled by the discovery of synthetic dyes from coal-tar by Perkins in the 19th century [49], which resulted in the significant growth of the textile industry at the dawn of the industrial revolution. [46, 50] Later, the discovery of the carcinogenic properties of benzo[a]pyrene, dibenzo[a,b]anthracene and other polyaromatics encouraged structure-activity studies of these compounds because it was the first indication of a disease caused by organic molecules rather

than microorganisms. [43]. These studies eventually led to the discovery of the photoconducting ability of anthracene and other PACs, which was the genesis of the study of their semiconducting ability and potential application in electronic devices. [16, 43, 51]

1.3 Synthesis of PACs

Understanding and controlling the synthesis of PACs is a key requirement for the growth of organic electronics. There is a vast number of organic synthetic methods in literature for the synthesis of these molecules. [43, 52–65]. However, in this thesis, we will focus only on eliminative cyclisation approaches because they are the most synthetically viable approach for the synthesis of PACs which, if well understood and controlled, can provide access to a wide variety of PACs.

1.3.1 Eliminative cyclisation

Eliminative cyclisation is an intramolecular cyclisation reaction that proceeds via two steps; planarisation and elimination. The planarisation step involves the initial cyclisation of the reactant molecule into a cyclised intermediate. The eliminative step involves the elimination of two adjacent groups bonded to the cyclising atoms, which leads to the restoration of aromaticity in the newly formed cycle, as illustrated in Scheme 1.1.

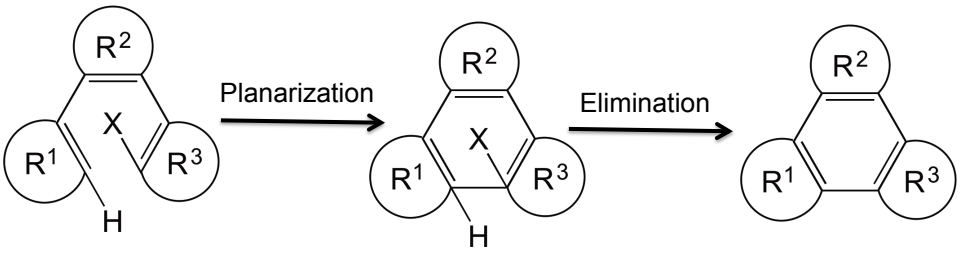

Scheme 1.1 General reaction scheme for eliminative cyclization, where R^1, R^2, R^3 represent different ring substituents and X stands for any leaving group

Eliminative cyclisation can be thermally or photochemically driven. The thermal process known as the Scholl reaction, involves an oxidative planarisation step followed by an oxidative elimination step. It is the most versatile thermally driven intramolecular cyclisation method for the synthesis of PACs and the only intramolecular cyclisation method that has been used to obtain multiple simultaneous cyclisations. [66] For example, Mullen and co-workers used the Scholl reaction to successfully make 126 new C-C bonds in a single step during the conversion of dendritic oligophenylenes to the corresponding symmetric hydrocarbons. [66–69]

The photochemically driven eliminative cyclisation is known as the Mallory reaction. It involves a planarisation step followed by either an oxidative or a thermal elimination step. It is an essential class of eliminative cyclisation because it provides a wide range of cyclisation routes as well as an alternative route for molecules that fail to cyclise thermally.

Scholl reaction

Despite its versatility, there is so far no agreed-upon reaction mechanism by which the Scholl reaction proceeds. Two commonly proposed reaction pathways involve

the formation of either a radical cation or arenium cation intermediate.

A schematic representation of the radical intermediate pathway is found in Scheme 1.2The reactant molecule **1.3** is oxidised to the radical cation intermediate **1.4**, which is then planarised to form the cyclised intermediate **1.5**. The elimination step is the least understood, [70] but the most common view is that it proceeds by deprotonation to **1.6**, followed by a simultaneous reduction and another deprotonation to form the product **1.7**. [71]

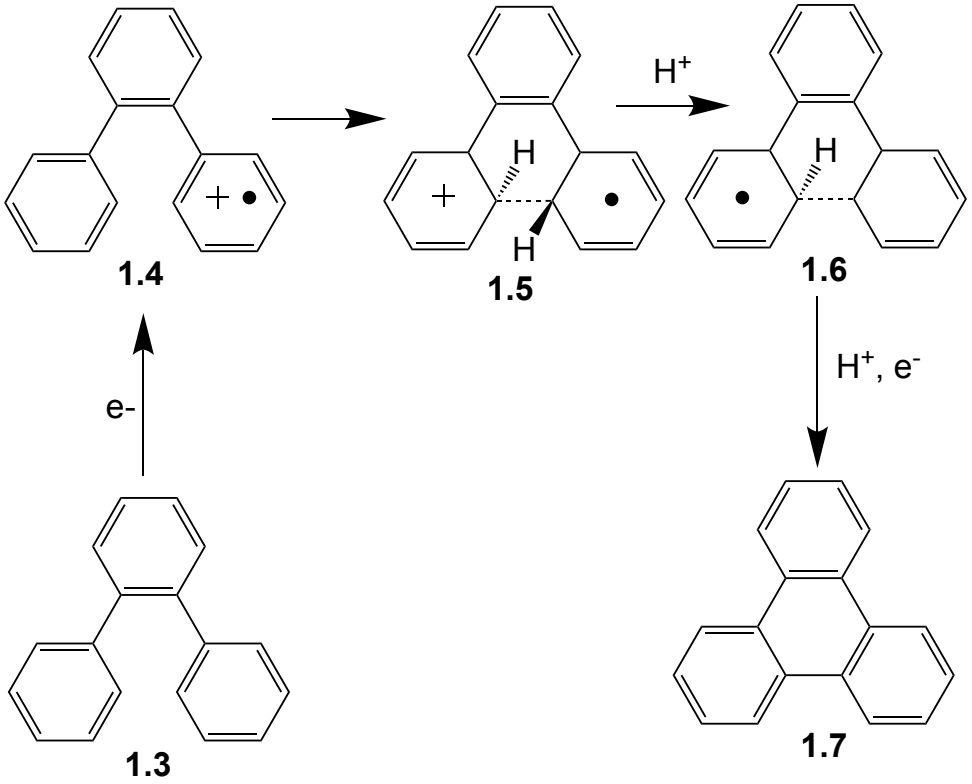

Scheme 1.2 Illustration of radical cation mechanism for the synthesis of ortho-terphenyl, **1.7**. [71]

In the arenium intermediate pathway illustrated in Scheme 1.3, the reactant molecule is believed to be protonated to form the arenium intermediate **1.4'**, which is then

planarised to the cyclised intermediate **1.5'**. The cyclised intermediate is then deprotonated to the product. [72–74]

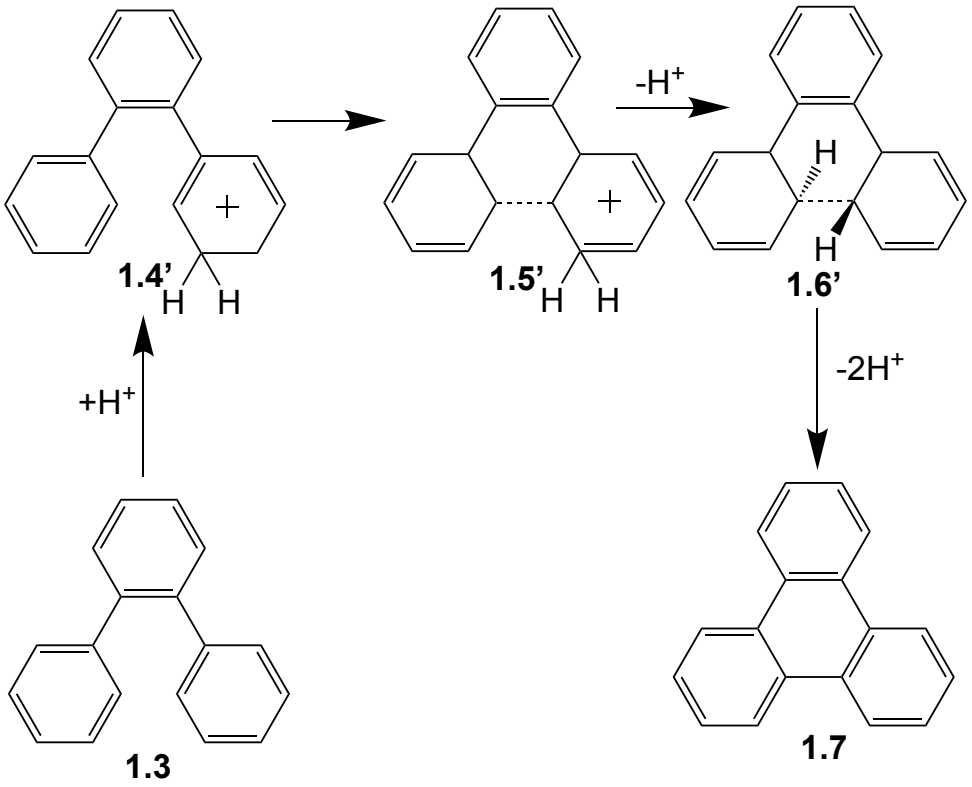

Scheme 1.3 Arenium mechanism pathway for the synthesis of ortho-terphenyl, **1.7**. [72]

The only evidence for the arenium intermediate pathway is based on computational studies; experimental studies favour the radical intermediate pathway. [71] For instance, Zhai and co-workers [70] argued that if the arenium intermediate pathway were the preferred pathway, the oxidising agent would play a role only in the oxidative dehydrogenation of the cyclised intermediate and weak oxidising agents like iodine or atmospheric oxygen would be effective. The failure of the Scholl reaction to yield any product in the presence of weak oxidising agents suggests

that the role of the oxidising agent is not limited to oxidative dehydrogenation. Since the Scholl reaction requires very harsh oxidative conditions such as $FeCl_3$ in CH_2Cl_2, $CuCl_2/AlCl_3$ in CS_2, $MoCl_5$ with or without $TiCl_4$ in CH_2Cl_2, $SbCl_5$, $TI(O_2CCF_3)_3$ in CF_3CO_2H or BF_3-OEt_2, CH_3SO_3H/DDQ, the oxidising agent clearly plays a major role. They also found that reactants with high oxidation potentials failed to yield products when an oxidising agent with a weaker oxidation potential was used. This also suggests that the radical intermediary pathway is the more likely pathway. [72–74] Based on this experimental evidence, all studies on the Scholl reaction in this thesis assume the radical intermediary pathway.

Mallory reaction

The Mallory reaction is another versatile synthetic method for the synthesis of PACs. In comparison with the Scholl reaction, it involves milder reaction conditions and applies to a broader range of substrates. [75–77] The most agreed-upon mechanism of the Mallory reaction is illustrated in Scheme 1.4. [76] The reactant molecule **1.8** absorbs a photon of light and is excited to a singlet excited state **1.9**, in which the molecule rearranges to a planarised, cyclised intermediate **1.10**. Elimination can then proceed oxidatively or non-oxidatively (when 'X' is a good leaving group) to give the product **1.11**. [76, 77]

1.3.2 Problems with eliminative cyclization

Although the Scholl and the Mallory reactions have been extensively studied experimentally, [78–84] there is a general lack of understanding as to why certain reactants fail to yield cyclisation products. One reason for this is that experimental studies have focused on optimising reaction conditions - solvent, oxidant, temperature - to identify experimental conditions that will lead to product formation. They do not provide fundamental information about the structural and

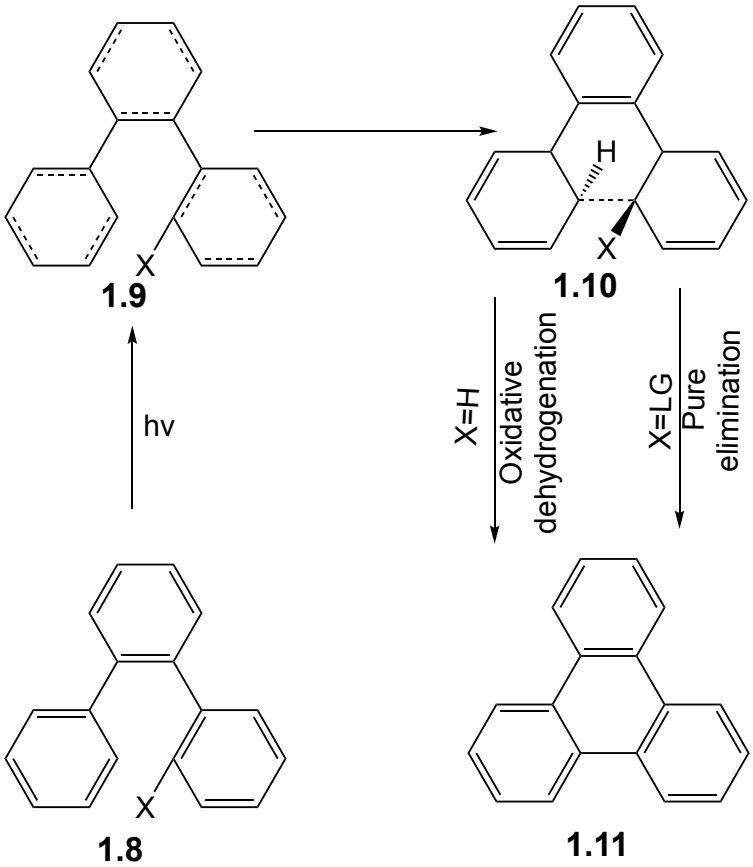

Scheme 1.4 Illustration of the reaction mechanism for Mallory reaction for the synthesis of ortho-terphenyl. LG represents a good leaving group. [76]

electronic attributes of the reactant molecules that will make them suitable candidates for eliminative cyclisation. Hence it will be important to perform detailed computational studies on a range of reactant molecules with diverse cyclisation modes, with the aim of providing a qualitative understanding of the fundamental structural and electronic factors that control the different mechanisms for these reactions.

1.3.3 Computational modelling

Chemical reactions, generally speaking, are determined by a complex physical interplay of the electronic and structural attributes of the reactants, along with conditions such as temperature, concentration, phase and solvent. [85] One of the major goals of chemistry is to control reactions to produce a relatively large yield of products. Designing a reaction to obtain large yields of a particular product of interest is one of the most challenging problems in synthetic chemistry. Most, if not all, organic chemists are devoted either to developing novel synthetic methods or altering the current synthetic methods by changing reaction conditions or reactant properties to maximise yield. However, a detailed understanding of the complex processes occurring during a reaction may enable the rational design of optimal processes.

Computational chemistry has emerged as a pivotal tool, for underpinning the mechanisms of complex chemical reactions. It enables a detailed understanding of the structural and electronic properties of reacting species, as well as elucidating the mechanism of reactions, which can help in designing new reactions or predicting the outcome of reactions. The latter can be done either by performing detailed mechanistic modelling or by developing rule-based parameters, known as reactivity predictors, that can be used to predict the products of a given reaction. Mechanistic modelling is a manual and time-consuming process, but gives comprehensive thermodynamical data. Reactivity predictors are faster, cheaper and amenable to automation, but are not quantitative.

Mechanistic modelling and reaction coordinate profiles

Fundamentally, computational chemistry is a quantum mechanical (QM) treatment of a chemical reaction that involves finding near exact solutions to the

Schrödinger equation for the reaction systems in question. A major approximation in solving the Schrödinger equation involves decoupling electronic motions from nuclear motions - the Born-Oppenheimer approximation. Solutions of the electronic motion for different nuclear coordinates lead to the construction of a multidimensional potential-energy surface (PES).

The PES is a graphical representation of the energy of a system at different nuclear coordinates. [86] Analysing and exploring the PES is key to understanding reaction mechanisms. Stationary points, whereby the first derivative of energy for one or more nuclear coordinates is zero, represent critical points that can further be characterised by performing second derivative calculations to confirm their nature. Stationary points with positive second derivatives for all nuclear coordinate displacements represent minima: reactants, products and intermediates. Alternatively, points with one direction of negative curvature are referred to as first-order saddle points. The direction of this negative second energy derivative indicates the vibrational coordinate along which the reaction proceeds through a transition state for the given reaction path. [87] Linking critical points on a PES surface establishes the minimum energy path of the reaction (MEP), which can otherwise be called the energy profile of the reaction.

Deciphering the energy profile of a chemical reaction is vital for understanding and explaining the reaction kinetics and thermodynamics. For instance, the determination of the transition state from the reaction profile explains the rate of the chemical reaction. Analysis of the energetics of the species that appear along the energy profile helps to understand the energy barriers required for the reactions as well as the relative stability of the products. [88]

Comparison between experimental observables and computational measurements depend on several factors. The first and most important of these is the computational. QM methods ranging from semi-empirical, and *ab initio* to density functional theory (DFT) are often used. Amongst these methods, DFT has emerged as the most popular and widely spread, largely because it gives a good comprise between accuracy and computational cost in comparison to the other methods.

Another essential approximation required for accurately modelling experimental observable is the basis set of the atomic orbital functions that are used in constructing the molecular orbitals of the system. The preferred basis sets are those that provide results at a minimal computational cost.

Finally, solvent effect plays a vital role in modelling many real chemical systems. The solvation approximation used is a crucial prerequisite in efficiently modelling any such chemical system. An extensive summary of the most critical computational approximation necessary to reproduce experimental observables will be covered in later chapters.

Generating the full PES for any realistically sized chemical system using any quantum chemical method is a costly and time-consuming process. One way to get around this is to intuitively guess starting geometries for all of the critical structures that constitute the MEP. This approach has been cleverly used to generate the energy profile of many chemical reactions at moderate cost, giving great insight into understanding these reactions.

Knowledge of the reaction mechanism for a common class of reaction can also be used to design some rule-based parameters or reactivity predictors that can be

used to predict the outcome of subsequent reactions in a far more cost-effective and automated manner.

Reactivity predictors

Reactivity predictors, commonly referred to as reactivity indices or reactivity descriptors, are a set of quantitative parameters that can be used to predict possible reaction outcomes or reaction centres in a molecule. [89] In particular, reactivity predictors aim to capture or describe the most essential interactions involved in forming the rate-determining transition state. [90] They can best be applied to reactions that have early transition states, for which there are only minor perturbations of the electronic and nuclear structures of the interacting species upon formation of the rate-determining transition state. [91]

The first calculated reactivity predictors for organic reactions were based on correlating chemical reactivity to atomic partial charges and free valence indices. [92] The basic rationale for calculating atomic charges was that the reorganisation of charges resulting from the polarisation of a molecule could be indicative of the most favourable site for either an electrophilic or nucleophilic attack. For instance in an aromatic electrophilic or nucleophilic substitution reaction, the carbon atom with the most negative partial charge will be the most responsive site for an electrophilic attack, and conversely, the carbon atoms with the most positive charge will be the most favourable site for nucleophilic attack.

The free valence index can be defined as the degree to which atoms in a molecule are bonded to one another relative to a theoretical maximum bonding power. [93] The rationale for this index was the premise that every atom in a molecule has

a valency that must be satisfied when forming bonds with other atoms in the molecule. This valency can be measured by comparing the total bond order of the atom to a theoretical maximum bond order expected for that atom type. Atoms with less than the required valency, also known as free valence, were considered to be reactive centres susceptible to new-bond formation. [93]

The use of both atomic partial charges and free valence index have found limited success due to many shortcomings. One shortcoming is that atomic partial charges and free valence indices are not experimental observable and have no agreed theoretical definitions or methods of quantification. [94]

As an alternative to partial atomic charge and free valence index, Fukui pioneered the development of a reactivity descriptor based on analysing electronic density distributions over only frontier molecular orbitals (FMOs), generally referred to as FMO theory. The basic tenet in this approach is that only the electrons in the FMO take part in chemical reactions. [95] Hence, organic reactions evolve through electronic overlap between FMOs of the reacting species. Reactivity predictors based on FMO theory have been the most popularly used reactivity predictors for most electrophilic and nucleophilic substitution reactions. [96]

The extensive application of FMO theory inspired the design of many more reactivity predictors such as chemical hardness, chemical softness, electrophilicity, ionisation potential (IP), electron affinity(EA), and nucleophilicity. [89,97–99] But despite the many published reactivity predictors, there is, so far, no robust reactivity predictor for eliminative cyclisation reactions. The existing reactivity predictors were focussed on changes in electron distribution computed via Hückel molecular orbital theory. [100–105] However, these reactivity predictors have been limited

only to polyaromatic hydrocarbons excluding heteroatom-containing molecules and are not commonly used for synthetic planning.

1.4 Objective of the present work

The aim of this study is to develop a more general and reliable computational model to cheaply and efficiently predict the outcome of eliminative cyclisation reactions under specified reaction conditions. In particular, this is to establish which reactions or sets of reaction conditions are likely to give products with preferably high yields or even to give any products at all. This is to be done in two stages. The first will establish a detailed reaction mechanism of eliminative cyclisation in order to grasp a full understanding of both the planarisation and the elimination steps. In particular, it will extend understanding on how oxidative-elimination and non-oxidative elimination proceed in the Mallory reaction, which will be a critical factor in understanding the role of the oxidising agent in eliminative cyclisation. Secondly, the knowledge acquired from elucidating the reaction mechanism will be used to establish a robust reactivity predictor for eliminative photocyclisation.

1.4.1 Scope of thesis

This work is divided into the following chapters:

Chapter Two: General overview of the computational quantum chemistry methods relevant to this study.

Chapter Three: Establish the reactivity mechanism for both the Mallory and Scholl reactions by studying the effects of alternating the position of heteroatoms in the molecule.

Chapter Four: The effects of different ring substituents on the photocyclisation of substituted benzylidene o-methyloximes is studied.

Chapter Five: Summary of existing reactivity predictors for photochemical cyclisation will be made as well as the setting grounds for the new reactivity predictor.

Chapter Six: Testing the new reactivity predictor on different molecules with varied structural diversity.

Chapter Seven: Conclusions and setting up some future work as well as providing some useful recommendations to synthetic chemists.

Bibliography

[1] S. Connolly, *The industrial revolution.* Chicago, Ill. : Heinemann Library, 2003.

[2] N. Smith, *The Industrial Revolution.* Events and outcomes, Evans, 2002.

[3] M. Barnhart, "A review of the industrial revolution in world historyÄ," *Journal of Business and Finance Librarianship*, vol. 15, no. 2, pp. 150–152, 2010.

[4] A. Thackray, "Science and technology in the industrial revolution," *History of Science*, vol. 9, no. 1, pp. 76–89, 1970.

[5] I. Inkster, *Science and Technology in the British Industrial Revolution*, p. 60 =88. London: Macmillan Education UK, 1991.

[6] R. Sarnoff, "Electronics: The new revolution," *Omega*, vol. 2, no. 4, pp. 543 – 547, 1974.

[7] P. Hills, "Human communication in an age of electronic revolution," *Science and Public Policy*, vol. 11, no. 6, pp. 335–337, 1984.

[8] V. Kumar, S. K. Mehta, B. K. Sehgal, and R. Singh, "Research and development in semiconductor devices in india," *IETE Technical Review*, vol. 20, no. 2, pp. 111–117, 2003.

[9] Y. Sun and J. Rogers, "Inorganic semiconductors for flexible electronics," *Advanced Materials*, vol. 19, no. 15, pp. 1897–1916, 2007.

[10] Y. Liu, K. He, G. Chen, W. R. Leow, and X. Chen, "Nature-inspired structural materials for flexible electronic devices," *Chemical Reviews*, vol. 117, no. 20, pp. 12893–12941, 2017.

[11] S. E. Root, S. Savagatrup, A. D. Printz, D. Rodriquez, and D. J. Lipomi, "Mechanical properties of organic semiconductors for stretchable, highly flexible, and mechanically robust electronics," *Chemical Reviews*, vol. 117, no. 9, pp. 6467–6499, 2017.

[12] V. Coropceanu, H. Li, P. Winget, L. Zhu, and J.-L. Bredas, "Electronic-structure theory of organic semiconductors: Charge-transport parameters and metal/organic interfaces," *Annual Review of Materials Research*, vol. 43, no. 1, pp. 63–87, 2013.

[13] A. Facchetti, "Organic electronics. Materials, Manufacturing and Applications. Edited by hagen klauk.," *Angewandte Chemie International Edition*, vol. 46, no. 9, pp. 1367–1368, 2006.

[14] C. Wang, H. Dong, L. Jiang, and W. Hu, "Organic semiconductor crystals," *Chemical Society Reviews*, vol. 47, pp. 422–500, 2018.

[15] X. Bai, K. Zong, J. Ly, J. S. Mehta, M. Hand, K. Molnar, S. Lee, B. Kahr, J. M. Mativetsky, A. Briseno, and S. S. Lee, "Orientation control of solution-processed organic semiconductor crystals to improve out-of-plane charge mobility," *Chemistry of Materials*, vol. 29, no. 17, pp. 7571–7578, 2017.

[16] J. E. Anthony, "Functionalized acenes and heteroacenes for organic electronics," *Chemical Reviews*, vol. 106, no. 12, pp. 5028–5048, 2006.

[17] C.-J. Zheng, W.-M. Zhao, Z.-Q. Wang, D. Huang, J. Ye, X.-M. Ou, X.-H. Zhang, C.-S. Lee, and S.-T. Lee, "Highly efficient non-doped deep-blue organic light-emitting diodes based on anthracene derivatives," *Journal of Materials Chemistry*, vol. 20, pp. 1560–1566, 2010.

[18] P.-Y. Gu, Y. Zhao, J.-H. He, J. Zhang, C. Wang, Q.-F. Xu, J.-M. Lu, X. W. Sun, and Q. Zhang, "Synthesis, physical properties, and light-emitting diode performance of phenazine-based derivatives with three, five, and nine fused six-membered rings," *The Journal of Organic Chemistry*, vol. 80, no. 6, pp. 3030–3035, 2015.

[19] Q. Zhang, Y. Divayana, J. Xiao, Z. Wang, E. Tiekink, H. Doung, H. Zhang, F. Boey, X. Sun, and F. Wudl, "Synthesis, characterization, and bipolar transporting behavior of a new twisted polycyclic aromatic hydrocarbon: 1',4'-diphenyl-naphtho-(2'.3':1.2)-pyrene-6'-nitro-7'-methyl carboxylate.," *ChemistryA European Journal*, vol. 16, no. 25, pp. 7422–7426, 2010.

[20] Z. Zhao, S. Chen, J. W. Y. Lam, P. Lu, Y. Zhong, K. S. Wong, H. S. Kwok, and B. Z. Tang, "Creation of highly efficient solid emitter by decorating pyrene core with AIE-active tetraphenylethene peripheries," *Chemical Communications*, vol. 46, pp. 2221–2223, 2010.

[21] M. Vasilopoulou, L. C. Palilis, A. Botsialas, D. G. Georgiadou, P. Bayiati, N. Vourdas, P. S. Petrou, G. Pistolis, N. A. Stathopoulos, and P. Argitis, "Flexible organic light emitting diodes (OLEDs) based on a blue emitting polyfluorene," *physica status solidi (c)*, vol. 5, no. 12, pp. 3658–3662, 2008.

[22] T. Hasegawa and J. Takeya, "Organic field-effect transistors using single crystals," *Science and Technology of Advanced Materials*, vol. 10, no. 2, pp. 024–314, 2009.

[23] Z. Bao, "Organic materials for thin film transistors." https://www.sigmaaldrich.com/technical-documents/articles/material-matters/organic-materials.html, 2007.

[24] B. Kumar, B. K. Kaushik, and Y. S. Negi, "Organic thin film transistors: Structures, models, materials, fabrication, and applications: A review," *Polymer Reviews*, vol. 54, no. 1, pp. 33–111, 2014.

[25] H. Klauk, "Organic thin-film transistors," *Chemical Society Reviews*, vol. 39, pp. 2643–2666, 2010.

[26] L.-K. Mao, J.-C. Hwang, T.-H. Chang, C.-Y. Hsieh, L.-S. Tsai, Y.-L. Chueh, S. S. Hsu, P.-C. Lyu, and T.-J. Liu, "Pentacene organic thin-film transistors with solution-based gelatin dielectric," *Organic Electronics*, vol. 14, no. 4, pp. 1170 – 1176, 2013.

[27] C. Reese, M. Roberts, M. mang Ling, and Z. Bao, "Organic thin film transistors," *Materials Today*, vol. 7, no. 9, pp. 20 – 27, 2004.

[28] R. Jin and K. Wang, "Rational design of diketopyrrolopyrrole-based small moleculesas donating materials for organic solar cells," *International Journal of Molecular Sciences*, vol. 16, no. 9, pp. 20326–20343, 2015.

[29] M. Scharber and N. Sariciftci, "Efficiency of bulk-heterojunction organic solar cells," *Progress in Polymer Science*, vol. 38, no. 12, pp. 1929 – 1940, 2013.

[30] L. Kazmerski, "Solar photovoltaics technology: No longer an outlier," in *Comprehensive Renewable Energy* (A. Sayigh, ed.), pp. 13 – 30, Oxford: Elsevier, 2012.

[31] R. J. Cogdell, T. H. Brotosudarmo, A. T. Gardiner, P. M. Sanchez, and L. Cronin, "Artificial photosynthesis solar fuels: Current status and future prospects," *Biofuels*, vol. 1, no. 6, pp. 861–876, 2010.

[32] T. Moore, A. Moore, D. Gust, J. Barber, R. Van Grondelle, L. Sun, and L. Hammarstr^m, "The design and synthesis of artificial photosynthetic antennas, reaction centres and membranes," *Philosophical Transactions of the Royal Society B: Biological Sciences*, vol. 357, no. 1426, pp. 1481–1498, 2002.

[33] H. Klauk, "Organic thin-film transistors," *Chemical Society Reviews*, vol. 39, pp. 2643–2666, 2010.

[34] J. E. Anthony, M. Heeney, and B. S. Ong, "Synthetic aspects of organic semiconductors," *MRS Bulletin*, vol. 33, no. 7, p. 698?705, 2008.

[35] A. Mishra and P. Bauerle, "Small molecule organic semiconductors on the move: Promises for future solar energy technology," *Angewandte Chemie International Edition*, vol. 51, no. 9, pp. 2020–2067, 2012.

[36] J. D. Myers and J. Xue, "Organic semiconductors and their applications in photovoltaic devices," *Polymer Reviews*, vol. 52, no. 1, pp. 1–37, 2012.

[37] G. Heimel, I. Salzmann, S. Duhm, and N. Koch, "Design of organic semiconductors from molecular electrostatics," *Chemistry of Materials*, vol. 23, no. 3, pp. 359–377, 2011.

[38] G. P. Moss, "Nomenclature of fused and bridged fused ring systems (IUPAC recommendations 1998)," *Pure and Applied Chemistry*, vol. 70, pp. 143–216, 01 1998.

[39] S. C. Rasmussen, "The nomenclature of fused-ring arenes and heterocycles: A guide to an increasingly important dialect of organic chemistry," *ChemTexts*, vol. 2, no. 4, p. 16, 2016.

[40] Y. Shen and C.-F. Chen, "Helicenes: Synthesis and applications," *Chemical Reviews*, vol. 112, no. 3, pp. 1463–1535, 2012.

[41] T. Fujikawa, Y. Segawa, and K. Itami, "Synthesis, structures, and properties of œÄ-extended double helicene: A combination of planar and nonplanar π-systems," *Journal of the American Chemical Society*, vol. 137, no. 24, pp. 7763–7768, 2015.

[42] M. Zander and G. Collin, "A review of the significance of polycyclic aromatic chemistry for pitch science," *Fuel*, vol. 72, no. 9, pp. 1281 – 1285, 1993.

[43] C. F. Murray, "Polycyclic aromatic hydrocarbons (Harvey, Ronald g.)," *Journal of Chemical Education*, vol. 75, no. 11, p. 1392, 1998.

[44] C. Pies, T. A. Ternes, and T. Hofmann, "Identifying sources of polycyclic aromatic hydrocarbons (PAHs) in soils: distinguishing point and non-point sources using an extended PAH spectrum and n-alkanes," *Journal of Soils and Sediments*, vol. 8, no. 5, p. 312, 2008.

[45] B.-K. Lee, "Sources, distribution and toxicity of polyaromatic hydrocarbons (PAHs) in particulate matter," in *Air Pollution* (V. Villanyi, ed.), ch. 5, Rijeka: InTech, 2010.

[46] N. M. Marinov, W. J. Pitz, C. K. Westbrook, M. J. Castaldi, and S. M. Senkan, "Modeling of aromatic and polycyclic aromatic hydrocarbon formation in premixed methane and ethane flames," *Combustion Science and Technology*, vol. 116-117, no. 1-6, pp. 211–287, 1996.

[47] G. Ana, M. Sridhar, and G. Emerole, "Contamination of surface waters by polycyclic aromatic hydrocarbons in two nigerian coastal communities," *Journal of Environmental Health Research*, vol. 11, no. 2, pp. 77–85, 2011.

[48] Z. Zelinkova and T. Wenzl, "The occurrence of 16 epa pahs in food.Äì A review," *Polycyclic Aromatic Compounds*, vol. 35, no. 2-4, pp. 248–284, 2015.

[49] J. Banerjee, "Sir william henry perkin and the coal-tar colours." http://www.victorianweb.org/science/perkin.html, 28 August 2014.

[50] R. D. Welham, "The early history of the synthetic dye industry," *Journal of the Society of Dyers and Colourists*, vol. 79, no. 3, pp. 98–105, 1963.

[51] A. G. Chynoweth and W. G. Schneider, "The photoconductivity of anthracene. I.," *The Journal of Chemical Physics*, vol. 22, no. 6, pp. 1021–1028, 1954.

[52] M. C. Kloetzel, *The Diels-Alder Reaction with Maleic Anhydride*, pp. 1–59. John Wiley and Sons, Inc., 2004.

[53] E. Clar and M. Zander, "Syntheses of coronene and 1: 2-7:8-dibenzocoronene," *Journal of the Chemical Society*, pp. 4616–4619, 1957.

[54] X. L. Feng, W. Pisula, and K. Müllen, "Large polycyclic aromatic hydrocarbons: Synthesis and discotic organization," *Pure and Applied Chemistry*, vol. 81, no. 12, pp. 2203–2224, 2009.

[55] M. Müller, C. Kübel, and K. Müllen, "Giant polycyclic aromatic hydrocarbons," *Chemistry A European Journal*, vol. 4, no. 11, pp. 2099–2109, 1998.

[56] L. T. Scott, M. M. Hashemi, D. T. Meyer, and H. B. Warren, "Corannulene. A convenient new synthesis," *Journal of the American Chemical Society*, vol. 113, no. 18, pp. 7082–7084, 1991.

[57] L. T. Scott, P.-C. Cheng, M. M. Hashemi, M. S. Bratcher, D. T. Meyer, and H. B. Warren, "Corannulene. A three-step synthesis1," *Journal of the American Chemical Society*, vol. 119, no. 45, pp. 10963–10968, 1997.

[58] A. Iuliano, P. Piccioli, and D. Fabbri, "Ring-closing olefin metathesis of 2,2'-divinylbiphenyls: A novel and general approach to phenanthrenes," *Organic Letters*, vol. 6, no. 21, pp. 3711–3714, 2004.

[59] M. C. Bonifacio, C. R. Robertson, J.-Y. Jung, and B. T. King, "Polycyclic aromatic hydrocarbons by ring-closing metathesis," *The Journal of Organic Chemistry*, vol. 70, no. 21, pp. 8522–8526, 2005.

[60] P. M. Donovan and L. T. Scott, "Elaboration of diaryl ketones into naphthalenes fused on two or four sides: A naphthoannulation procedure," *Journal of the American Chemical Society*, vol. 126, no. 10, pp. 3108–3112, 2004.

[61] M. B. Goldfinger, K. B. Crawford, and T. M. Swager, "Directed electrophilic cyclizations: Efficient methodology for the synthesis of fused polycyclic aromatics," *Journal of the American Chemical Society*, vol. 119, no. 20, pp. 4578–4593, 1997.

[62] M. B. Goldfinger and T. M. Swager, "Fused polycyclic aromatics via electrophile-induced cyclization reactions: Application to the synthesis of graphite ribbons," *Journal of the American Chemical Society*, vol. 116, no. 17, pp. 7895–7896, 1994.

[63] L. F. Fieser, *The Elbs Reaction*, pp. 129–154. John Wiley and Sons, Inc., 2004.

[64] A. H. Lewin and T. Cohen, "Mechanism of the copperinduced pschorr cyclization. New phenol synthesis involving hydroxylation of the intermediate radical by cupric ion," *The Journal of Organic Chemistry*, vol. 32, no. 12, pp. 3844–3850, 1967.

[65] D. F. DeTar, *The Pschorr Synthesis and Related Diazonium Ring Closure Reactions*, pp. 409–462. John Wiley and Sons, Inc., 2004.

[66] V. S. Iyer, M. Wehmeier, J. D. Brand, M. A. Keegstra, and K. Mullen, ""from hexa-peri-hexabenzocoronene to superacenes"," *Angewandte Chemie International Edition in English*, vol. 36, no. 15, pp. 1604–1607, 1997.

[67] M. D. Watson, A. Fechtenkotter, and K. Mullen, "Big is beautiful- "Aromaticity" revisited from the viewpoint of macromolecular and supramolecular benzene chemistry," *Chemical Reviews*, vol. 101, no. 5, pp. 1267–1300, 2001.

[68] C. D. Simpson, J. D. Brand, A. J. Berresheim, L. Przybilla, H. J. Rader, and K. Mullen, "Synthesis of a giant 222 carbon graphite sheet," *Chemistry A European Journal*, vol. 8, no. 6, pp. 1424 –1429, 2002.

[69] C. D. Simpson, G. Mattersteig, K. Martin, L. Gherghel, R. E. Bauer, H. J. Rader, and K. Mullen, "Nanosized molecular propellers by cyclodehydrogenation of polyphenylene dendrimers," *Journal of the American Chemical Society*, vol. 126, no. 10, pp. 3139–3147, 2004.

[70] L. Zhai, R. Shukla, S. H. Wadumethrige, and R. Rathore, "Probing the arenium-ion (protontransfer) versus the cation-radical (electron transfer)

mechanism of Scholl reaction using DDQ as oxidant," *The Journal of Organic Chemistry*, vol. 75, no. 14, pp. 4748–4760, 2010.

[71] B. T. King, J. Kroulik, C. R. Robertson, P. Rempala, C. L. Hilton, J. D. Korinek, and L. M. Gortari, "Controlling the Scholl reaction," *The Journal of Organic Chemistry*, vol. 72, no. 7, pp. 2279–2288, 2007.

[72] R. Rathore, A. S. Kumar, S. V. Lindeman, and J. K. Kochi, "Preparation and structures of crystalline aromatic cation-radical salts. triethyloxonium hexachloroantimonate as a novel (one-electron) oxidant," *The Journal of Organic Chemistry*, vol. 63, no. 17, pp. 5847–5856, 1998.

[73] R. Rathore and J. K. Kochi, "Radical-cation catalysis in the synthesis of diphenylmethanes via the dealkylative coupling of benzylic ethers," *The Journal of Organic Chemistry*, vol. 60, no. 23, pp. 7479–7490, 1995.

[74] S. H. Wadumethrige and R. Rathore, "A facile synthesis of elusive alkoxy-substituted hexa-peri-hexabenzocoronene," *Organic Letters*, vol. 10, no. 22, pp. 5139–5142, 2008.

[75] W. M. Moore, D. D. Morgan, and F. R. Stermitz, "The photochemical conversion of stilbene to phenanthrene. The nature of the intermediate," *Journal of the American Chemical Society*, vol. 85, no. 6, pp. 829–830, 1963.

[76] F. B. Mallory, C. S. Wood, and J. T. Gordon, "Photochemistry of stilbenes III. Some aspects of the mechanism of photocyclization to phenanthrenes," *Journal of the American Chemical Society*, vol. 86, no. 15, pp. 3094–3102, 1964.

[77] F. B. Mallory and C. W. Mallory, *Photocyclization of Stilbenes and Related Molecules*, pp. 1–456. John Wiley and Sons, Inc., 2004.

[78] T. Bach and J. P. Hehn, "Photochemical reactions as key steps in natural product synthesis," *Angewandte Chemie International Edition*, vol. 50, no. 5, pp. 1000 –1045, 2011.

[79] F. B. Mallory, K. E. Butler, A. Berube, E. D. Luzik, C. W. Mallory, E. J. Brondyke, R. Hiremath, P. Ngo, and P. J. Carroll, "Phenacenes: A family of graphite ribbons. Part 3: Iterative strategies for the synthesis of large phenacenes," *Tetrahedron*, vol. 57, no. 17, pp. 3715 – 3724, 2001.

[80] S. B. Singh and G. R. Pettit, "Antineoplastic agents. Isolation, structure, and synthesis of combretastatin C-1," *The Journal of Organic Chemistry*, vol. 54, no. 17, pp. 4105–4114, 1989.

[81] T. R. Kelly, C. T. Jagoe, and Q. Li, "Synthesis of (.+-.)cervinomycins A1 and A2," *Journal of the American Chemical Society*, vol. 111, no. 12, pp. 4522–4524, 1989.

[82] S. Takeo, S. Shigeru, and H. Kazuo, "A new route to polycondensed aromatics: Photolytic formation of triphenylene and dibenzo[fg,op]naphthacene ring systems," *Bulletin of the Chemical Society of Japan*, vol. 44, no. 9, pp. 2484–2490, 1971.

[83] F. B. Mallory, K. E. Butler, A. C. Evans, E. J. Brondyke, C. W. Mallory, C. Yang, and A. Ellenstein, "Phenacenes: A family of graphite ribbons. 2. Syntheses of some [7]Phenacenes and an [11]Phenacene by stilbene-like photocyclizations," *Journal of the American Chemical Society*, vol. 119, no. 9, pp. 2119–2124, 1997.

[84] L. Liu, B. Yang, T. J. Katz, and M. K. Poindexter, "Improved methodology for photocyclization reactions," *The Journal of Organic Chemistry*, vol. 56, no. 12, pp. 3769–3775, 1991.

[85] M. A. Kayala, C.-A. Azencott, J. H. Chen, and P. Baldi, "Learning to predict chemical reactions," *Journal of Chemical Information and Modeling*, vol. 51, no. 9, pp. 2209–2222, 2011.

[86] D. Heidrich, W. Kliesch, and W. Quapp, *Analysis of Multidimensional Potential Energy Surfaces — Stationary and Critical Points —*, pp. 31–100. Berlin, Heidelberg: Springer Berlin Heidelberg, 1991.

[87] O. Novaro and S. Castillo, "Multibody analysis of potential energy surfaces for first- and second-row tetramers I. The tetrahedral structures of P4 and N4," *International Journal of Quantum Chemistry*, vol. 26, no. 3, pp. 411 – 423, 1984.

[88] E. Kraka and D. Cremer, "Computational analysis of the mechanism of chemical reactions in terms of reaction phases: Hidden intermediates and hidden transition states," *Accounts of Chemical Research*, vol. 43, no. 5, pp. 591–601, 2010.

[89] Y. E. Zevatskii and D. V. Samoilov, "Some modern methods for estimation of reactivity of organic compounds," *Russian Journal of Organic Chemistry*, vol. 43, no. 4, pp. 483–500, 2007.

[90] R. F. Bader and K. E. Laidig, "The prediction and calculation of properties of atoms in molecules," *Journal of Molecular Structure: THEOCHEM*, vol. 234, pp. 75 – 94, 1991.

[91] T. Brinck and M. Liljenberg, *The Use of Quantum Chemistry for Mechanistic Analyses of SE Ar Reactions*, pp. 83–105. John Wiley and Sons, Inc, 2015.

[92] G. W. Wheland, "A quantum mechanical investigation of the orientation of substituents in aromatic molecules," *Journal of the American Chemical Society*, vol. 64, no. 4, pp. 900–908, 1942.

[93] F. H. Burkitt, C. A. Coulson, and H. C. Longuet-Higgins, "Free valence in unsaturated hydrocarbons," *Transactions of the Faraday Society*, vol. 47, pp. 553–564, 1951.

[94] K. Fukui, T. Yonezawa, and H. Shingu, "A molecular orbital theory of reactivity in aromatic hydrocarbons," *The Journal of Chemical Physics*, vol. 20, no. 4, pp. 722–725, 1952.

[95] K. Fukui, K. Morokuma, T. Yonezawa, and C. Nagata, "Charge transfer mechanism of reaction of conjugated molecules," *The Journal of Chemical Physics*, vol. 32, no. 6, pp. 1743–1747, 1960.

[96] W. Langenaeker, K. Demel, and P. Geerlings, "Electrophilic substitution on mono-substituted benzenes," *Journal of Molecular Structure: THEOCHEM*, vol. 234, pp. 329 – 342, 1991.

[97] R. G. Parr and W. Yang, "Density functional approach to the frontier-electron theory of chemical reactivity," *Journal of the American Chemical Society*, vol. 106, no. 14, pp. 4049–4050, 1984.

[98] P. Thanikaivelan, J. Padmanabhan, V. Subramanian, and T. Ramasami, "Chemical reactivity and selectivity using Fukui functions: basis set and population scheme dependence in the framework of B3LYP theory," *Theoretical Chemistry Accounts*, vol. 107, no. 6, pp. 326–335, 2002.

[99] L. S. † and P. Kolandaivel, "Study of effective hardness and condensed Fukui functions using AIM, ab initio, and DFT methods," *Molecular Physics*, vol. 103, no. 4, pp. 547–556, 2005.

[100] W. H. Laarhoven, "Photochemical cyclizations and intramolecular cycloadditions of conjugated arylolefins. Part I: Photocyclization with dehydrogena-

tion," *Recueil des Travaux Chimiques des Pays-Bas*, vol. 102, no. 4, pp. 185–204, 1983.

[101] W. Laarhoven, T. Cuppen, and R. Nivard, "Photodehydrocyclizations in stilbene-like compounds II: Photochemistry of distyrylbenzenes," *Tetrahedron*, vol. 26, no. 4, pp. 1069 – 1083, 1970.

[102] M. Scholz, M. Muhlstadt, and F. Dietz, "Die richtung der photocyclisierung naphthalinsubstituierter athylene," *Tetrahedron Letters.*, vol. 8, no. 7, pp. 665 – 668, 1967.

[103] K. A. Muszkat, G. Seger, and S. Sharafi-Ozeri, "Electronic overlap population as a measure of reactivity in electrocyclic reactions. Part 2.-photocyclization and photodimerization reactions," *Journal of the Chemical Society, Faraday Transactions 2*, vol. 71, pp. 1529–1544, 1975.

[104] K. Muzkat and S. Sharafi-Ozeri, "Electronic overlap population as measure of reactivity in electrocyclic reactions, stilbenes and analogs," *Chemical Physics Letters*, vol. 20, no. 4, pp. 397 – 400, 1973.

[105] P. R.-G. C. Minot and C. Thal, "Photocyclisation de stilbènes,et de composès indoliques apparentès: Contribution à l'utilisation des indices de réactivitè," *Tetrahedron*, vol. 36, no. 9, pp. 1209–1214, 1980.

CHAPTER 2

Computational Methods

2.1 Introduction

In order to design a model for predicting eliminative cyclisation through plotting reaction coordinate profiles or simple rule-based parameters, a set of molecular properties will have to be calculated. These properties would all be determined computationally since this study is purely theoretical. In this chapter, the various computational chemistry methods that are relevant to understanding the modelling done in this study will be described in the simplest way possible without including any mathematic formulas. This will be followed by a brief description of the different methods that will be used to map out reaction coordinate diagrams. Finally, a summary of the computational details used in this study will be presented.

2.2 Electronic structure methods

Electronic structure is a branch of chemistry that uses computational algorithms to find approximate mathematical solutions for describing the behaviour of electrons in molecules and how electronic energies change as a function of atom positions. [1–5] Electronic structure theories are commonly used in determining molecular energies, electronic charge density distributions, dipoles, reaction-coordinates energy profiles as well as predicting spectroscopic observables such as infrared transition frequencies and nuclear magnetic resonance chemical shifts. [6–23]

All electronic structure models yield approximate solutions to the electronic Schrödinger equation because analytical solutions are only possible for one-electron systems such the hydrogen atom. [3] Therefore, computational quantum chemistry methods are mostly classified based on the approximations that they make in solving this equation. [4]

The main classes of computational quantum chemistry methods are: those based on approximations made onto the form and composition of the wave-function (wave function theories); and those based on computing energy from the density alone (density functional theory).

Wave function-based methods are variational, meaning that the energy obtained from any trial wave function is an upper bound of the exact energy. [24] Density functional-based methods are not variational, but, if parameterised appropriately, can lead to reasonably accurate predictions of relative energies at lower computational cost. [25–29]

2.2.1 Wave function methods: Hartree-Fock theory

The Hartree-Fock method is the simplest wave function based method and forms the foundation for all other wave-function based methods. [30–32] In the Hartree-Fock method, a many-electrons wave-function is expressed as an antisymmetrised product of one electron function, also known as molecular orbitals. [30] This wave function does not allow for the instantaneous interactions between electrons. [33]It instead assumes that each electron in the system feels only a time averaged electrostatic effect created by all the other electrons. [34] For this reason, the Hartree-Fock method is said to employ a mean-field approximation. [35]

In practice, a Hartree-Fock wave-function is represented as a single determinant, which ensures that electrons are indistinguishable and are associated with all other orbitals. This determinantal representation of the Hartree-Fock wave function is commonly known as the Slater determinant. [4] The elements in a Slater determinant are molecular orbitals expressed as a linear combinations of atomic orbital

functions. The coefficients for the atomic orbitals play a central role in determining the energy and electronic properties of systems. [34] In order to obtain the best estimate of the energy of a system, the orbital coefficients are adjusted iteratively until the energy is minimised according to the variational principle. This approach is known as the self-consistent field (SCF) approach since the optimal shape of the orbital relies on the energy and vice versa. [34, 36]

The energies calculated by the Hartree-Fock method are usually about 99% accurate in terms of absolute energy. [37] Unfortunately, the remaining 1%, although seemingly small, is important for describing changes in valence electron density, energies and chemical behaviour. For instance, even for a small molecule like H_2 at its equilibrium geometry, this small fraction of energy is approximately 110kJmole^{-1}, which is of the order of a chemical bond. [35] The unaccounted 1% is known as the correlation energy, and results from the fact that the mean-field approximation neglects the instantaneous interactions between electrons. [4]

Correlation energy can be divided into two main components: dynamic and static correlation. Dynamic correlation is associated with the motion of electrons as they avoid each other and is most important in bond breaking processes. Static correlation results from the use of a single determinant wave function, [38] and is most important for distorted from their equilibrium geometry and for low lying excited states. [4]

2.2.2 Wave function methods: Post Hartree-Fock

Post Hartree-Fock methods are extensions of the Hartree-Fock method that account for the correlation energies by constructing new wave functions that implicitly correct for these energies. These wave functions are constructed from the

single-determinant Hartree-Fock wave function. [4]

A single-determinant wave function from the Hartree-Fock method is made-up of a total of M molecular orbitals that result from the linear combination of M atomic orbitals. After optimisation of the wave function, only the N orbitals with the lowest energies are occupied by electrons. Consequently, this results in a total of M-N unoccupied orbitals often referred to as virtual orbitals. [35] New determinants, also known as configurations, can be constructed by promoting one or more electrons to these unoccupied orbitals. [4]

Post Hartree-Fock wave functions are simply approximate wave functions that are constructed from mixing the new configurations. All existing post Hartree-Fock methods differ only in the manner in which these configurations are constructed and in the manner in which their mixing coefficients are determined.

The simplest post Hartree-Fock method is a configuration interactions method wherein the molecular electronic wave function is expressed as a linear combination of a Hartree-Fock wave function and many other wave functions that are constructed by promoting electrons from ground-state occupied orbitals to unoccupied orbitals. [39–49] Methods in which excited-state determinants are built by promoting one electron at a time to the unoccupied orbital are referred to as configuration interaction singles (CIS). When both single and double electrons are promoted, the method is referred to as configuration interaction singles and doubles (CISD). [48, 49]

2.2.3 Density functional theory

Density functional theory is a class of electronic-structure method that relies on the use of electron density to compute molecular energies and electronic properties. It is based on the Hohenberg-Kohn theorem, which states that the total ground-state energy of a system can be obtained as a functional of its electron density. [50, 51] This means that there is a one-to-one mapping of the energy of a system to its electron density made possible through the density functional.

The electron density is simply the integral over all space of the square of the wave function, which is the same as the electron probability density, whereas a functional is the function of a function. For instance, a function acts on a number to generate another number. In the same way, a functional acts on a function to generate a number. Unfortunately, the exact functional for mapping the electron-density of a system to its total ground-state energy is unknown, so has to be estimated of approximated.

In density functional theory, the total energy of a system can be expressed as a sum of energy functionals for: 1) the electrons kinetic energy, which describes the motion of the electrons in the field of the nuclei; 2) electron-electron repulsion energy; 3) electron-nuclear attraction energy; 4) the exchange energy, which describes motions of electrons with the same spin, and; 5) the correlation energy, which describes the motion of electrons with different spins. Exact functionals exist only for the electron-electron repulsion and the electron-nuclear attraction energies, which have exact classical expressions in terms of electron density. There are no exact functionals for the other three terms. The kinetic energy functional is the most problematic since it makes the largest contribution to the total energy. Consequently, a small relatively error in the kinetic energy leads to a large absolute

error in the total energy. [52]

To determine expressions for the functional form of the electrons kinetic energy, Kohn and Sham derived a set of equations using concepts similar to those of the Hartree-Fock method. In their approach, the electronic kinetic energy is solved for a one-electron system in a manner similar to the Hartree-Fock method except that Kohn-Sham orbitals are used in place of the Hartree-Fock orbitals. [50, 53]

The two remaining terms, the exchange energy and the correlation energy, commonly referred to collectively as the exchange-correlation energy, are the only unknowns with no universal functional form. Existing density functional methods differ in the manner in which these functionals are expressed. [54] Currently, there is a plethora of existing exhange-correlation functionals with more being designed and published on a regular basis [52, 55–60]

2.2.4 Excited-state wave function methods

An electronic excited state is a quantum state of a system that has a higher energy than the ground-state. It can be defined as an electronic state in which one or more electrons have been promoted from a lower energy state to a higher energy state. Excited-states in which the spins of all electrons are paired are referred to as a singlet electronic excited-states, meanwhile those with two unpaired spins are referred to as triplet electronic excited states. [61]

Wave function-based methods for calculating excited-state energies can be divided into single-reference methods or multi-reference methods. In single-reference methods, only the mixing coefficient of the configurations that make up the wave function are optimised when minimising the energy of the wave function. [62] In

multi-reference methods, both the mixing coefficients and the orbitals of the configuration they represent are optimised when minimising the energy. The latter approach corrects for both static and dynamic correlations. [63]

2.2.5 Density functional methods for excited states

The extension of density functional theory to compute excited state energies and properties is known as time-dependent density functional theory (TDDFT). [64–66]

In practice, excited-state energies and their properties are often calculated using the Casida's formulation of TDDFT. [67] A detailed formulation of this approach can be found in the following references. [67–69] In this formulation TDDFT can be classified as 'full' TDDFT or Tamm-Dancoff approximation to TDDFT. [67–69]

The Tamm-Dancoff approximation is conceptually similar to CIS but, with the DFT correction applied to each electronic state before the CI matrix is diagonalised to find ground and excited-state energies and properties. Effectively, it uses the Kohn-Sham orbitals to construct the one-electron densities without optimising these densities. On the other hand, 'full' TDDFT includes extra terms that allow the Kohn-Sham orbitals to be iteratively optimised during excited-state calculation. [70]

2.2.6 Basis sets

Basis sets are mathematical functions used in wave function and density functional-based methods to describe molecular orbitals and densities respectively. [71] They are important because they transform the Hartree-Fock and Kohn-Sham equations into algebraic equations that are suitable for efficient computational implementation. In general, the choice of the basis set determines how close the trial wave

function is to the true wave function of the system. The mathematical functions making up these basis sets are often atomic orbitals, wherein the two most common are the Slater-type orbitals and Gaussian-type orbitals. [72, 73]

Slater-type orbitals are solutions of the Schrödinger equation for the hydrogen-like atoms. They have the property that they form a cusp at the nucleus (i.e. r=0) and decay exponentially at long distances from the nucleus. However, integral calculations using Slater orbitals are computationally difficult to solve. [74–76]

Gaussian orbitals have analytic integrals, which are simpler to solve computationally. However, they do not provide the correct behaviour at long distances from the nucleus because they decay exponentially. [76, 77]

For most practical applications, basis sets are formed by expanding Slater orbitals as a linear combination of Gaussian orbitals. An example of this type of basis set is the STO-3G basis set, in which each Slater orbital is represented as a linear combination of three Gaussian-type orbitals. This basis set is generally referred to as a minimal basis set because each orbital is represented by only one basis function. [78, 79]

Minimal basis sets are not well suited for modelling anisotropic effects, the reason being that, their basis sets exponents do not vary, and as a consequence, the orbitals have a fixed size and do not expand or contract. [78, 79] Basis sets that allow orbital sizes to vary are most often referred to as split-valence basis sets. In these basis sets, each valence orbital is represented by two or more basis functions that have different exponents. An example of a split-valence basis set is 6-31G. in which, each core orbital is represented by one basis function consisting of 6

Gaussian functions. The valence orbitals are each represented by two basis functions, wherein one is composed of 3 Gaussian and the other one is composed of one Gaussian function.

Polarisation functions are higher angular momentum functions that are added to a basis set. They increase the flexibility of a basis set, which enables better description of inter-electronic cusp as well as anisotropic variations that occur during bonding. [80] For instance, an electron on an opposite site of the nucleus may not always be well described by an s-orbital. However, adding a p-function, which has a higher angular momentum, enables a better description of the electron probability. Thus, polarisation functions involve adding some p functions to an s-orbital, a d-function to a p-orbital and an f-function to the d-orbital. An example of a split-valence basis with some polarisation functions is the 6-31G(p,d).

Diffuse functions are used to describe the behaviour of electrons at large distances from the nucleus. They are Gaussian basis functions with a small exponent that increases the flexibility of atomic orbitals, at long distances from the nucleus. [24,80] These functions are denoted by a "+" sign, for instance 6-31+G(p,d).

2.2.7 Solvent model

Solvation can generally be perceived as an interaction between a solute and a solvent that leads to a stabilisation of the mixed system. [81,82] Simply, it corresponds to an energy favourable process of surrounding a solute by solvent molecules.

Electronic structure methods model the properties of molecules as isolated systems in vacuum; but in the real world, molecules are not always isolated. [83] Including a solvation correction accounts for the stabilisation interactions that the

system would have experienced in a solvated medium. [83]

There are two model types used in modelling solvent effects; explicit and implicit. [81, 84] Explicit solvation models take into account the detail interactions between each solvent molecule and the solute molecule. [85] They represent an intuitively realistic picture of solute-solvent interactions, are extremely time consuming and computationally very expensive. [85]

Implicit solvation models account for solute-solvent interactions by presenting the solvent as a uniform polarisable medium with a fixed dielectric constant wherein the solute is placed in a cavity. [86] The energy resulting from this interaction is given as a sum of terms that includes: 1) free energy required to form the solute cavity, which is the work required to create the cavity plus the entropic penalty resulting from the reorganisation of the solvent molecules around the solute; 2) the van der Waals interaction between the solute and the solvent; 3) the electrostatic potential resulting from the polarisation between solute and solvent molecules; and finally 4) the free energy from hydrogen bonding. [87, 88]

There are many existing implicit solvation models that differ from one another based on: the size and shape of the solute cavity considered; the level of solute description; the description of the dielectric medium; the method used in calculating the cavity; and the manner in which charges are distributed. [87] The most common implicit solvation model is the polarisation continuum model often abbreviated as PCM. [88] In this study, the conductor-like polarisation continuum model (CPCM) [87] was used, mostly because it is currently the only implicit solvation model for which analytical gradients and Hessian are available for both the ground and excited-states.

2.3 Characterising the potential energy surface

The potential energy surface is a plot of energy as a function of all internal coordinates of a given molecular system. [89, 90] This is constructed from computing electronic energies at different nuclear configurations. The most important points on the potential energy surface are those in which the gradients of the energy along all internal coordinates equal zero. These points are commonly referred to as stationary points. The nature of these points is confirmed by computing the second derivative of energies with respect to atomic displacements. This information is stored in the Hessian matrix. When the Hessian matrix is diagonalised, the number of negative eigenvalues is referred to as the Hessian index. It corresponds to the number of vibrational modes along which the energy decreases with atomic displacement along the corresponding eigenvectors.

Stationary points in which the Hessian index is zero are known as minima, and they usually involve reactants, intermediates, and products. [91] Meanwhile, points with non-zero Hessian index are known as saddle points. A saddle point with only one Hessian index is known as a first order saddle point. If the coordinates of this saddle correspond to the most critical change that needs to occur for the reaction to proceed, then this point is the transition state for the reaction under consideration. [91]

Reaction minimum energy paths, routinely referred to as reaction coordinate profiles, are plots that connect reactants, transition states, intermediates and products' energies.. [31] In practice, reaction coordinate profiles are computed by determining the individual energies of reactants, products, intermediates, and transition states. [92] The energies of these species are obtained from single point energy cal-

culations on their equilibrium geometric structures, which are mostly obtained from geometry optimisation calculations. [93]

Obtaining transition-states energies are comparatively harder and are hardly obtained from normal geometry optimisation calculations. This is because it is often difficult to locate transition-state structures. [94] In practice, the process of locating transition-state structures generally involve two steps: 1) designing approximate guess transition-state structures; and 2) refining these structures to precisely locate the first-order saddle point using surface-walking techniques, which are often in-built algorithms in quantum mechanical software packages. [95, 96] Of the two steps, the first step is often the more tricky because it involves a high level of chemical intuition and good knowledge of the form of the transition state in order to ease the refinement process. In general, a sufficiently good guess has one Hessian index. [97] In this thesis, two approaches were employed to determine guess transition-state structures for instances where reaction coordinate diagrams were computed. These approaches were the freezing-string method [98] and a method based on computing a series of constrained geometry optimisations.

2.3.1 Geometry optimisation

Geometry optimisation is a general procedure for obtaining the equilibrium geometry of a molecule. [96] For reactant, intermediates and products, this involves obtaining a structure in which the forces on all the atoms are zero.

In practice, a guess structure or an approximate structure of a molecule is built using a molecular builder software. The energy of the guess molecule is minimised by computing the derivatives of the energy for different atom positions. [96] In this process, atoms position are displaced by some computed step that is predicted to

reduce the energy gradient. If the gradient is is equal to zero or below a specified threshold, the process stops; otherwise a new displacement is made. [99] This process is iterative and it repeats until the geometry is converged to the minima structure in which the forces on all atoms are zero. For each cycle in the geometry optimisation, a single point energy calculation is performed to obtain the energies of the wave function or electron density at that nuclear configuration. The end result is an equilibrium structure with associated energy.

2.3.2 Constrained geometry optimisation

A constrained geometry optimisation is one on which one or more coordinates are held fixed meanwhile all other coordinates are free to relax to their equilibrium position. This method was used as one approach for determining guess transition state structures. This was done by performing a series of constrained geometry optimisations, whereby the distance between the bond being formed or broken, depending on the transition state being searched were constrained. For forming bonds, which generally involved the formation of the cyclised intermediate, the distance between the two atoms forming the new bond was constrained and a value of 0.1 Å was subtracted from this distance during each constrained geometry optimisation. For bond breaking, which involved the elimination of a leaving group, the distance between the bond being broken were increased by 0.1 Å in each constrained geometry optimisation. Finally, the coordinates of the constrained structure with the largest energy was selected as the guess transition-state structure.

This approach is manual but guarantees that the guess transition state structure found is the structure closest to the first-order saddle point for the reaction path being considered.

2.3.3 Freezing-string method

The freezing-string method is an automated method for determining guess transition state structures. In this method, the reactant and the product coordinates are interpolated inwardly towards the transition state. Each node created from each interpolation is partially optimised orthogonally to the reaction path, and then frozen before the next node is interpolated. [98] At the end of the interpolation, an output is printed out with coordinates of all the nodes generated along the reaction path with their associated energies. The node with the highest energy was used as the guess transition state structure.

2.4 Computational details

In this thesis, all ground state geometries and energies were calculated using density functional theory (DFT) incorporating the Becke-3-Lee-Yang-Parr (B3LYP) functional, [100–102]. DFT is a method of choice that offers a favourable compromise between accuracy and computational cost. [103, 104] The B3LYP functional was selected because it is well parametrised for calculating geometries and energies of organic molecules and also because it is one of the few functionals for which ground and excited-state analytical gradients and Hessians are available. [105, 106] All singlet electronic excited-states gradients, geometries and energies were calculated using the TDDFT and also using B3LYP functional. All ground and excited-state properties were computed using the 6-31G(d,p) basis set because it is the basis set that was used in parameterising the B3LYP functional and so it affords near-optimal error cancellation between basis set superposition errors (BSSE) and dispersion contributions to the energy. [107] Finally, solvation corrections to the free energy were computed using the conductor-like polarisation continuum model (C-PCM) [87, 88] with a dielectric constant of either 8.93 or 32.6 chosen to resem-

ble dichloromethane and methanol, respectively. All calculations were performed using Q-chem 4.4. [108]

Bibliography

[1] R. J. Boyd, "Theoretical and computational chemistry," in *Reference Module in Chemistry, Molecular Sciences and Chemical Engineering*, Elsevier, 2019.

[2] M. Hofmann and H. F. Schaefer, "Computational chemistry," in *Encyclopedia of Physical Science and Technology (Third Edition)* (R. A. Meyers, ed.), pp. 487 – 506, New York: Academic Press, third edition ed., 2003.

[3] V. A. Rassolov and S. Garashchuk, "Computational complexity in quantum chemistry," *Chemical Physics Letters*, vol. 464, no. 4, pp. 262 – 264, 2008.

[4] E. Lewars, "Chapter 7 - personal computers in computational chemistry," in *Mathematical Physics in Theoretical Chemistry* (S. Blinder and J. House, eds.), Developments in Physical and Theoretical Chemistry, pp. 219 – 260, Elsevier, 2019.

[5] K. Roy, S. Kar, and R. N. Das, "Chapter 5 - computational chemistry," in *Understanding the Basics of QSAR for Applications in Pharmaceutical*

Sciences and Risk Assessment (K. Roy, S. Kar, and R. N. Das, eds.), pp. 151 – 189, Boston: Academic Press, 2015.

[6] L. Serrano and Manuela, "Quantum chemistry of the excited state: 2005 overview," *Journal of Molecular Structure: THEOCHEM*, vol. 729, no. 1, pp. 99 – 108, 2005.

[7] M. S. Kodikara, R. Stranger, and M. G. Humphrey, "Computational studies of the nonlinear optical properties of organometallic complexes," *Coordination Chemistry Reviews*, vol. 375, pp. 389 – 409, 2018.

[8] D. L. Monego, M. B. da Rosa, and P. do Nascimento, "Applications of computational chemistry to the study of the antiradical activity of carotenoids: A review," *Food Chemistry*, vol. 217, pp. 37 – 44, 2017.

[9] T. Cowen, K. Karim, and S. Piletsky, "Computational approaches in the design of synthetic receptors A review," *Analytica Chimica Acta*, vol. 936, pp. 62 – 74, 2016.

[10] L. Mammino, "Incorporating information on green chemistry into theoretical chemistry courses," *Current Opinion in Green and Sustainable Chemistry*, vol. 13, pp. 76 – 80, 2018.

[11] F.-X. Coudert and A. H. Fuchs, "Computational characterization and prediction of metal-organic framework properties," *Coordination Chemistry Reviews*, vol. 307, pp. 211 – 236, 2016.

[12] M. M. Bounab, K. djameleddine, H. Stephane, Rayenne, M. Fatiha, and N. Leila, "Molecular dynamics and quantum mechanics study of the [2-oxo-n-phenyl-3-oxazolidinesulfonamidecyclodextrin] complex," *Journal of Molecular Liquids*, vol. 222, pp. 777 – 782, 2016.

[13] O. Engkvist, P.-O. Norrby, N. Selmi, Y. hong Lam, Z. Peng, E. C. Sherer, W. Amberg, T. Erhard, and L. A. Smyth, "Computational prediction of chemical reactions: current status and outlook," *Drug Discovery Today*, vol. 23, no. 6, pp. 1203 – 1218, 2018.

[14] J. Sellier, M. Nedjalkov, and I. Dimov, "An introduction to applied quantum mechanics in the wigner monte carlo formalism," *Physics Reports*, vol. 577, pp. 1 – 34, 2015.

[15] "Computational modeling for formulation design," *Drug Discovery Today*, vol. 24, no. 3, pp. 781 – 788, 2019.

[16] J. Desclaux, J. Dolbeault, M. Esteban, and P. Indelicato, "Computational approaches of relativistic models in quantum chemistry," in *Special Volume, Computational Chemistry*, vol. 10 of *Handbook of Numerical Analysis*, pp. 453 – 483, Elsevier, 2003.

[17] "Chapter 21 - computational quantum chemistry: A new approach to atmospheric nucleation," in *Applications of Theoretical Methods to Atmospheric Science* (M. E. Goodsite and M. S. Johnson, eds.), vol. 55 of *Advances in Quantum Chemistry*, pp. 449 – 478, Academic Press, 2008.

[18] C. Sherrill, "Chapter 4 bond breaking in quantum chemistry," vol. 1 of *Annual Reports in Computational Chemistry*, pp. 45 – 56, Elsevier, 2005.

[19] Eric, M. Defranceschi, W. Kutzelnigg, C. L. Bris, and Y. Maday, "Computational quantum chemistry: A primer," in *Special Volume, Computational Chemistry*, vol. 10 of *Handbook of Numerical Analysis*, pp. 3 – 270, Elsevier, 2003.

[20] A. J. Fry, "Computational applications in organic electrochemistry," *Current Opinion in Electrochemistry*, vol. 2, no. 1, pp. 67 – 75, 2017.

[21] M. R. Blomberg and P. E. Siegbahn, "Quantum chemistry as a tool in bioenergetics," *Biochimica et Biophysica Acta (BBA) - Bioenergetics*, vol. 1797, no. 2, pp. 129 – 142, 2010.

[22] P. G. D. Benedetti and F. Fanelli, "Computational modeling approaches to quantitative structure-binding kinetics relationships in drug discovery," *Drug Discovery Today*, vol. 23, no. 7, pp. 1396 – 1406, 2018.

[23] K. Doitomi and H. Hirao, "Hybrid computational approaches for deriving quantum mechanical insights into metal-orrganic frameworks," *Tetrahedron Letters*, vol. 58, no. 24, pp. 2309 – 2317, 2017.

[24] W. Richards, "Chapter 11 - wave functions and orbitals," in *Quantum Pharmacology (Second Edition)* (W. Richards, ed.), pp. 117 – 129, Butterworth-Heinemann, second edition ed., 1983.

[25] K. R. Brorsen, Y. Yang, M. V. Pak, and S. Hammes-Schiffer, "Is the accuracy of density functional theory for atomization energies and densities in bonding regions correlated?," *The Journal of Physical Chemistry Letters*, vol. 8, no. 9, pp. 2076–2081, 2017.

[26] S. McKechnie, G. H. Booth, A. J. Cohen, and J. M. Cole, "On the accuracy of density functional theory and wave function methods for calculating vertical ionization energies," *The Journal of Chemical Physics*, vol. 142, no. 19, p. 194114, 2015.

[27] J. C. Howard, J. D. Enyard, and G. S. Tschumper, "Assessing the accuracy of some popular dft methods for computing harmonic vibrational frequencies of water clusters," *The Journal of Chemical Physics*, vol. 143, no. 21, p. 214103, 2015.

[28] I. Konstantinov, S. Ewart, H. Brown, C. Eddy, J. Mendenhall, and S. Munjal, "Accurate density functional theory (dft) protocol for screening and designing chain transfer and branching agents for ldpe systems," *Molecular Systems Design and Engineering*, vol. 3, pp. 228–242, 2018.

[29] N. Mardirossian and M. Head-Gordon, "Thirty years of density functional theory in computational chemistry: An overview and extensive assessment of 200 density functionals," *Molecular Physics*, vol. 115, no. 19, pp. 2315–2372, 2017.

[30] J. C. Morrison, "Chapter 5 - many-electron atoms," in *Modern Physics (Second Edition)* (J. C. Morrison, ed.), pp. 95 – 115, Boston: Academic Press, second edition ed., 2015.

[31] D.-T. Tuan, "The geometric approximation of physical properties," *Chemical Physics Letters*, vol. 7, no. 1, pp. 115 – 120, 1970.

[32] S. Blinder, "Chapter 1 - introduction to the hartree-fock method," in *Mathematical Physics in Theoretical Chemistry* (S. Blinder and J. House, eds.), Developments in Physical and Theoretical Chemistry, pp. 1 – 30, Elsevier, 2019.

[33] V. Magnasco, "7 - many-electron wavefunctions: Slater, hartree-fock and related methods," in *Elementary Methods of Molecular Quantum Mechanics* (V. Magnasco, ed.), pp. 255 – 361, Amsterdam: Elsevier Science B.V., 2007.

[34] A. Szabo and N. S. Ostlund, *Modern Quantum Chemistry: Introduction to Advanced Electronic Structure Theory*. New York, USA: Dover Publications, 1996.

[35] D. W. Rogers, *Computational Chemistry Using the PC*. Hoboken, New Jersey: John Wiley and Sons, 2003.

[36] V. Gupta, "3 - self-consistent field molecular orbital theory," in *Principles and Applications of Quantum Chemistry* (V. Gupta, ed.), pp. 63 – 125, Boston: Academic Press, 2016.

[37] N. F. Johnson and M. Reina, "The accuracy of the hartree-fock approximation for quantum dots," *Journal of Physics: Condensed Matter*, vol. 4, no. 47, pp. L623–L628, 1992.

[38] L. Piela, "Chapter 10 - correlation of the electronic motions," in *Ideas of Quantum Chemistry (Second Edition)* (L. Piela, ed.), pp. 577 – 662, Oxford: Elsevier, second edition ed., 2014.

[39] M. B. Ruiz and R. Tróger, "Chapter twelve - configuration interaction study of the 3P ground state of the carbon atom," in *Novel Electronic Structure Theory: General Innovations and Strongly Correlated Systems* (P. E. Hoggan, ed.), vol. 76 of *Advances in Quantum Chemistry*, pp. 223 – 238, Academic Press, 2018.

[40] C. F. Bunge, "Chapter one - present status of selected configuration interaction with truncation energy error," in *Novel Electronic Structure Theory: General Innovations and Strongly Correlated Systems* (P. E. Hoggan, ed.), vol. 76 of *Advances in Quantum Chemistry*, pp. 3 – 34, Academic Press, 2018.

[41] L. G. Jiao, L. R. Zan, L. Zhu, and Y. K. Ho, "Full configuration-interaction calculations of the angular quantities for helium atom," *Computational and Theoretical Chemistry*, vol. 1135, pp. 1 – 5, 2018.

[42] E. Sun, T. Ren, S. Shan, Q. Liu, H. Xu, and B. Yan, "Multireference configuration interaction study of dichlorocarbene," *Chemical Physics*, vol. 459, pp. 54 – 58, 2015.

[43] D. C. Allan and J. Phillips, "Configuration interaction of hydropathic waves enables ubiquitin functionality," *Physica A: Statistical Mechanics and its Applications*, vol. 491, pp. 377 – 381, 2018.

[44] S. Zhao, J. Cui, R. Li, and B. Yan, "Configuration interaction study of electronic structures of CdCl including spin-orbit coupling," *Chemical Physics Letters*, vol. 677, pp. 92 – 98, 2017.

[45] W. Sotoyama, H. Sato, A. Matsuura, and N. Sawatari, "Ab initio configuration interaction singles (CIS) study on polycyclic aromatic molecules (II): Predicting fluorescence quantum yields by calculating the excitation energies," *Journal of Molecular Structure: THEOCHEM*, vol. 756, no. 1, pp. 35 – 38, 2005.

[46] M. Erturk and L. Meissner, "Chapter seven - size-extensivity corrections in single- and multireference configuration interaction calculations," in *Electron Correlation in Molecules ab initio Beyond Gaussian Quantum Chemistry* (P. E. Hoggan and T. Ozdogan, eds.), vol. 73 of *Advances in Quantum Chemistry*, pp. 145 – 160, Academic Press, 2016.

[47] L. Meissner, "A posteriori corrections to the configuration interaction method with singles and doubles," *Chemical Physics Letters*, vol. 263, no. 3, pp. 351 – 359, 1996.

[48] W. Sotoyama, H. Sato, A. Matsuura, and N. Sawatari, "Ab initio configuration interaction singles (CIS) study on polycyclic aromatic molecules (I): Correlation between calculated and observed excitation energies," *Journal of Molecular Structure: THEOCHEM*, vol. 759, no. 1, pp. 165 – 169, 2006.

[49] J.-L. Heully and J.-P. Malrieu, "Four self-consistent dressing to achieve size-consistency of singles and doubles configuration interaction," *Chemical Physics Letters*, vol. 199, no. 6, pp. 545 – 550, 1992.

[50] H. S. Yu, S. L. Li, and D. G. Truhlar, "Perspective: Kohn-sham density functional theory descending a staircase," *The Journal of Chemical Physics*, vol. 145, no. 13, p. 130901, 2016.

[51] "Chapter 4 - density functional theory," in *Mathematical Physics in Theoretical Chemistry* (S. Blinder and J. House, eds.), Developments in Physical and Theoretical Chemistry, pp. 119 – 159, Elsevier, 2019.

[52] F. Jensen, *Introduction to Computational Chemistry*. USA: John Wiley & Sons, Inc., 2006.

[53] R. Stowasser and R. Hoffmann, "What do the kohn-sham orbitals and eigenvalues mean?," *Journal of the American Chemical Society*, vol. 121, no. 14, pp. 3414–3420, 1999.

[54] M. Hanas and M. Makowski, "Assessing accuracy of exchange-correlation functionals for singlet-triplet excitations," *Computational and Theoretical Chemistry*, vol. 1060, pp. 52 – 57, 2015.

[55] D. Bagayoko, "Understanding density functional theory (dft) and completing it in practice," *AIP Advances*, vol. 4, no. 12, p. 127104, 2014.

[56] C. Ochsenfeld, "Linear scaling exchange gradients for hartre-fock and hybrid density functional theory," *Chemical Physics Letters*, vol. 327, no. 3, pp. 216 – 223, 2000.

[57] E. Bene and A. Nagy, "The correlation energy in terms of density moments along the adiabatic connection in the density functional theory," *Chemical Physics Letters*, vol. 324, no. 5, pp. 475 – 481, 2000.

[58] J. Mulak and Z. Gajek, "Chapter 16 - density functional theory approach," in *The Effective Crystal Field Potential* (J. Mulak and Z. Gajek, eds.), pp. 185 – 209, Oxford: Elsevier Science Ltd, 2000.

[59] G. Faussurier, "Density-functional theory and average-atom model formulated in terms of functional integrals," *Journal of Quantitative Spectroscopy and Radiative Transfer*, vol. 65, no. 1, pp. 207 – 222, 2000.

[60] D. Kashchiev, "Chapter 8-density-functional approach," in *Nucleation* (D. Kashchiev, ed.), pp. 97 – 112, Oxford: Butterworth-Heinemann, 2000.

[61] S. Perun, T. Jörg, and C. M. Marian, "Singlet and triplet excited states and intersystem crossing in free-base porphyrin: Tddft and dft/mrci study," *ChemPhysChem*, vol. 9, no. 2, pp. 282–292, 2008.

[62] C. M. Isborn, N. Luehr, I. S. Ufimtsev, and T. J. Matinez, "Excited-state electronic structure with configuration interaction singles and tamm-dancoff time-dependent density functional theory on graphical processing units," *Journal of Chemical Theory and Computation*, vol. 7, no. 6, pp. 1814–1823, 2011.

[63] J. Wang, S. Manivasagam, and A. K. Wilson, "Multireference character for 4d transition metal-containing molecules," *Journal of Chemical Theory and Computation*, vol. 11, no. 12, pp. 5865–5872, 2015.

[64] E. Runge and E. K. U. Gross, "Density-functional theory for time-dependent systems," *Physical Review Letters*, vol. 52, pp. 997–1000, 1984.

[65] D. P. Chong, *Recent Advances in Density Functional Methods*. WORLD SCIENTIFIC, 1995.

[66] S. Hirata, M. Head-Gordon, and R. J. Bartlett, "Configuration interaction singles, time-dependent hartree,Äìfock, and time-dependent density functional theory for the electronic excited states of extended systems," *The Journal of Chemical Physics*, vol. 111, no. 24, pp. 10774–10786, 1999.

[67] M. E. Casida, C. Jamorski, K. C. Casida, and D. R. Salahub, "Molecular excitation energies to high-lying bound states from time-dependent density-functional-response theory: Characterization and correction of the time-dependent-local-density-approximation ionization threshold," *The Journal of Chemical Physics*, vol. 108, no. 11, pp. 4439–4449, 1998.

[68] D. J. Tozer and N. C. Handy, "Improving virtual kohn-sham orbitals and eigenvalues: Application to excitation energies and static polarizabilities," *The Journal of Chemical Physics*, vol. 109, no. 23, pp. 10180–10189, 1998.

[69] J. Liu and J. M. Herbert, "An efficient and accurate approximation to time-dependent density functional theory for systems of weakly coupled monomers," *The Journal of Chemical Physics*, vol. 143, no. 3, p. 034106, 2015.

[70] C. Walter, V. Kramer, and B. Engels, "On the applicability of time-dependent density functional theory (tddft) and semiempirical methods to the computation of excited-state potential energy surfaces of perylene-based dye-aggregates," *International Journal of Quantum Chemistry*, vol. 117, no. 6, p. e25337, 2017.

[71] D. COOK, "4 - atomic orbitals," in *Ab Initio Valence Calculations in Chemistry* (D. COOK, ed.), pp. 39 – 53, Butterworth-Heinemann, 1974.

[72] V. Magnasco, "Chapter 12 - atomic orbitals," in *Elementary Molecular Quantum Mechanics (Second Edition)* (V. Magnasco, ed.), pp. 467 – 481, Oxford: Elsevier, second edition ed., 2013.

[73] I. S. Ulusoy and A. K. Wilson, "Chapter 2 - slater and gaussian basis functions and computation of molecular integrals," in *Mathematical Physics in Theoretical Chemistry* (S. Blinder and J. House, eds.), Developments in Physical and Theoretical Chemistry, pp. 31 – 61, Elsevier, 2019.

[74] J. Yasui, "Chapter eight - introducing a polynomial expression of molecular integrals for algebraic the molecular orbital (MO) equation," in *Electron Correlation in Molecules ab initio Beyond Gaussian Quantum Chemistry* (P. E. Hoggan and T. Ozdogan, eds.), vol. 73 of *Advances in Quantum Chemistry*, pp. 161 – 172, Academic Press, 2016.

[75] N. MARCH, "Chapter 7 - electron exchange and slater determinants," in *Self-Consistent Fields in Atoms* (N. MARCH, ed.), pp. 89 – 100, Pergamon, 1975.

[76] J. E. Avery and J. S. Avery, "Chapter seven - 4-center sto interelectron repulsion integrals with coulomb sturmians," in *Novel Electronic Structure Theory: General Innovations and Strongly Correlated Systems* (P. E. Hoggan, ed.), vol. 76 of *Advances in Quantum Chemistry*, pp. 133 – 146, Academic Press, 2018.

[77] V. Magnasco, "Chapter 18 - evaluation of molecular integrals," in *Elementary Molecular Quantum Mechanics (Second Edition)* (V. Magnasco, ed.), pp. 789 – 830, Oxford: Elsevier, second edition ed., 2013.

[78] J.E., O. Taurian, A. Bouferguene, and P. Hoggan, "Chapter 4 - on a transformation for the electrostatic potential, generated by the product of two 1s

slater type orbitals, giving an efficient expression," in *Proceedings of MEST 2012: Exponential Type Orbitals for Molecular Electronic Structure Theory* (P. E. Hoggan, ed.), vol. 67 of *Advances in Quantum Chemistry*, pp. 65 – 71, Academic Press, 2013.

[79] D. COOK, "5 - the molecular orbital and valence bond methods," in *Ab Initio Valence Calculations in Chemistry* (D. COOK, ed.), pp. 54 – 74, Butterworth-Heinemann, 1974.

[80] C. M. Quinn, "1 - essential atomic orbital theory," in *Computational Quantum Chemistry* (C. M. Quinn, ed.), pp. 1 – 56, London: Academic Press, 2002.

[81] D. M. Chipman, "Reaction field treatment of charge penetration," *The Journal of Chemical Physics*, vol. 112, no. 13, pp. 5558–5565, 2000.

[82] E. Cances and B. Mennucci, "The escaped charge problem in solvation continuum models," *The Journal of Chemical Physics*, vol. 115, no. 13, pp. 6130–6135, 2001.

[83] J. Tomasi, B. Mennucci, and R. Cammi, "Quantum mechanical continuum solvation models," *Chemical Reviews*, vol. 105, no. 8, pp. 2999–3094, 2005.

[84] J. Zhang, H. Zhang, T. Wu, Q. Wang, and D. van der Spoel, "Comparison of implicit and explicit solvent models for the calculation of solvation free energy in organic solvents," *Journal of Chemical Theory and Computation*, vol. 13, no. 3, pp. 1034–1043, 2017.

[85] C. J. Fennell, C. W. Kehoe, and K. A. Dill, "Modeling aqueous solvation with semi-explicit assembly," *Proceedings of the National Academy of Sciences*, vol. 108, no. 8, pp. 3234–3239, 2011.

[86] S. Bandaru, N. J. English, and J. M. D. MacElroy, "Implicit and explicit solvent models for modeling a bifunctional arene ruthenium hydrogen-storage catalyst: A classical and ab initio molecular simulation study," *Journal of Computational Chemistry*, vol. 35, no. 9, pp. 683–691, 2014.

[87] T. N. Truong and E. V. Stefanovich, "A new method for incorporating solvent effect into the classical, ab initio molecular orbital and density functional theory frameworks for arbitrary shape cavity," *Chemical Physics Letters*, vol. 240, no. 4, pp. 253 – 260, 1995.

[88] V. Barone and M. Cossi, "Quantum calculation of molecular energies and energy gradients in solution by a conductor solvent model," *The Journal of Physical Chemistry A*, vol. 102, no. 11, pp. 1995–2001, 1998.

[89] S. Sato, "A new method of drawing the potential energy surface," *Bulletin of the Chemical Society of Japan*, vol. 28, no. 7, pp. 450–453, 1955.

[90] K. Fukui, "Formulation of the reaction coordinate," *The Journal of Physical Chemistry*, vol. 74, no. 23, pp. 4161–4163, 1970.

[91] R. G. Bone, C. W. Murray, R. D. Amos, and N. C. Handy, "Stationary points on the potential energy surface of (C2H2)3," *Chemical Physics Letters*, vol. 161, no. 2, pp. 166 – 174, 1989.

[92] T. Taketsugu and M. S. Gordon, "Dynamic reaction path analysis based on an intrinsic reaction coordinate," *The Journal of Chemical Physics*, vol. 103, no. 23, pp. 10042–10049, 1995.

[93] C. F. Jackels, Z. Gu, and D. G. Truhlar, "Reaction-path potential and vibrational frequencies in terms of curvilinear internal coordinates," *The Journal of Chemical Physics*, vol. 102, no. 8, pp. 3188–3201, 1995.

[94] S. Mallikarjun Sharada, P. M. Zimmerman, A. T. Bell, and M. Head-Gordon, "Automated transition state searches without evaluating the hessian," *Journal of Chemical Theory and Computation*, vol. 8, no. 12, pp. 5166–5174, 2012.

[95] H. B. Schlegel, "Exploring potential energy surfaces for chemical reactions: An overview of some practical methods," *Journal of Computational Chemistry*, vol. 24, no. 12, pp. 1514–1527, 2003.

[96] J. Baker, "An algorithm for the location of transition states," *Journal of Computational Chemistry*, vol. 7, no. 4, pp. 385–395, 1986.

[97] P. J. Berti and V. L. Schramm, "Transition state structure of the solvolytic hydrolysis of nad," *Journal of the American Chemical Society*, vol. 119, no. 50, pp. 12069–12078, 1997.

[98] A. Behn, P. M. Zimmerman, A. T. Bell, and M. Head-Gordon, "Efficient exploration of reaction paths via a freezing string method," *The Journal of Chemical Physics*, vol. 135, no. 22, p. 224108, 2011.

[99] H. B. Schlegel, "Geometry optimization," *Wiley Interdisciplinary Reviews: Computational Molecular Science*, vol. 1, no. 5, pp. 790–809, 2011.

[100] A. D. Becke, "Density functional thermochemistry. III. The role of exact exchange," *The Journal of Chemical Physics*, vol. 98, no. 7, pp. 5648–5652, 1993.

[101] C. Lee, W. Yang, and R. G. Parr, "Development of the Colle-Salvetti correlation-energy formula into a functional of the electron density," *Physical Review B*, vol. 37, pp. 785–789, 1988.

[102] P. J. Stephens, F. J. Devlin, C. F. Chabalowski, and M. J. Frisch, "Ab initio calculation of vibrational absorption and circular dichroism spectra using density functional force fields," *The Journal of Physical Chemistry*, vol. 98, no. 45, pp. 11623–11627, 1994.

[103] P. H.-Y. Cheong, C. Y. Legault, J. M. Um, N. Celebi-Olcum, and K. N. Houk, "Quantum mechanical investigations of organocatalysis: Mechanisms, reactivities, and selectivities," *Chemical Reviews*, vol. 111, no. 8, pp. 5042–5137, 2011.

[104] T. Sperger, I. A. Sanhueza, and F. Schoenebeck, "Computation and experiment: A powerful combination to understand and predict reactivities," *Accounts of Chemical Research*, vol. 49, no. 6, pp. 1311–1319, 2016.

[105] D. Chen, J. Liu, H. Ma, Q. Zeng, and W. Liang, "Analytical derivative techniques for tddft excited-state properties: Theory and application," *Science China Chemistry*, vol. 57, no. 1, pp. 48–57, 2014.

[106] Q. Zeng and W. Liang, "Analytic energy gradient of excited electronic state within TDDFT/MMpol framework: Benchmark tests and parallel implementation," *The Journal of Chemical Physics*, vol. 143, no. 13, p. 134104, 2015.

[107] J. Tirado-Rives and W. L. Jorgensen, "Performance of b3lyp density functional methods for a large set of organic molecules," *Journal of Chemical Theory and Computation*, vol. 4, no. 2, pp. 297–306, 2008.

[108] Y. Shao, Z. Gan, E. Epifanovsky, A. T. B. Gilbert, M. Wormit, J. Kussmann, A. W. Lange, A. Behn, J. Deng, X. Feng, D. Ghosh, M. Goldey, P. R. Horn, L. D. Jacobson, I. Kaliman, R. Z. Khaliullin, T. Kús, A. Landau, J. Liu, E. I. Proynov, Y. M. Rhee, R. M. Richard, M. A. Rohrdanz, R. P. Steele, E. J.

Sundstrom, H. L. Woodcock III, P. M. Zimmerman, D. Zuev, B. Albrecht, E. Alguire, B. Austin, G. J. O. Beran, Y. A. Bernard, E. Berquist, K. Brandhorst, K. B. Bravaya, S. T. Brown, D. Casanova, C.-M. Chang, Y. Chen, S. H. Chien, K. D. Closser, D. L. Crittenden, M. Diedenhofen, R. A. DiStasio Jr., H. Dop, A. D. Dutoi, R. G. Edgar, S. Fatehi, L. Fusti-Molnar, A. Ghysels, A. Golubeva-Zadorozhnaya, J. Gomes, M. W. D. Hanson-Heine, P. H. P. Harbach, A. W. Hauser, E. G. Hohenstein, Z. C. Holden, T.-C. Jagau, H. Ji, B. Kaduk, K. Khistyaev, J. Kim, J. Kim, R. A. King, P. Klunzinger, D. Kosenkov, T. Kowalczyk, C. M. Krauter, K. U. Lao, A. Laurent, K. V. Lawler, S. V. Levchenko, C. Y. Lin, F. Liu, E. Livshits, R. C. Lochan, A. Luenser, P. Manohar, S. F. Manzer, S.-P. Mao, N. Mardirossian, A. V. Marenich, S. A. Maurer, N. J. Mayhall, C. M. Oana, R. Olivares-Amaya, D. P. O'Neill, J. A. Parkhill, T. M. Perrine, R. Peverati, P. A. Pieniazek, A. Prociuk, D. R. Rehn, E. Rosta, N. J. Russ, N. Sergueev, S. M. Sharada, S. Sharmaa, D. W. Small, A. Sodt, T. Stein, D. Stück, Y.-C. Su, A. J. W. Thom, T. Tsuchimochi, L. Vogt, O. Vydrov, T. Wang, M. A. Watson, J. Wenzel, A. White, C. F. Williams, V. Vanovschi, S. Yeganeh, S. R. Yost, Z.-Q. You, I. Y. Zhang, X. Zhang, Y. Zhou, B. R. Brooks, G. K. L. Chan, D. M. Chipman, C. J. Cramer, W. A. Goddard III, M. S. Gordon, W. J. Hehre, A. Klamt, H. F. Schaefer III, M. W. Schmidt, C. D. Sherrill, D. G. Truhlar, A. Warshel, X. Xua, A. Aspuru-Guzik, R. Baer, A. T. Bell, N. A. Besley, J.-D. Chai, A. Dreuw, B. D. Dunietz, T. R. Furlani, S. R. Gwaltney, C.-P. Hsu, Y. Jung, J. Kong, D. S. Lambrecht, W. Liang, C. Ochsenfeld, V. A. Rassolov, L. V. Slipchenko, J. E. Subotnik, T. Van Voorhis, J. M. Herbert, A. I. Krylov, P. M. W. Gill, and M. Head-Gordon, "Advances in molecular quantum chemistry contained in the q-chem 4 program package," *Mol. Phys.*, vol. 113, pp. 184–215, 2015.

CHAPTER 3

Effect of Position and Nature of Heteroatom in Eliminative Cyclisation

3.1 Introduction

It has long been recognised that the most powerful insights into the nature of the physical world come when theory and experiment are unified:

"Experiment without theory is blind, but theory without experiment is mere intellectual play" – Immanuel Kant (1724-1804)

With a particular focus on directly connecting theory and experiment, this work seeks to elucidate and understand the factors that control reactivity in a synthetically important class of aromatic-ring forming reactions; those that involve both intramolecular cyclisation and elimination processes. [1]

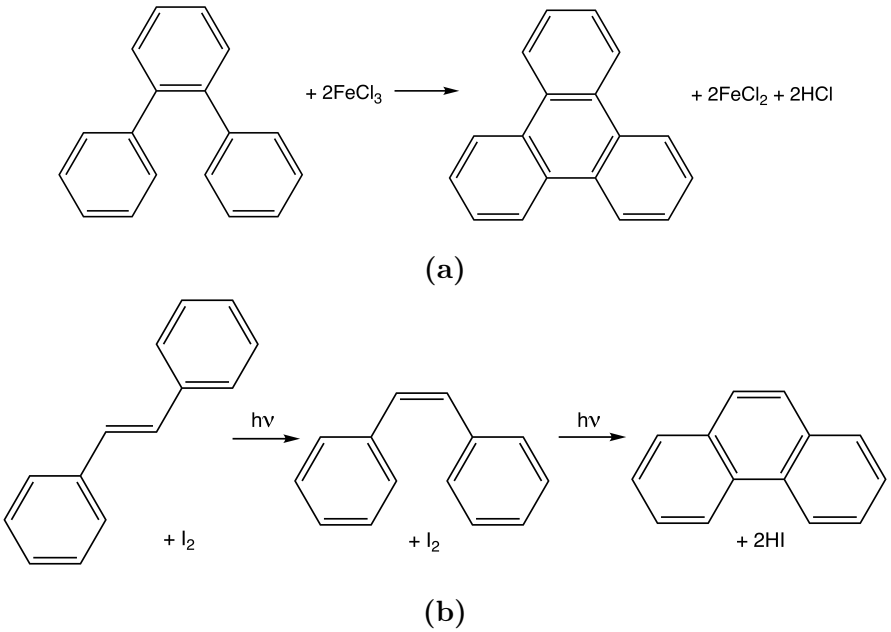

Fig. 3.1 Balanced equations for prototypical (a) thermal [Scholl] and (b) photochemical [Mallory] oxidative cyclodehydrogenation reactions

For example, the Scholl reaction [2–5] (Fig. 3.1(a)) is a thermal oxidative cyclodehydrogenation process that is used in the synthesis of atomically-precise nanomaterials with useful electronic properties such as polythiophene semiconducting polymers, [6,7] polypyrrole conducting polymers [8,9] and very large polyaromatic hydrocarbons that are often referred to as nano-graphenes. [1,10,11]

Mallory reactions, [12–17] on the other hand, are photo-activated cyclisation processes whose elimination step may be either oxidative (Fig. 3.1(b)) or purely eliminative. They may be used to access a wider range of products from a wider range of readily accessible starting materials than the Scholl reaction. In particular, they do not need to be pre-aligned for ring formation, but can form the unconnected ring structure via trans-cis isomerisation and/or bond rotation. The cyclising centres may be heteroatoms and/or may have non-hydrogenic leaving groups attached. Mallory reactions are also more tolerant to functional group substitution than Scholl reactions. However, the photoexcitation process can be reversible, or lead to alternative photoproducts, which can result in lower yields. [18–20]

The most likely proposed mechanisms for the Scholl [1,21–23] and Mallory [18, 20,24] reactions are illustrated in Fig. 3.2 and Fig. 3.3, and key similarities and differences between them are summarised in Table 3.1.

Table 3.1 Key steps in Mallory and Scholl cyclisation processes, highlighting the similarities and differences between them.

	Mallory	Scholl
Mechanism	Photoexcite ↓ Cyclise ↓ Oxidise and dehydrogenate/ Eliminate	Oxidise ↓ Cyclise ↓ Dehydrogenate with further oxidation

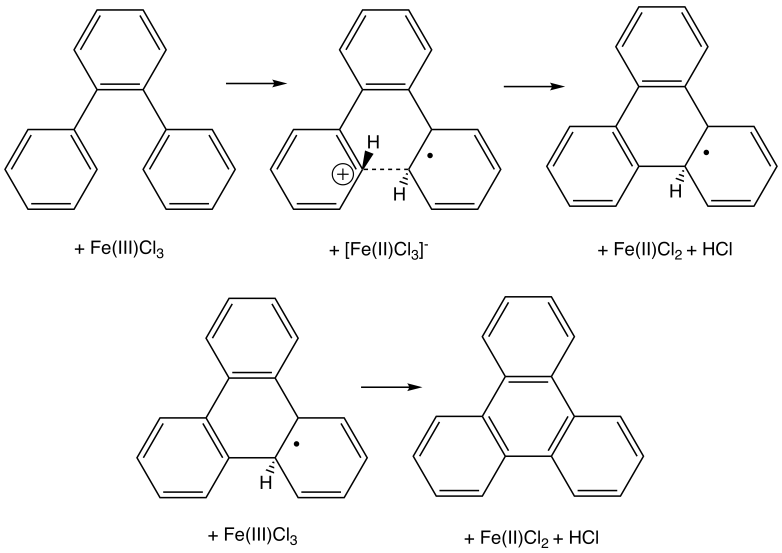

Fig. 3.2 Thermal cyclisation (Scholl reaction) proceeds via oxidative photocyclisation and elimination (top), followed by a second oxidative elimination step (bottom)

For Scholl reactions and oxidative Mallory reactions, cyclisation is initiated by

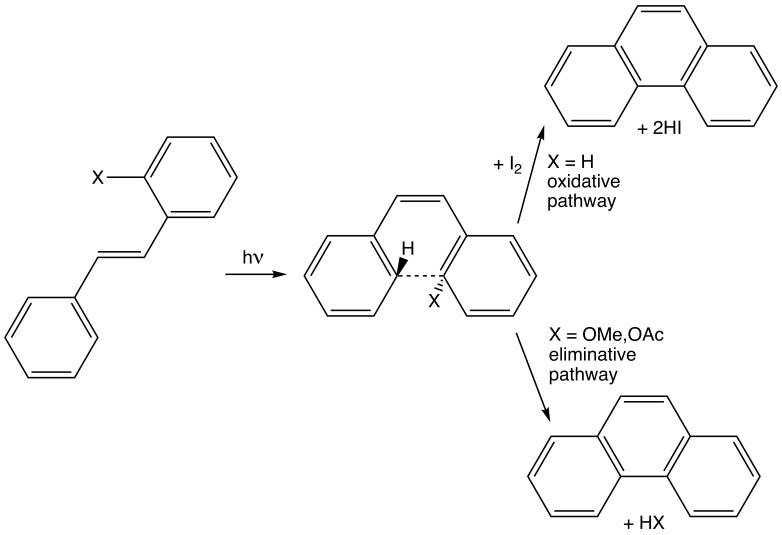

Fig. 3.3 Mallory reaction mechanism: trans-cis isomerisation and cyclisation occur in first step, followed by either oxidative dehydrogenation (if oxidant present) or elimination (if reactant contains appropriately positioned leaving group)

moving electrons either electrochemically to another molecule, or photochemically to another electronic state, and the dehydrogenation step is electrochemically driven. However, redox coupling is not required for the Mallory process to proceed through the purely eliminative pathway.

Although the general mechanisms illustrated in Fig. 3.2 and Fig. 3.3 are reasonably well-supported by experimental and computational evidence, [1,18,20–24] they fall well short of providing the level of detail that is useful for synthetic chemists; given a reactant and set of reaction conditions, will a product form? Which set of reaction conditions should be tried first, if multiple reaction pathways are possible?

The Woodward-Hoffmann rules [25–27], provide a simple, general and powerful model to answer questions of this nature for electrocyclisation reactions, which are a much simpler class of cyclisation reaction that are atom-economical and in-

volve only concerted electron-transfer processes. The Woodward-Hoffmann rules were later generalised by Baldwin to describe a wider range of electrocyclisation reactions involving heteroatoms and unusual ring features, [28, 29] and map onto modern quantum chemical calculations through conceptual DFT [30]. However, all of these approaches lack information about the dehydrogenation/elimination process, so cannot be applied to the mechanistically more complex Scholl and Mallory reactions.

To address this deficiency, Laarhoven developed reactivity predictors for all-hydrocarbon photocyclisation reactions based upon bond order analysis within Hückel molecular orbital theory. [31–34]. The physical rationale behind this approach is that the number and/or strength of the existing π bonds at the cyclising centres should decrease upon photo-excitation, facilitating the formation of a new intramolecular σ bond. Unfortunately, Laarhoven's rules turn out to be neither robust, nor generalisable, nor powerful, nor simple. They cannot be easily applied to molecules containing heteroatoms, do not apply at all to Scholl reactions, contain no information about reaction conditions or geometrical structure, and can fail to predict reaction outcomes correctly even where applicable.

Our aim here is to perform detailed mechanistic studies of both Mallory and Scholl reactions, to determine the key steric and electronic factors that control reactivity, with a view to developing simple, powerful, general and unified reactivity predictors for these synthetically important classes of aromatic ring-forming reactions. We will focus particularly on structural modifications whose impact on reactivity is poorly explained by existing reactivity models; inclusion of heteroatoms and varying ring sizes within the photocyclising ring system. Aromatic substituent effects on elimination reactions are already well understood [35, 36] so will not be investigated in further detail here.

3.2 Methods

All reactants have the same basic framework structure (Fig. 3.4) with varying rings, as illustrated in Table 3.2.

Fig. 3.4 Framework structure for all reactants (left) and products (right) within our data set of molecules that undergo eliminative cyclisation.

Reaction pathways are mapped out at B3LYP [37] using a 6-31G(d,p) basis [38] for all atoms except Cl^- (6-31+G(d)) [39, 40] and Fe (LanL2DZ) [41]. Vertical excitation energies are computed at TD-B3LYP [42] with the same atomic orbital basis. Gibbs free energies are computed from ground and excited state electronic energies, ground state harmonic frequencies, moments of inertia and molecular masses using standard statistical thermodynamics formulae, discarding the imaginary frequency of each transition state. Solvation corrections to the free energy are computed using the conductor-like continuum solvation model [43] as implemented in QChem4.2 [44, 45] with a dielectric constant of 8.93 chosen to resemble dichloromethane. Complete details of all species involved in each reaction pathway are provided as in Appendix (A).

All *ab initio* and statistical thermodynamics calculations are performed using QChem4.2. [44]

Table 3.2 IUPAC names and schematic representation of all molecules in our data set

IUPAC name	R_1	R_2	R_3
cis-1,2-diphenylethylene	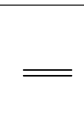	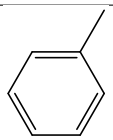	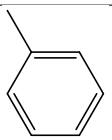
3,4-diphenylpyrrole	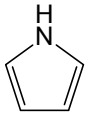	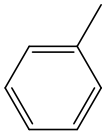	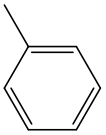
3,4-diphenylthiophene		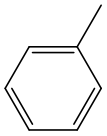	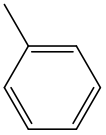
1,2-diphenylbenzene		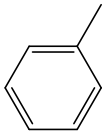	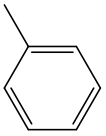
2,2'-(1,2-phenylene)dipyridine		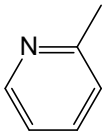	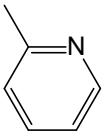
2,2'-(1,2-phenylene)dithiophene		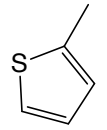	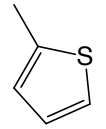
2,2'-(1,2-phenylene)dipyrrole		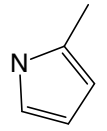	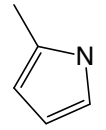
3,3'-(1,2-phenylene)dipyridine		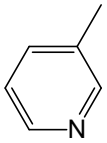	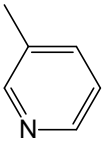
3,3'-(1,2-phenylene)dithiophene	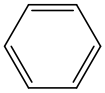	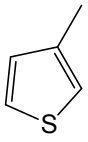	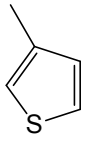
3,3'-(1,2-phenylene)dipyrrole		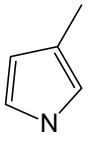	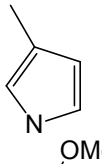
1-(2-methoxyphenyl)-2-phenylbenzene		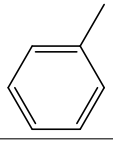	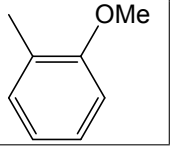

3.3 Results and Discussion

3.3.1 Thermal cyclisation

A prototypical reaction coordinate diagram for the radical cation mediated thermal oxidative cyclodehydrogenation of 1,2-diphenylbenzene is illustrated in Fig. 3.5, and key thermodynamic parameters for all structural variants reported in Table 3.3.

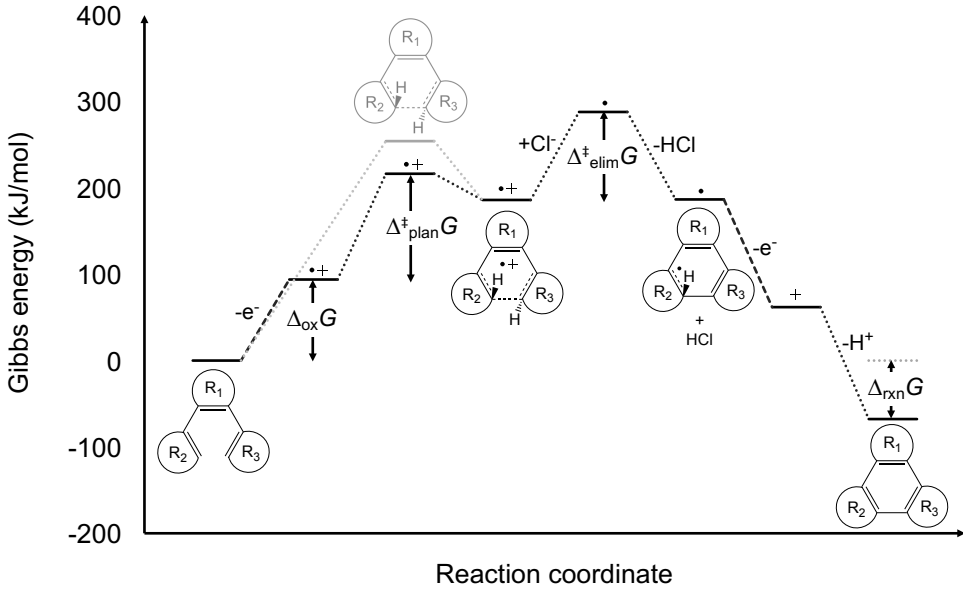

Fig. 3.5 Reaction coordinate diagram for the thermal oxidative dehydrogenation of 1,2-diphenylbenzene (R_1 = benzene, R_2 = R_3 = phenyl), proceeding via the radical cation mechanism. The greyed-out lines represent the energy required for the planarisation step of the reaction to proceed in a single step, in the absence of a strong oxidising agent.

On the whole, the data presented in Table 3.3 are consistent with experimental

observations reported in the literature; [6–9, 46, 47] oxidative cyclodehydrogenation for all heteroaromatic molecules under investigation – except the dipyridine derivatives, for which no experimental data is available – occurs in the presence of strong oxidising agents at room temperature. The substantial negative $\Delta_{\mathrm{rxn}}G$ values provide a strong thermodynamic driving force. The Gibbs energies of activation indicate that each reaction step, except the planarisation of 3,4-diphenylpyrrole, should be thermally accessible at room temperature, assuming each molecule possesses $\frac{3N_{\mathrm{atom}}}{2}RT$ J mol^{-1} thermal energy ($\approx$ 120 kJ mol^{-1} at 298.15 K). Although it is unlikely that all the available thermal energy would be channeled into the reaction coordinate, it is also likely that we have overestimated barrier heights, as the continuum solvation model we have used does not account for explicit solvent stabilisation of the radical cation intermediates, which is likely to have a significant stabilising effect. [48, 49] Finally, we note that the intrinsic accuracy of B3LYP for modelling isomerization reactions, [50] reaction enthalpies [51, 52] and activation energies [51, 52] lies in the 6 – 10 kJ mol^{-1} range.

Table 3.3 Key thermodynamic quantities controlling the thermodynamic stability (Gibbs energy of reaction, $\Delta_{\text{rxn}}G$) and kinetic reactivity (Gibbs energy of oxidation, $\Delta_{\text{ox}}G$ and Gibbs energies of activation, $\Delta^{\ddagger}_{\text{plan}}G$ and $\Delta^{\ddagger}_{\text{elim}}G$) of candidate molecules for thermal oxidative cyclodehydrogenation (Scholl reaction).

R_1	$R_2 = R_3$	Both	Scholl			-oxidant
		$\Delta_{\text{rxn}}G$ (kJ mol^{-1})	$\Delta_{\text{ox}}G$ (kJ mol^{-1})	$\Delta^{\ddagger}_{\text{plan}}G$ (kJ mol^{-1})	$\Delta^{\ddagger}_{\text{elim}}G$ (kJ mol^{-1})	$\Delta^{\ddagger}_{\text{plan}}G$ (kJ mol^{-1})
pyrrole	phenyl	-54.5	56.1	136.6	99.4	291.2
thiophene	phenyl	-55.0	98.8	93.9	73.0	307.2
benzene	phenyl	-67.7	93.9	122.5	101.9	254.1
benzene	2-pyridine	-71.8	118.3	103.5	73.0	246.4
benzene	2-thiophene	-97.7	60.0	98.2	106.4	264.2
benzene	2-pyrrole	-87.9	1.7	105.1	121.3	194.8
benzene	3-pyridine	-71.8	117.7	89.1	58.4	240.9
benzene	3-thiophene	-93.3	68.8	37.6	115.8	187.3
benzene	3-pyrrole	-90.8	6.5	46.1	118.9	172.4

To the best of our knowledge, the only previous studies of oxidative cyclodehydrogenation reactions have either been performed entirely in the gas phase [22] or largely focussed on the arenium cation mechanism [53] that has since been experimentally shown [23] to be less plausible than the radical cation mechanism investigated here. However, they do report solvation-corrected $\Delta^{\ddagger}_{\text{plan}}G$ values for 1,2-diphenylbenzene of 114.2 kJ mol^{-1} at B3LYP/6-31G* and 105.9 kJ mol^{-1} at BHandHLYP/6-31G* that agree reasonably with the 122.5 kJ mol^{-1} reported here.

High-level gas phase CASPT2/6-31G* calculations of the initial barrier to planarisation, $\Delta^{\ddagger}_{\text{plan}}G$, for 2,2'-(1,2-phenylene)dithiophene and 3,3'-(1,2-phenylene)dithiophene

reactions have been computed in the absence of oxidant, in the context of modelling the factors that control photoswitchability of these molecules. [54] In principle, their reported gas phase values are not directly comparable to our solvation-corrected values. However, the polarity of the molecule does not change substantially upon planarisation in the absence of oxidant, so the corresponding solvation free energy change is also small, according to the continuum solvation model we use (full details accessible in Appendix (A)). Therefore, the difference between their reported values of 236.0 kJ mol^{-1} and 193.3 kJ mol^{-1}, respectively, and ours of 264.2 kJ mol^{-1} and 187.3 kJ mol^{-1}, are largely due to differences in electronic structure models. This finding is consistent with the results of a recent benchmarking study for a series of electrocyclisation reactions [55] which shows that hybrid generalised gradient functionals like B3LYP can be in error by up to 35 kJ mol^{-1} for barrier heights, although the RMSD error for B3LYP is only around 6 kJ mol^{-1}.

Overall, our model qualitatively and semi-quantitatively reproduces existing experimental and computational data, so can be confidently used to identify trends in reactivity due to inclusion of heteroatoms and variation of ring sizes within the cyclising ring system.

From Table 3.3, it is clear that the Gibbs energy of oxidation, $\Delta_{ox}G$, is most strongly influenced by the identity of the terminal rings, but not the position of the heteroatom within the cyclising ring system. Pyridine increases the barrier to oxidation relative to benzene, thiophene decreases it, and pyrrole substantially decreases it. As expected, these trends are roughly correlated with the oxidation potentials of each ring substituent drawn from the literature [56, 57] and reported in Table 3.4

Table 3.4 Oxidation potentials of ring substituents, measured under the same experimental conditions [57]

Molecule	E_{ox} (V)
benzene	2.08
pyridine	1.82
thiophene	1.60
pyrrole	0.76

Gibbs energies of activation for planarisation, $\Delta^{\ddagger}_{plan}G$, are substantially decreased by having a heteroatom adjacent to the photocyclising site, and slightly decreased by the presence of a thiophene ring anywhere within the cyclising system. This suggests that the primary determinant of the barrier to oxidative cyclisation is the ability to alleviate ring strain.

Gibbs energies of activation for elimination, $\Delta^{\ddagger}_{elim}G$ obey similar trends to those of oxidation, only in the opposite direction. For molecules with terminal ring substituents, pyrrole and thiophene both raise the barrier while pyridine substantially decreases it. Substitution of the central ring by pyrrole has little effect while thiophene substituent lowers the barrier for reasons that are not entirely clear to us.

Taking all of the above competing effects into account, the molecule with lowest overall rate-determining free energy barrier is 3,4-diphenylthiophene.

3.3.2 Oxidative photocyclisation

A prototypical reaction coordinate diagram for the oxidative photocyclisation of 1,2-diphenylbenzene is illustrated in Fig. 3.6, and key thermodynamic parameters for all structural variants reported in Table 3.5.

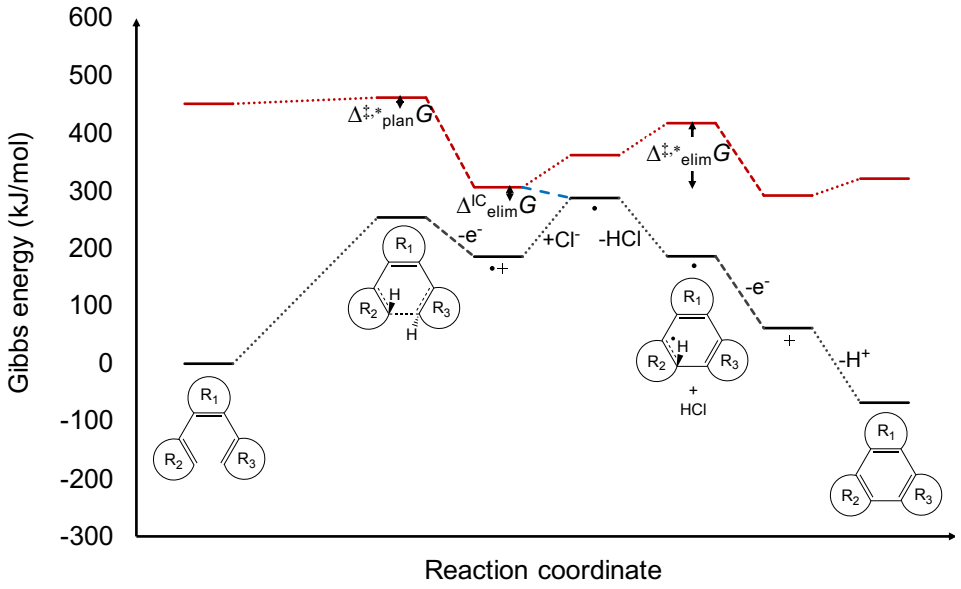

Fig. 3.6 Ground (black) and excited state (red) reaction coordinate diagrams for the photochemical oxidative dehydrogenation of 1,2-diphenylbenzene (R_1 = benzene, R_2 = R_3 = phenyl), with internal conversion proposed to occur during the first step of the elimination process, as indicated in blue.

Table 3.5 Key thermodynamic quantities controlling the thermodynamic stability (Gibbs energy of intersystem crossing, $\Delta^{\mathrm{IC}}_{\mathrm{elim}}G$) and kinetic reactivity (excited state Gibbs energies of activation, $\Delta^{\ddagger,*}_{\mathrm{plan}}G$ and $\Delta^{\ddagger,*}_{\mathrm{elim}}G$) of candidate molecules for photochemical oxidative cyclodehydrogenation (Mallory reaction). Gibbs energies of reaction are the same as for the Scholl reaction, as reported in Table 3.3.

R_1	$R_2 = R_3$	Mallory		
		$\Delta^{\ddagger,*}_{\mathrm{plan}}G$ (kJ mol^{-1})	$\Delta^{\ddagger,*}_{\mathrm{elim}}G$ (kJ mol^{-1})	$\Delta^{\mathrm{IC}}_{\mathrm{elim}}G$ (kJ mol^{-1})
ethene	phenyl	19.2	85.2	-52.8
pyrrole	phenyl	14.9	148.3	-11.6
thiophene	phenyl	17.8	123.1	-26.6
benzene	phenyl	10.7	111.3	-18.6
benzene	2-pyridine	8.8	105.3	-28.0
benzene	2-thiophene	36.8	92.7	-69.3
benzene	2-pyrrole	32.6	155.3	-44.9
benzene	3-pyridine	6.0	117.3	-31.9
benzene	3-thiophene	-73.1	155.3	-39.1
benzene	3-pyrrole	-20.7	214.3	-31.7

As far as we are aware, there are no prior mechanistic studies covering all stages of the oxidative Mallory photocyclisation process. However, the first step in the photocyclisation of 2,2'-(1,2-phenylene)dithiophene and 3,3'-(1,2-phenylene)dithiophene has been extensively investigated [24,54] in light of their potential utility as molecular photoswitches. Although our vertical excitation energies are not directly comparable with the adiabatic values reported in the literature [54], our results are nonetheless consistent with previous findings that planarisation proceeds sponta-

neously in the first excited state for 3,3'-(1,2-phenylene)dithiophene, and partial planarisation proceeds spontaneously for 2,2'-(1,2-phenylene)dithiophene.

Overall, the $\Delta^{\ddagger,*}_{\text{plan}}G$ values presented in Table 3.5 imply that planarisation proceeds either readily (low positive values) or spontaneously (negative values) following photo-excitation for all molecules in our data set. Planarisation appears to be strongly enhanced by the presence of a heteroatom adjacent to the photocyclising centre, but retarded by distant heteroatoms within 5-membered rings, or the presence of an ethylene bridge within the molecule.

By analogy with the Scholl mechanism data presented in the previous section, a number of these reactions could proceed thermally in the excited state, with $\Delta^{\ddagger,*}_{\text{elim}}G$ values < 120 kJ mol^{-1}. However, it is far more likely that they undergo a thermodynamically favourable internal conversion ($\Delta^{\text{IC}}_{\text{elim}}G < 0$), mediated by vibronic interactions with the oxidant.

Comparing the data presented in Table 3.3 and Table 3.5, it appears that photomediated oxidative cyclodehydrogenation reactions will occur more readily and under milder conditions than their thermal counterparts, with free energy barriers that are less sensitive to the identity of the reactants.

3.3.3 Eliminative photocyclisation

Finally, it remains to compare the oxidative and purely eliminative photocyclisation processes illustrated in Fig. 3.7. Synthetically, the oxidative route is easier, as it does not require appropriate leaving groups to be pre-attached to the photocyclising rings in appropriate positions, although the eliminative route has a shorter work-up as the low molecular weight elimination product can simply be distilled off from the reaction mixture.

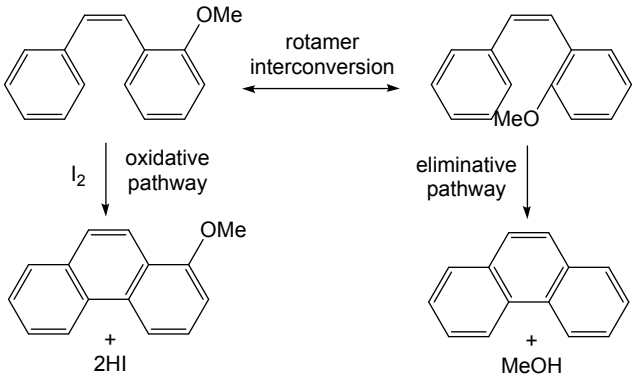

Fig. 3.7 Oxidative (left) and eliminative (right) photocyclisation pathways

Reaction coordinate diagrams for 1-(2-methoxyphenyl)-2-phenylbenzene, a prototypical molecule that can undergo both oxidative and eliminative photocyclisation, are illustrated in Fig. 3.8. Key thermodynamic parameters for both pathways are reported in Table 3.6, along with 1,2-diphenylbenzene reference data.

Table 3.6 Gibbs energies of reaction ($\Delta_{\mathrm{rxn}}G$), Gibbs energies of activation ($\Delta^{\ddagger,*}_{\mathrm{plan}}G$, $\Delta^{\ddagger,*}_{\mathrm{elim}}G$) and Gibbs energies of internal conversion ($\Delta^{\mathrm{IC}}_{\mathrm{elim}}G$) capturing key characteristics of the potential energy surfaces for oxidative and purely eliminative photocyclisation of 1-(2-methoxyphenyl)-2-phenylbenzene (R_1 = benzene, R_2 = phenyl, R_3 = 2-methoxyphenyl).

Molecule	Pathway	$\Delta_{\mathrm{rxn}}G$ (kJ mol^{-1})	$\Delta^{\ddagger,*}_{\mathrm{plan}}G$ (kJ mol^{-1})	$\Delta^{\ddagger,*}_{\mathrm{elim}}G$ (kJ mol^{-1})	$\Delta^{\mathrm{ISC}}_{\mathrm{elim}}G$ (kJ mol^{-1})
1,2-diphenylbenzene	oxidative	-67.7	10.7	111.3	-18.6
1-(2-methoxyphenyl)-2-phenylbenzene	oxidative	-51.7	41.0	154.6	17.5
1-(2-methoxyphenyl)-2-phenylbenzene	eliminative	-91.8	45.8	8.7	-168.1

In contrast to the unsubstituted parent molecule 1,2-diphenylbenzene, 1-(2-methoxyphenyl)-2-phenylbenzene has an unfavourable free energy of internal conversion along the

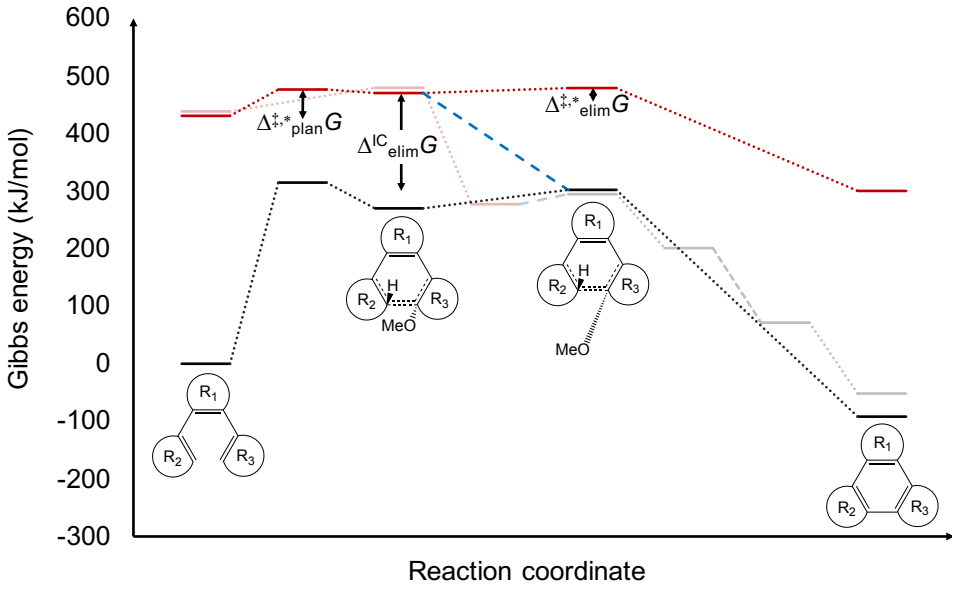

Fig. 3.8 Ground (black) and excited state (red) reaction coordinate diagrams for the photochemical eliminative cyclisation of 1-(2-methoxyphenyl)-2-phenylbenzene (R_1 = benzene, R_2 = phenyl, R_3 = 2-methoxyphenyl). For reference, the proposed oxidative pathway is shown greyed-out.

oxidative pathway, higher free energy of planarisation and lower overall thermodynamic stability of the products, i.e. it is disfavoured over the unsubstituted molecule in every respect. Therefore, adding on a methoxy leaving group is a poor synthetic strategy unless the eliminative pathway is strongly favourable.

The eliminative pathway has a low energy barrier for progression from the planar intermediate to the excited state product and the internal conversion along this pathway is strongly exergonic, suggesting that the reaction could proceed via either pathway. However, as there is no obvious mechanism for the internal conversion to occur, we hypothesise that this reaction proceeds to completion in the excited state.

Finally, we note that the free energies of activation for planarisation, $\Delta^{\ddagger,*}_{\text{plan}}G$, are the largest of all reactants considered in this study, regardless of which rotamer is involved and which pathway is being followed.

3.4 Conclusions

Oxidative Mallory reactions appear to optimally balance synthetic convenience (ease of preparation of reactants, mild conditions, tolerant to chemical diversity in reactants) against favourable kinetic and thermodynamic properties. Thermal oxidative cyclodehydrogenation (Scholl) reactions are far more sensitive to the nature of the rings comprising the reactant molecules, which can have both disadvantages (capricious reactivity) and advantages (controllability). There does not seem to be any additional advantage pursuing eliminative photocyclisation over oxidative, from the limited results presented here. Future work on how the nature of the reactant affects the outcome of the reaction would studied in order to investigate the interplay between substituent effects, ring strain and heteroatom effects. Beyond

this, it would also be useful and synthetically relevant to investigate the influence of different solvents and/or solvation models, and the importance of the choice of oxidant.

Bibliography

[1] M. Kivala, D. Wu, X. Feng, C. Li, and K. Müllen, "Cyclodehydrogenation in the synthesis of graphene-type molecules," *Mat. Sci. Tech.*, 2012.

[2] R. Scholl and C. Seer, "Abspaltung aromatisch gebundenen wasserstoffs und verknüpfung aromatischer kerne durch aluminiumchlorid," *Eur. J. Org. Chem.*, vol. 394, no. 2, pp. 111–177, 1912.

[3] R. Scholl and C. Seer, "Über die abspaltung aromatisch gebundenen wasserstoffs unter verknüpfung aromatischer kerne durch aluminiumchlorid," *Eur. J. Inorg. Chem.*, vol. 55, no. 1, pp. 109–117, 1922.

[4] P. Kovacic and C. Wu, "Reaction of ferric chloride with benzene," *J. Polymer Sci. A*, vol. 47, no. 149, pp. 45–54, 1960.

[5] P. Kovacic, C. Wu, and R. W. Stewart, "Reaction of ferric chloride with alkylbenzenes," *J. Am. Chem. Soc.*, vol. 82, no. 8, pp. 1917–1923, 1960.

[6] A. C. Grimsdale, K. Leok Chan, R. E. Martin, P. G. Jokisz, and A. B. Holmes, "Synthesis of light-emitting conjugated polymers for applications in electroluminescent devices," *Chem. Rev.*, vol. 109, no. 3, pp. 897–1091, 2009.

[7] R. Rieger, D. Beckmann, W. Pisula, W. Steffen, M. Kastler, and K. Müllen, "Rational optimization of benzo [2, 1-b; 3, 4-b?] dithiophene-containing polymers for organic field-effect transistors," *Adv. Mat.*, vol. 22, no. 1, pp. 83–86, 2010.

[8] A. Bhattacharya and A. De, "Conducting composites of polypyrrole and polyaniline a review," *Prog. Solid State Chem.*, vol. 24, no. 3, pp. 141–181, 1996.

[9] Y. Q. Lu, G. Q. Shi, C. Li, and Y. Q. Liang, "Thin polypyrrole films prepared by chemical oxidative polymerization," *J. Appl. Polym. Sci.*, vol. 70, no. 11, pp. 2169–2172, 1998.

[10] A. K. Geim and K. S. Novoselov, "The rise of graphene," *Nature Mat.*, vol. 6, no. 3, pp. 183–191, 2007.

[11] J. Wu, W. Pisula, and K. Müllen, "Graphenes as potential material for electronics," *Chem. Rev.*, vol. 107, no. 3, pp. 718–747, 2007.

[12] F. B. Mallory, J. T. Gordon, C. S. Wood, L. C. Lindquist, and M. L. Savitz, "Photochemistry of stilbenes .1.," *J. Am. Chem. Soc.*, vol. 84, no. 22, pp. 4361–4362, 1962.

[13] F. B. Mallory, C. S. Wood, and J. T. Gordon, "Photochemistry of stilbenes .2. Substituent effects on rates of phenanthrene formation," *J. Am. Chem. Soc.*, vol. 85, no. 6, pp. 828–829, 1963.

[14] F. B. Mallory, C. S. Wood, and J. T. Gordon, "Photochemistry of stilbenes .3. Some aspects of mechanism of photocyclization to phenanthrenes," *J. Am. Chem. Soc.*, vol. 86, no. 15, pp. 3094–3102, 1964.

[15] C. S. Wood and F. B. Mallory, "Photochemistry of stilbenes .4. Preparation of substituted phenanthrenes," *J. Org. Chem.*, vol. 29, no. 11, pp. 3373–3377, 1964.

[16] A. Sudhakar, T. J. Katz, and B. W. Yang, "Synthesis of a helical metallocene oligomer," *J. Am. Chem. Soc.*, vol. 108, pp. 2790–2791, MAY 14 1986.

[17] L. B. Liu, B. W. Yang, T. J. Katz, and M. K. Poindexter, "Improved methodology for photocyclization reactions," *J. Org. Chem.*, vol. 56, pp. 3769–3775, JUN 7 1991.

[18] F. B. Mallory and C. W. Mallory, "Photocyclization of stilbenes and related molecules," *Org. React.*, vol. 30, pp. 1–456, 1984.

[19] Y. Tominaga and R. N. Castle, "Photocyclization of aryl- and heteroaryl-2-propenoic acid derivatives. Synthesis of polycyclic heterocycles," *J. Heterocyc. Chem.*, vol. 33, pp. 523–538, MAY-JUN 1996.

[20] K. B. Jorgensen, "Photochemical oxidative cyclisation of stilbenes and stilbenoids - the Mallory reaction," *Molecules*, vol. 15, pp. 4334–4358, JUN 2010.

[21] O. Hammerich and V. D. Parker, "Kinetics and mechanisms of reactions of organic cation radicals in solution," *Advances in physical organic chemistry*, vol. 20, pp. 55–189, 1984.

[22] M. Di Stefano, F. Negri, P. Carbone, and K. Müllen, "Oxidative cyclodehydrogenation reaction for the design of extended 2d and 3d carbon nanostructures: A theoretical study," *Chem. Phys.*, vol. 314, no. 1, pp. 85–99, 2005.

[23] L. Zhai, R. Shukla, S. H. Wadumethrige, and R. Rathore, "Probing the arenium-ion (proton transfer) versus the cation-radical (electron transfer) mechanism of scholl reaction using ddq as oxidant," *J. Org. Chem.*, vol. 75, no. 14, pp. 4748–4760, 2010.

[24] D. Guillaumont, T. Kobayashi, K. Kanda, H. Miyasaka, K. Uchida, S. Kobatake, K. Shibata, S. Nakamura, and M. Irie, "An ab initio mo study of the photochromic reaction of dithienylethenes," *J. Phys. Chem. A*, vol. 106, no. 31, pp. 7222–7227, 2002.

[25] R. B. Woodward and R. Hoffmann, "Stereochemistry of electrocyclic reactions," *J. Am. Chem. Soc.*, vol. 87, no. 2, pp. 395–397, 1965.

[26] R. Hoffmann and R. B. Woodward, "Selection rules for concerted cycloaddition reactions," *J. Am. Chem. Soc.*, vol. 87, no. 9, pp. 2046–2048, 1965.

[27] R. B. Woodward and R. Hoffmann, "The conservation of orbital symmetry," *Angewandte Chemie*, vol. 8, no. 11, pp. 781–853, 1969.

[28] J. E. Baldwin, "Rules for ring-closure," *J. Chem. Soc. - Chem. Comm.*, no. 18, pp. 734–736, 1976.

[29] K. Gilmore, R. K. Mohamed, and I. V. Alabugin, "The baldwin rules: revised and extended," *Wiley Interdisciplinary Reviews: Computational Molecular Science*, vol. 6, no. 5, pp. 487–514, 2016.

[30] P. Geerlings, P. W. Ayers, A. Toro-Labbe, P. K. Chattaraj, and F. De Proft, "The Woodward-Hoffmann rules reinterpreted by conceptual Density Functional Theory," *Acc. Chem. Res.*, vol. 45, pp. 683–695, MAY 2012.

[31] W. H. Laarhoven, T. J. H. Cuppen, and R. J. F. Nivard, "Photodehydrocyclizations in stilbene-like compounds," *Rec. Trav. Chim. - J. Roy. Neth. Chem.*, vol. 87, no. 7, pp. 687–698, 1968.

[32] W. H. Laarhoven, T. J. H. Cuppen, and R. J. F. Nivard, "Photodehydrocyclizations in stilbene-like compounds. 2. Photochemistry of distyrylbenzenes," *Tetrahedron*, vol. 26, no. 4, pp. 1069–1083, 1970.

[33] W. H. Laarhoven, T. J. H. Cuppen, and R. J. F. Nivard, "Photodehydrocyclizations in stilbene-like compounds. 3. Effect of steric factors," *Tetrahedron*, vol. 26, no. 20, pp. 4865–4881, 1970.

[34] W. H. Laarhoven, "Photochemical cyclizations and intramolecular cycloadditions of conjugated arylolefins .1. Photocyclization with dehydrogenation," *Rec. Trav. Chim. - J. Roy. Neth. Chem.*, vol. 102, no. 4, pp. 185–204, 1983.

[35] C. J. M. Stirling, "Leaving groups and nucleofugality in elimination and other organic reactions," *Acc. Chem. Res.*, vol. 12, no. 6, pp. 198–203, 1979.

[36] B. T. King, J. Kroulík, C. R. Robertson, P. Rempala, C. L. Hilton, J. D. Korinek, and L. M. Gortari, "Controlling the scholl reaction," *J. Org. Chem.*, vol. 72, no. 7, pp. 2279–2288, 2007.

[37] A. D. Becke, "A new mixing of hartree–fock and local density-functional theories," *J. Chem. Phys.*, vol. 98, no. 2, pp. 1372–1377, 1993.

[38] W. J. Hehre, R. Ditchfield, and J. A. Pople, "Self-consistent molecular orbital methods. xii. further extensions of gaussian-type basis sets for use in molecular orbital studies of organic molecules," *J. Chem. Phys.*, vol. 56, no. 5, pp. 2257–2261, 1972.

[39] M. M. Francl, W. J. Pietro, W. J. Hehre, J. S. Binkley, M. S. Gordon, D. J. DeFrees, and J. A. Pople, "Self-consistent molecular orbital methods. xxiii. a polarization-type basis set for second-row elements," *J. Chem. Phys.*, vol. 77, no. 7, pp. 3654–3665, 1982.

[40] M. J. Frisch, J. A. Pople, and J. S. Binkley, "Self-consistent molecular orbital methods 25. supplementary functions for gaussian basis sets," *J. Chem. Phys.*, vol. 80, no. 7, pp. 3265–3269, 1984.

[41] P. J. Hay and W. R. Wadt, "Ab initio effective core potentials for molecular calculations. potentials for the transition metal atoms scandium to mercury," *J. Chem. Phys*, vol. 82, no. 1, pp. 270–283, 1985.

[42] S. Hirata and M. Head-Gordon, "Time-dependent density functional theory within the tamm–dancoff approximation," *Chem. Phys. Lett.*, vol. 314, no. 3, pp. 291–299, 1999.

[43] V. Barone and M. Cossi, "Quantum calculation of molecular energies and energy gradients in solution by a conductor solvent model," *J. Phys. Chem. A*, vol. 102, no. 11, pp. 1995–2001, 1998.

[44] Y. Shao, Z. Gan, E. Epifanovsky, A. T. Gilbert, M. Wormit, J. Kussmann, A. W. Lange, A. Behn, J. Deng, X. Feng, and *et al*, "Advances in molecular quantum chemistry contained in the q-chem 4 program package," *Molecular Physics*, vol. 113, no. 2, pp. 184–215, 2015.

[45] A. W. Lange and J. M. Herbert, "Polarizable continuum reaction-field solvation models affording smooth potential energy surfaces," *J. Phys. Chem. Lett.*, vol. 1, no. 2, pp. 556–561, 2009.

[46] H. C. Kang and K. E. Geckeler, "Enhanced electrical conductivity of polypyrrole prepared by chemical oxidative polymerization: effect of the preparation

technique and polymer additive," *Polymer*, vol. 41, no. 18, pp. 6931–6934, 2000.

[47] D. Stanke, M. L. Hallensleben, and L. Toppare, "Graft copolymers and composites of poly (methyl methacrylate) and polypyrrole part i," *Synthetic metals*, vol. 72, no. 1, pp. 89–94, 1995.

[48] C. P. Kelly, C. J. Cramer, and D. G. Truhlar, "Adding explicit solvent molecules to continuum solvent calculations for the calculation of aqueous acid dissociation constants," *J. Phys. Chem. A*, vol. 110, no. 7, pp. 2493–2499, 2006.

[49] E. F. da Silva, H. F. Svendsen, and K. M. Merz, "Explicitly representing the solvation shell in continuum solvent calculations," *J. Phys. Chem. A*, vol. 113, no. 22, pp. 6404–6409, 2009.

[50] J. Tirado-Rives and W. L. Jorgensen, "Performance of b3lyp density functional methods for a large set of organic molecules," *J. Chem. Theor. Comp.*, vol. 4, no. 2, pp. 297–306, 2008.

[51] D. H. Ess and K. Houk, "Activation energies of pericyclic reactions: Performance of dft, mp2, and cbs-qb3 methods for the prediction of activation barriers and reaction energetics of 1, 3-dipolar cycloadditions, and revised activation enthalpies for a standard set of hydrocarbon pericyclic reactions," *J. Phys. Chem. A*, vol. 109, no. 42, pp. 9542–9553, 2005.

[52] V. Guner, K. S. Khuong, A. G. Leach, P. S. Lee, M. D. Bartberger, and K. Houk, "A standard set of pericyclic reactions of hydrocarbons for the benchmarking of computational methods: the performance of ab initio, density functional, casscf, caspt2, and cbs-qb3 methods for the prediction of activa-

tion barriers, reaction energetics, and transition state geometries," *J. Phys. Chem. A*, vol. 107, no. 51, pp. 11445–11459, 2003.

[53] P. Rempala, J. Kroulík, and B. T. King, "Investigation of the mechanism of the intramolecular scholl reaction of contiguous phenylbenzenes," *J. Org. Chem.*, vol. 71, no. 14, pp. 5067–5081, 2006.

[54] A. Perrier, S. Aloise, M. Olivucci, and D. Jacquemin, "Inverse versus normal dithienylethenes: computational investigation of the photocyclization reaction," *J. Phys. Chem. Lett.*, vol. 4, no. 13, pp. 2190–2196, 2013.

[55] A. Karton and L. Goerigk, "Accurate reaction barrier heights of pericyclic reactions: Surprisingly large deviations for the cbs-qb3 composite method and their consequences in dft benchmark studies," *J. Comput. Chem.*, vol. 36, no. 9, pp. 622–632, 2015.

[56] N. Weinberg and H. Weinberg, "Electrochemical oxidation of organic compounds," *Chemical Reviews*, vol. 68, no. 4, pp. 449–523, 1968.

[57] J. W. Loveland and G. Dimeler, "Anodic voltammetry to+ 2.0 volts. application to hydrocarbons and oxidation stability studies," *Analytical Chemistry*, vol. 33, no. 9, pp. 1196–1201, 1961.

CHAPTER 4

Substituent Effects on Substituted Benzylidene O-methyloximes

4.1 Substituents in organic reactions

In organic chemistry, substituents play an important role in understanding, controlling, and predicting the fate of most reactions. For instance, in predicting the acidity of many acids as well as the rate and product distribution of nucleophilic/electrophilic addition and substitution reactions. [1–4] Substituent effects may be transmitted geometrically or electronically. The geometrical effect of substituents is observed through steric hindrance while the electronic effects can either be transmitted via inductive or resonance effects. In general, the electronic effects of substituents are often more important because they affect the position and distribution of electrons in molecules, which is what chemistry is all about.

4.1.1 Inductive effect of substituents

Substituent inductive effects involve polarisation that results in partial separation of charges between the substituent and the substrate. [5] Substituents that pull electron density away from the substrate are referred to as inductive electron withdrawing groups. Meanwhile, those that push electron density towards the substrate are referred to as inductive electron-donating groups. Examples of both inductive electrons donating and withdrawing groups are represented in Table 4.1.

Table 4.1 Some examples of inductive electron-donating and electron withdrawing groups, where R represents an alkyl group.

Electron donating groups	Electron withdrawing groups
O^-, CO_2^-, CR_3	NR_3^+, NO_2, CN, X(F, Cl, Br, I), RCO, OR, NR_2

An example of the role of substituent inductive effects can be illustrated in an

aromatic ring system. In aromatic compounds, substituent inductive effects act by either activating or deactivating the ring.

Inductive electron-donating groups are ring activators. [6] They activate the ring by donating a pair of electrons into the ring, which increases the electron density of the ring. For instance, in electrophilic substitution reactions, activated rings are important for stabilising the carbocation intermediate, which leads to a reduction in transition-state energies for substitution. [7] On the other hand, inductive electron withdrawing groups act as ring deactivators. They deactivate the ring by pulling electron density away from the ring, thereby destabilising the carbocation. The polarisation effects of these groups on an aromatic ring are illustrated in Fig. 4.1

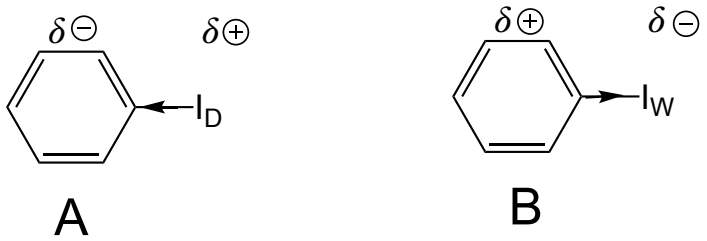

Fig. 4.1 Illustration of ring activation (A) and deactivation (B) due to the presence of inductive electron-donating groups, I_D, and electron withdrawing groups, I_W, respectively. δ - represent electron rich site meanwhile δ + represent electron-deficient site.

4.1.2 Resonance effect

A resonance effect involves the polarisation of a molecule resulting from the interaction of a lone pair of electrons or π-system of the substituent with the conjugated electrons in the parent molecule or substrate. Substituents with a lone pair of electrons or C=C bond (e.g. -vinyl, -aryl) on the atoms adjacent to the

substrate molecule can donate these electrons to the π-conjugation of the system. Such substituents are referred to as resonance electron-donating groups. On the other hand, substituents with an electronegative atom involved in a π-bond have the ability to pull electron density away from their substrate. Hence they are referred to as resonance electron-withdrawing groups. Some examples of resonance electron-donating and electron-withdrawing groups are presented in Table 4.2.

Table 4.2 Example of resonance electron-donating and electron-withdrawing groups, where R represents an alkyl group.

Resonance electron-donating groups	Resonance electron-withdrawing groups
OCH_3, -NH_2, -X[F, Cl, Br, I], -vinyl, -aryl	NO_2, -CN, C=O

In aromatic ring systems, substituent resonance effects are important in predicting the most reactive sites in aromatic compounds. [8] When a resonance electron-donating group is attached to an aromatic ring, it donates a pair of electrons to the conjugated system of the ring, which leads to the formation of different resonance structures as the electron is delocalised. The different resonance structures allow the electron density to be located on the ortho and para position, as illustrated in Scheme 4.1. For this reason, resonance electron-donating groups are often referred to as ortho/para directional substituents because they activate these positions by making them more nucleophilic, which has a consequence of reducing the barrier for electrophilic substitution on these sites.

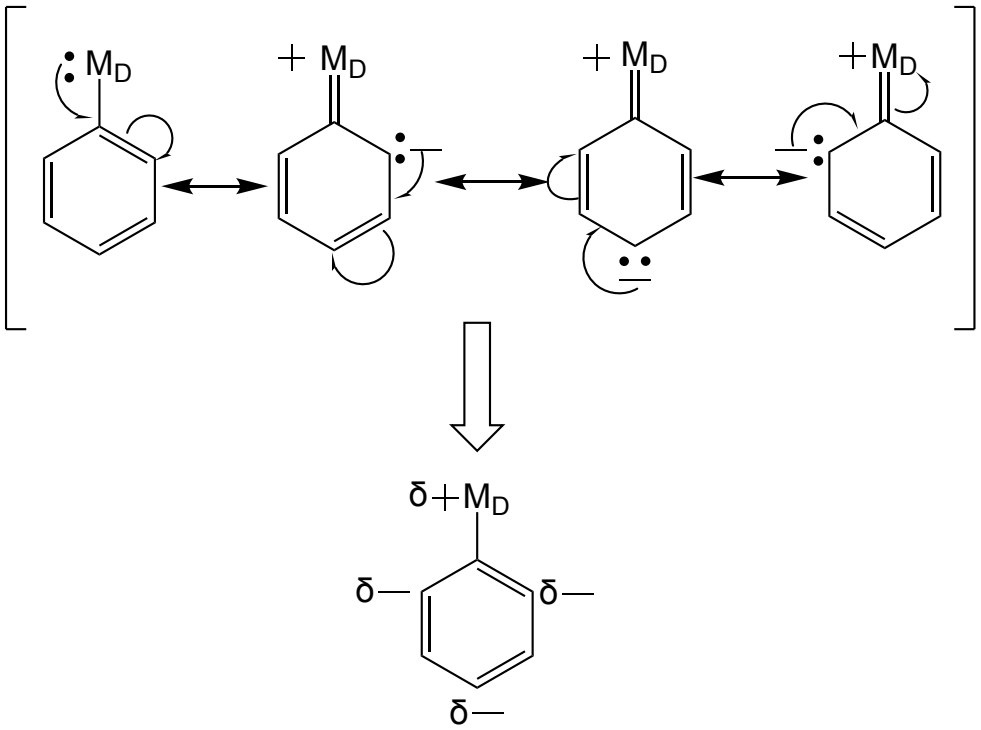

Scheme 4.1 Illustration of ortho/para ring activation by resonance electron-donating substituents, M_D. The double-headed arrow shows the direction of the formation of the different resonant structures with localised electron density. The bottom structure represents the net effect of electron-donating resonance effect with δ - showing the activated sites.

When a resonance electron-withdrawing group is attached to the ring, the resonance structures that result from their electron-withdrawing effect allow the charge to be localised on the meta-position as shown in Fig. 4.3. Consequently, resonance electron-withdrawing groups are generally referred to as meta-directional groups.

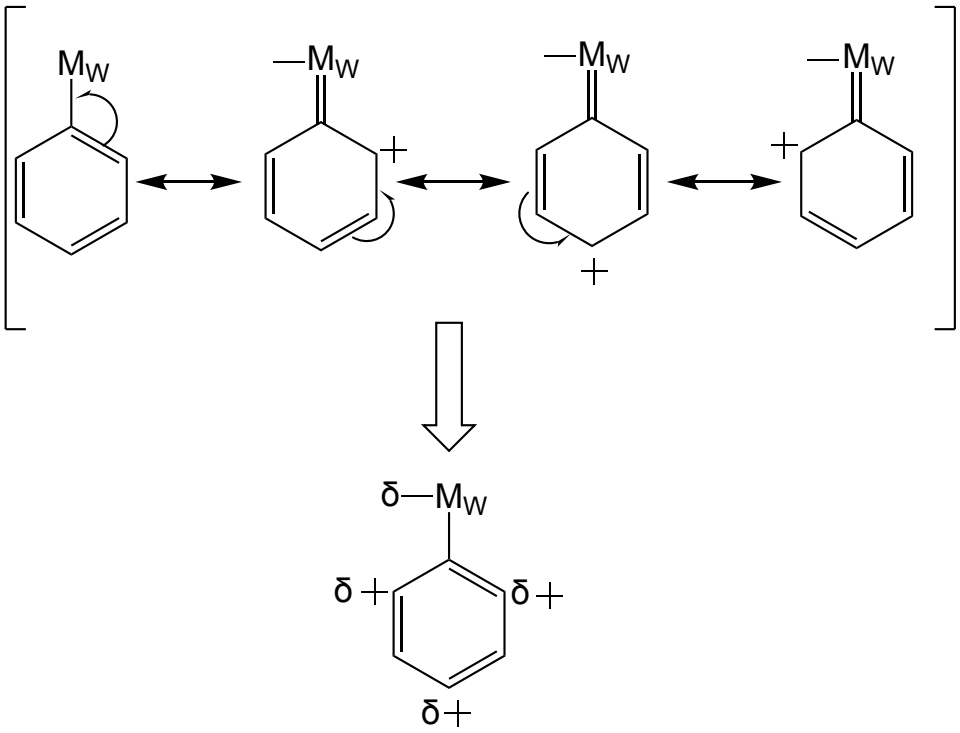

Scheme 4.2 Illustration of meta ring activation by resonance electron-withdrawing substituents, M_W. The double-headed arrow shows the direction of formation of the different resonant structures with regions of depletion of electron density. The bottom structure represents the net effect of electron-withdrawing resonance effect on a benzene ring with $\delta +$ showing the deactivated sites.

It is not routinely possible to decouple inductive and resonance effects of substituents. However, most inductive electron-withdrawing groups are also resonance electron-withdrawing groups and it is a rule of thumb that resonance effects of most substituents dominate over their inductive effects. The only exceptions to these rules are halogens, which have an unusual substituent effect on aromatic rings. They deactivate the ring but, at the same time, act as ortho/para directional groups. This is because halogens are highly electronegative and this leads to

their ring deactivating ability. However, they are still capable of donating a lone pair of electrons to the ring, which leads to their ortho/para-directional ability.

The importance of substituents in controlling reactions are not limited to predicting reaction rates and site selectivity. They are also useful in altering some chemical and physical properties such as melting and boiling point, solubility, photochromic, and self-assembly mode of molecules. Hence the choice of a substituent is a crucial requirement to take into account during synthetic planning.

4.2 Substituent effects in cyclisation

For the past 100 years, substituent effects have been explored and studied for almost all reactions in chemistry. [9–27] Despite these plethora of studies, there is still the need for a generalisation of how substituents could be used in controlling eliminative cyclisation reactions. However, before examining the importance and application of substituent in eliminative cyclisation, it is necessary to review the basic steps in these reactions and how substituents can be important in controlling each step.

4.2.1 Basic steps in eliminative cyclisation

Eliminative cyclisation in the simplest case can be described as a two-step process as shown in Fig. 4.2, which can be thermally or photochemically driven.

In the thermally driven reaction, the first step involves an oxidative electron transfer from the reactant to a strong oxidising agent, which enables the planarisation step to proceed. The second step involves an oxidative dehydrogenation of the planar intermediate to form the product.

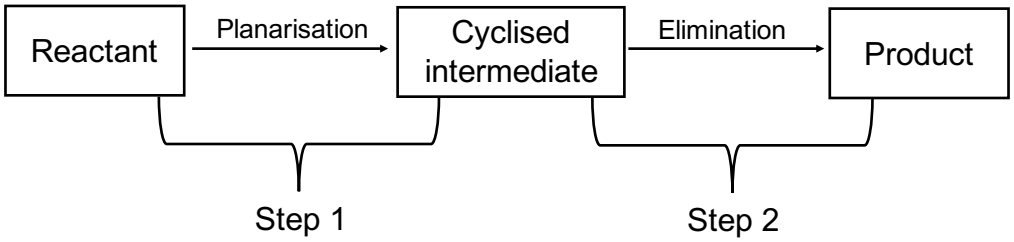

Fig. 4.2 Illustration of the two main steps in eliminative cyclisation.

In photochemical eliminative cyclisation, the first step involves the absorption of light, which enables the planarisation step. Meanwhile, the second step can either proceed via a thermal oxidative dehydrogenation of the planar intermediate or via a non-oxidative elimination of a leaving group, in which case a good leaving group is required.

In both thermal and photochemical cyclisation reactions, it is important to know how substituent effects can be used in controlling reaction rates and product distribution.

4.2.2 Substituent effects on thermal eliminative cyclisation

Several theoretical and experimental studies have been performed to decipher the role of substituents as directing and blocking groups on aromatic rings in thermal eliminative cyclisation reaction. [28–30] It has been concluded from these studies that both the number and position of the electron-donating group(s) in a reactant molecule are crucial for successful thermal cyclisation reactions. This conclusion is evident because electron donating groups increase the electron density around the ring, and as a consequence lower the barrier of oxidation, which in effect

reduces the overall energy barrier for planarisation and elimination. However, electron withdrawing-groups have an opposite effect of decreasing the oxidation potential of the precursor molecule as they pull electrons away from the ring, which consequently increases the oxidation barrier, and eventually the barrier for planarisation and elimination. Apart from acting as blocking groups, steric effects were found to be of little importance in controlling thermal cyclisation reactions. [31] These observations are unsurprising because thermal cyclisation, like every other reaction for which substituent effects have extensively been studied, are reactions that proceed in the ground electronic state.

4.2.3 Substituent effects on photochemical eliminative cyclisation

In photochemical cyclisation, there is still no generalisation on the role and importance of substituent effects. A possible reason for this can be attributed to the fact previous studies [32–43] were based on oxidative photocyclisation reaction, which is more dependent on the oxidising agent and solvation medium. In non-oxidative photochemical eliminative cyclisation reactions, which proceed in the absence of oxidising agents and involve the actual elimination of a leaving group, it is likely that substituent effects may be important. However, for these reactions, there are presently no studies on the effect of substituents on their reaction mechanisms.

For this reason, this chapter is aimed at investigating the role of substituents in non-oxidative eliminative photocyclisation reactions, using substituted-benzylidene O-methyloximes as a test case. This will be done computationally by mapping out stationary points on the potential energy surfaces of the ground and first singlet electronic excited states for a series of substituted-benzylidene O-methyloximes that are capable of undergoing non-oxidative eliminative photocyclisation reac-

tions. The results obtained from this computation will be compared against experimental results obtained from the synthesis of substituted-benzylidene O-methyloximes. [44] However, this study is not intended to correlate calculated energies with experimental yields, which depend on purification and other experimental variables. Rather, experimental yields will be considered only for judging whether the calculated energies correctly predict the formation of a product or not.

4.3 Methods

4.3.1 Data set

The data set is composed of a series of para- and ortho-substituted-benzylidene O-methyloximes, whose experimental syntheses are all known with the methoxyl group acting as the leaving group. [44] The para-substituted compounds lead to only one product and, as a consequence, they have only one rotamer. A scaffold for the reactant and product of the para-substituted compound is illustrated in Scheme 4.3. The different substituents represented by R are presented in Table 4.3.

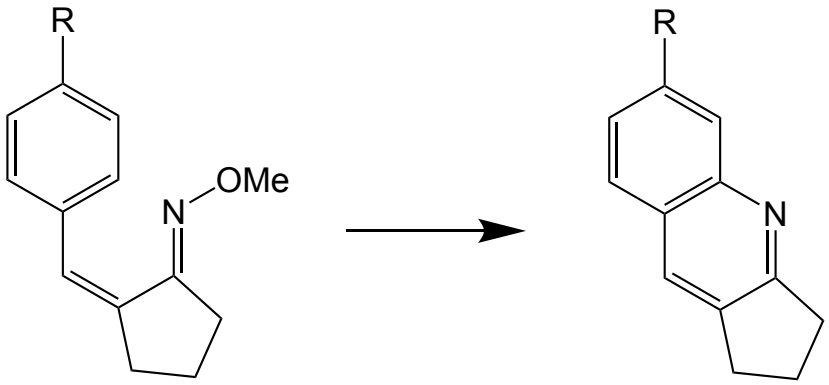

Scheme 4.3 Scaffold of reactant (left) and product (right) of para-substituted-benzylidene O-methyloximes. *R* represents the substituent and the methoxy group is the leaving group, which is eliminated during cyclisation.

Table 4.3 IUPAC names for the different para substituents of benzylidene O-methyloximes with corresponding abbreviation for the *R* group.

IUPAC name	*R*
Para-dimethylamino-benzylidene O-methyloximes	NMe_2
Para-amino-benzylidene O-methyloximes	NH_2
Para-methoxy-benzylidene O-methyloximes	OMe
Para-hydroxy-benzylidene O-methyloximes	OH
Methoxy-benzylidene O-methyloximes	H
Para-chloro-benzylidene O-methyloximes	Cl
Para-cyano-benzylidene O-methyloximes	CN
Para-nitro-benzylidene O-methyloximes	NO_2

The ortho-substituted-benzylidene O-methyloximes compounds have two rotamers as presented in Scheme 4.4. Each rotamer can cyclise into a different isomer. The

IUPAC names as well as the substituents, R, are presented in Table 4.4.

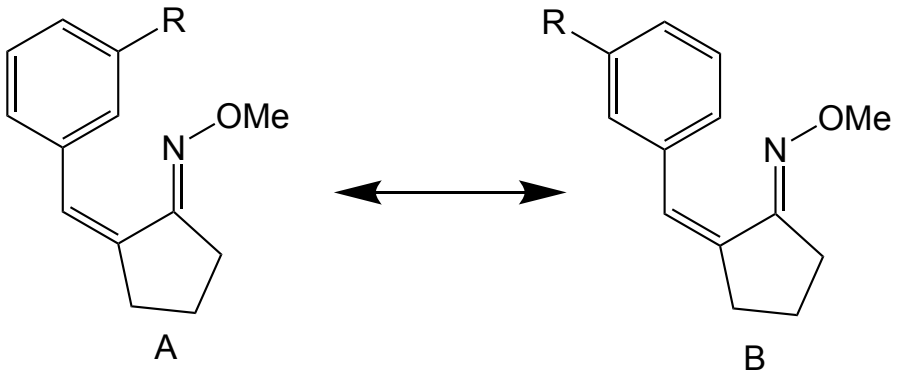

Scheme 4.4 Illustration of rotamers A and B of ortho-substituted-benzylidene O-methyloximes, where the R represents the substituent and the methoxy group is the leaving group.

Table 4.4 IUPAC names for ortho-substituent-benzylidene O-methyloximes with corresponding abbreviation for the R group

IUPAC name	R
Ortho-dimethylamino-benzylidene O-methyloximes	NMe_2
Ortho-amino-benzylidene O-methyloximes	NH_2
Ortho-methoxy-benzylidene O-methyloximes	OMe
Ortho-hydroxy-benzylidene O-methyloximes	OH
Ortho-floro-benzylidene O-methyloximes	F
Ortho-chloro-benzylidene O-methyloximes	Cl
Ortho-cyano-benzylidene O-methyloximes	CN
Ortho-nitro-benzylidene O-methyloximes	NO_2

4.3.2 Computational procedure

Firstly, a ground-state geometry optimisation was performed for the reactant, intermediate, and product guess structures for the unsubstituted O-methyloxime. This was followed by a vibrational frequency calculation to ensure that the optimised geometries were local minima. Initial-guess geometries for transition-state structures for both planarisation and elimination were then determined using the freezing string method (FSM) [45,46], which is described in chapter 2. These guess transition-state structures were then used as starting geometries for the transition-state search using an in-built surface-walking transition state search algorithm [47] implemented in QChem4.4. [48]

Before each transition-state search, a vibrational frequency calculation was first performed on the guess transition-state structure. The gradients and Hessians from this calculation were read into the in-built surface-walking transition-state search in QChem4.4. Another vibrational-frequency calculation was performed on the optimised transition-state structure to ensure that only one imaginary frequency was present and that the vibrational mode of this frequency corresponded to the vibration of the bond being formed or broken.

Once all the optimised structures were obtained, a Python script was implemented to add the various substituents to the optimised unsubstituted structures. This was done in a way that the coordinates of each atom in the unsubstituted compounds remained fixed.

Optimised geometries were then obtained for each substituted species. This was done using a fixed-geometry optimisation procedure wherein the main frame of the unsubstituted compound was held fixed and only the coordinates of the sub-

stituents added were allowed to relax.

Finally, a single-point energy calculation was performed on all optimised geometries using the conductor-like polarisation continuum model to account for solvent correction. This was done using a dielectric constant of 32.6, which represents the dielectric constant of methanol. A similar procedure was performed for the first singlet electronic excited states for all the systems.

4.4 Results and Discussion

4.4.1 Unsubstituted benzylidene O-methyloximes

The reaction coordinate diagram for the unsubstituted benzylidene O-methyloximes is presented in Fig. 4.3.

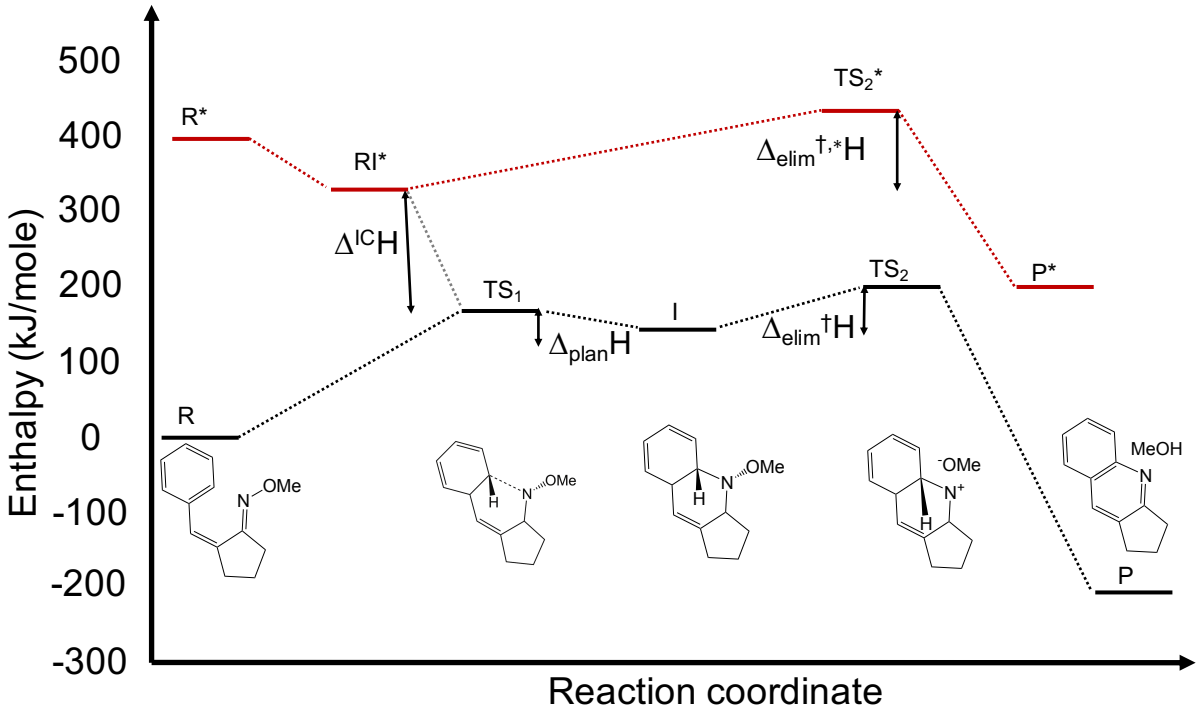

Fig. 4.3 Ground (black) and first singlet electronic excited-state (red) reaction coordinate diagram for the photochemical eliminative cyclisation of unsubstituted O-methyloxime, with internal conversion proposed for vibrational relaxation of the reactant as represented by the grey line. R, TS_1, I, TS_2, and P represent the ground-state energies of reactant, transition-state for planarisation, intermediate, transition state for elimination, and product respectively at ground-state geometry. R^* represents the first singlet electronic excited-state energy of the reactant at ground-state geometry. RI^*, $TS_2{}^*$, and P^* represent the first singlet electronic excited energies of the reactant, transition-state for elimination, and product respectively at excited-state geometry.

In Fig. 4.3, R, TS_1, I, TS_2, and P represent the relative energies of the reactant, transition-state energy for planarisation, cyclised-intermediate, transition-state en-

ergy for elimination, and product in the ground-state respectively. R^* corresponds to the first singlet electronic excited-state energy of the reactant at ground-state geometry meanwhile, RI^* corresponds to the first singlet electronic excited state-energy of the reactant at excited-state geometry. TS_2^* corresponds to the excited-state transition-state energy for elimination and P^* is the excited-state energy of the product at excited-state geometry.

Geometry optimisation in the first singlet excited state, beginning at all possible rotamers of the reactant and intermediate all converged to the same structure, RI^*. This structure is very similar to the ground-state transitions-state structure for planarisation, TS_1. 3D ball-and-stick digrams of RI^* and TS_1, generated using IQmol2.1 from their optimised geometric coordinates as produced from the QChem4.4 output, are presented in Fig. 4.4 and Fig. 4.5, respectively. The distance between atoms 1 and 2 is 1.982 Å and 1.864 Å for RI^* and TS_1, respectively. This resemblance in structures can potentially lead to a strong coupling between the two states. Hence, there is a likelihood that excited-state deactivation can proceed via internal conversion from RI^* to TS_1, with $\Delta^{IC}H$, corresponding to the energy released from vibrational relaxation. On the basis of this hypothesis, the ground-state enthalpies of planarisation, $\Delta_{plan}H$, and elimination $\Delta^{\dagger}_{elim}H$ can be calculated.

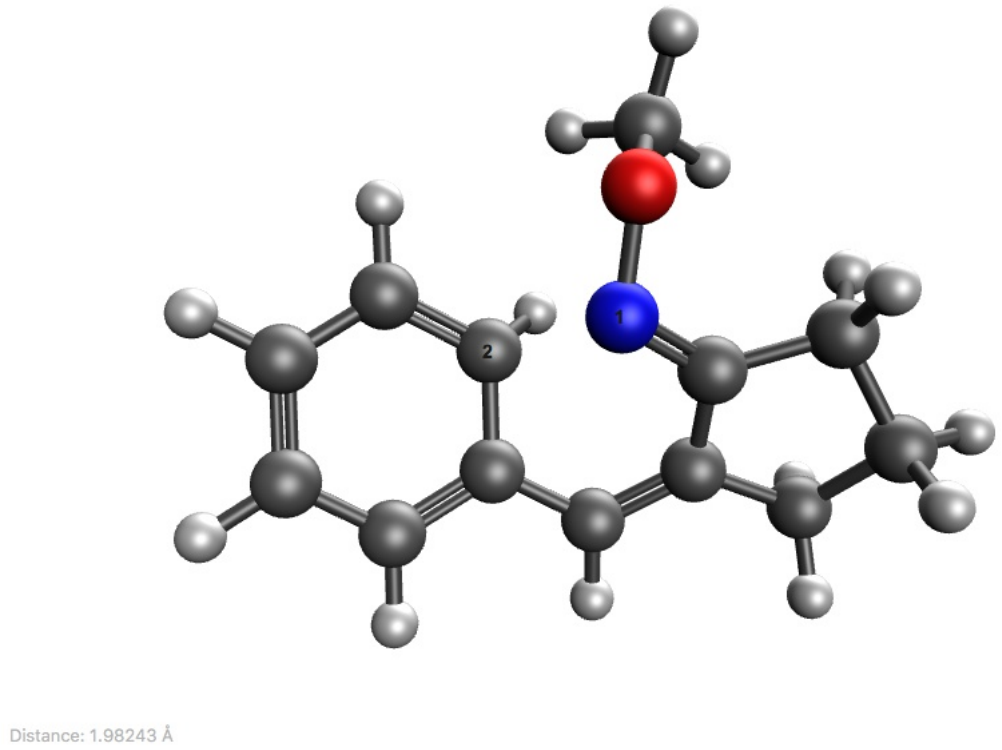

Fig. 4.4 3D ball-and-stick image of RI* generated using IQmol2.1. The balls represent atoms and the sticks connecting the balls represent bonds connecting the atoms. The blue and red ball represent a nitrogen and an oxygen atom respectively. The dark grey balls represent carbon atoms, and the light-grey balls represent hydrogen atoms. Atom 1 and 2 correspond to atoms forming the new bond in the planar intermediate.

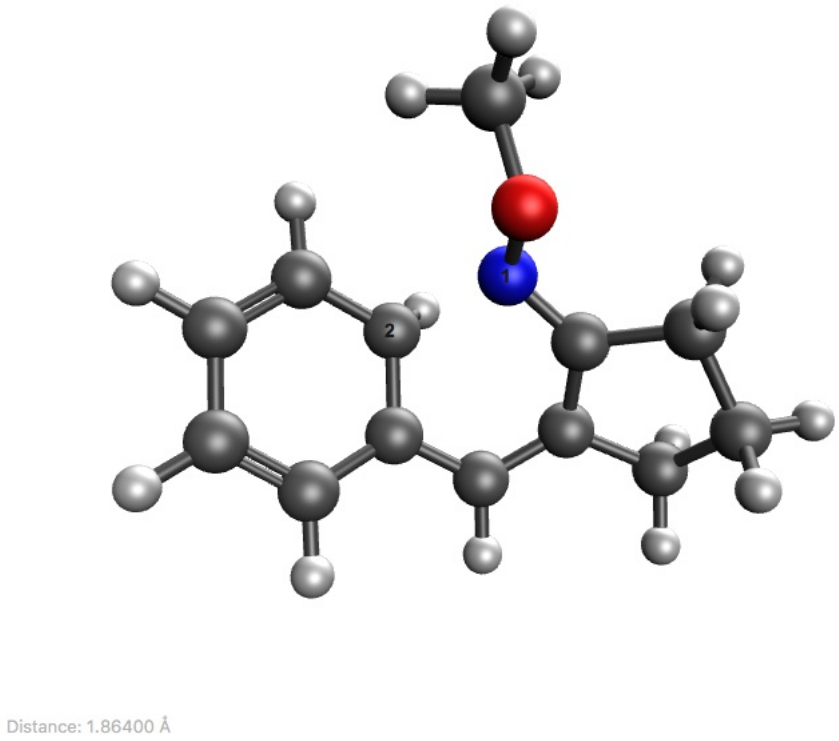

Fig. 4.5 3D ball-and-stick image of TS_1 generated using IQmol2.1, where the blue and red ball represent a nitrogen and an oxygen atom respectively. The dark grey balls represent carbon atoms, and the light-grey balls represent hydrogen atoms. Atom 1 and 2 correspond to atoms forming the new bond in the planar intermediate.

Since approximately 173 kJ mol^{-1} of energy is released in the formation of the cyclised intermediate for the ground-state reaction path, elimination via the ground-state pathway can be considered to be valid. This amount of energy should be sufficient to overcome the enthalpy/entropic barrier to drive elimination. Alternatively, if elimination is considered to proceed in the first singlet electronic excited-state, then about 108 kJ mol^{-1} of energy will be required to overcome this barrier.

However, since reacting species often follow the minimum energy path of the reaction, it is likely that elimination will not proceed in the excited state.

It should be noted that the accuracy of the computed energies is limited by the approximations made in computational modelling and also the methods used. In this model, some error may be included due to the non-inclusion of zero-point energy correction and thermochemical corrections. Also, the solvent-correction model used does not explicitly account for solvent interactions. Moreover, the error associated with B3LYP/6-31G(d,p) for reaction energy is within the range of 6-10 kJ mol^{-1}. [49, 50] In spite of these inaccuracies, it is still expected that the shape of the reaction coordinate diagram, Fig. 4.3, should be qualitatively correct given that only relative energies are considered.

4.4.2 Para-substituted benzylidene O-methyloximes

The results obtained from calculating the enthalpies for key elementary steps in the photocyclisation of para-substituted benzylidene O-methyloximes are reported in Table 4.5. All enthalpies are reported in kJ mol^{-1}.

Table 4.5 Results of enthalpy (kJ mol^{-1}) of internal($\Delta^{IC}H$), planarisation ($\Delta^{\dagger}_{plan}H$), ground-state elimination ($\Delta^{\dagger}_{elim}H$), elimination in the first singlet electronic excited-state ($\Delta^{\dagger,*}_{elim}H$), and photocyclisation experimental yields obtained from literature. [44]

Molecule	$\Delta^{IC}H$	$\Delta^{\dagger}_{plan}H$	$\Delta^{\dagger}_{elim}H$	$\Delta^{\dagger,*}_{elim}H$	Yield(%)
NMe_2	-150.8	-24.4	57.7	89.1	26
NH_2	-152.8	-19.9	58.9	99.8	36
OMe	-154.6	-22.9	60.9	104.1	53
OH	-153.1	-18.5	61.1	107.5	36
H	-148.7	-24.3	56.6	108.6	29
Cl	-151.9	-20.7	62.3	111.3	-
CN	-149.2	-18.8	62.5	113.4	-
NO_2	-147.4	-18.5	63.1	138.0	-

The results in Table 4.5 are presented in order of decreasing electron-donating ability ($NMe_2 > NH_2 > OMe > OH$) and increasing electro- withdrawing ability ($Cl < CN < NO_2$) of R. According to these results, it can be observed that both the ground and the first singlet electronic excited-state enthalpies of elimination, $\Delta^{\dagger}_{elim}H$ and $\Delta^{\dagger,*}_{elim}H$ respectively, are sensitive to the strength and nature of R. In this respect, enthalpies for elimination increase as the electron-donating power of R decrease, meanwhile the same increases as the electron-withdrawing ability of R increases. These trends imply that the barrier for elimination is influenced by the nature of the para-substituent. Comparing these enthalpies of elimination between both states, shows that enthalpies of elimination in the ground-state (57-62 kJ mol^{-1}) are lower than those of the first singlet electronic excited-state (89-138

kJ mol^{-1}). This means that less energy is required to drive elimination in the ground-state than in the first singlet electronic excited-state. Consequently, this increases the likelihood for a ground-state elimination pathway over the excited state pathway.

It can also be inferred from Table 4.5 that the enthalpies for planarisation are all negative. This shows that planarisation in these systems is thermodynamically favourable regardless of the nature of the substituent. Consequently, it can be hypothesised that elimination is rate limiting step. This is supported by the fact that no cyclisation products were obtained from the experimental synthesis for systems with electron withdrawing substituents, [44] which were found to have the largest enthalpies for elimination both in the ground and in the first singlet electronic excited-state.

4.4.3 Ortho-substituted benzylidene O-methyloximes

The enthalpies of elimination for ortho-substituted benzylidene O-methyloximes are reported in Table 4.6. All enthalpies are reported in kJ mol^{-1}.

Table 4.6 Ground and first singlet electronic excited-state enthalpies for elimination in rotamers A and B for ortho-substituted benzylidene O-methyloximes, Scheme 4.4. $\Delta^{\dagger}_{elim}$H, and $\Delta^{\dagger,*}_{elim}$H ground and first singlet electronic excited-state enthalpies. All enthalpies are recorded in kJ mol^{-1}. Yields were obtained from experimental published literature. [44]

Molecule	Rotamer A			Rotamer B		
	$\Delta^{\dagger}_{elimA}$H	$\Delta^{\dagger,*}_{elimA}$H	Yield(%)	$\Delta^{\dagger}_{elimB}$H	$\Delta^{\dagger,*}_{elimB}$H	Yield(%)
NMe_2	41.3	98.6	-	29.9	87.4	6
NH_2	30.0	92.0	-	32.8	94.7	26
OMe	53.6	101.2	-	45.9	106.6	63
OH	49.1	90.6	-	42.9	105.3	30
H	56.6	108.6	29	56.6	108.6	29
F	56.9	109.2	-	53.5	110.6	-
Cl	59.3	124.3	-	59.2	110.1	-
CN	62.5	117.3	-	70.9	107.7	-
NO_2	79.8	127.2	-	79.6	104.0	-

Considering that the barrier for planarisation is a downhill process, as shown in section 4.4.1, only the ground and excited-state enthalpies of elimination for ortho-substituted benzylidene O-methyloximes are reported in Table 4.6. These enthalpies are presented in decreasing order of the electron-donating power to the increasing electron-withdrawing power of R. Each rotamer in Scheme 4.4 represent different starting geometry that can either lead to isomer A or B, whose scaffold structures are illustrated in Fig. 4.6.

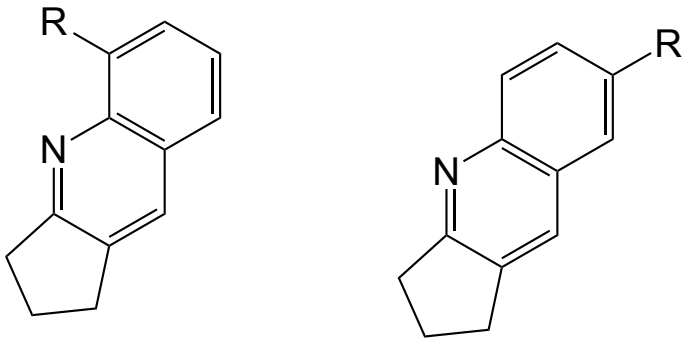

Fig. 4.6 Structure of isomer A (left) and isomer (B), which can respectively be synthesised from the photocyclisation of rotamer A or B of ortho-substituted-benzylidene O-methyloximes, Scheme 4.4. R represents the substituent and the methoxy group is the leaving group.

According to Table 4.6, it can be observed for both rotamer A and B that electron-donating groups all have a stabilising effect on the barrier for elimination for both the ground and the first singlet electronic excited-state. Meanwhile, electron-withdrawing groups all have a destabilising effect. However, it can be observed for rotamer B that the rotamer with R = F has a ground-state enthalpy of elimination, $\Delta^{\dagger}_{elim}$H, of 53.5 kJ mol^{-1}, which is slightly more stable than that the rotamer with R = H, whose ground-state enthalpy of elimination, $\Delta^{\dagger}_{elim}$H, is 56.6 kJ mol^{-1}. This should probably result from the fact that although fluorine is an inductive ring deactivating group, it also possesses a resonance electron-donating ability which activates the ring at the ortho and para positions, with the para position being more activated. This could also explain why R = Cl in rotamer A has a ground state enthalpy of elimination, $\Delta^{\dagger}_{elim}$H, of 56.9 kJ mol^{-1}, which is only about 0.3 kJ mol^{-1} different from that of R = H.

It can also be observed from Table 4.6 that the enthalpies for elimination for rotamer B are much lower than those of rotamer A. This can be linked to both

geometrical and electronic effects of the substituents. This could be because of the resonance-stabilisation effect from having a substituent on the para-position to the cyclisation centre. This resonance-stabilisation effect could also explain why the enthalpies of rotamer A and B are much lower than those previously obtained for para-substituted-benzylidene O-methyloximes in section 4.4.2.

Finally, enthalpies of elimination are much lower in the ground-state than in the first singlet electronic excited-state for both rotamers. This should further support a ground-state elimination pathway over an excited-state elimination pathway.

4.4.4 Literature context

From experimental studies, [44] product yields were recorded only for rotamer B, with electron-donating substituents Table 4.6. However, even though there were no reported experimental yields for compounds with R = F and Cl, cyclisation products were observed in complex mixtures whose purifications were not pursued. Finally compounds with electron-withdrawing groups, R = CN, NO_2 failed to form any product. [44]

Comparing the ground-state barrier for elimination with the experimental results shows that the enthalpies calculated in Table 4.6 correlate well with experimental results. Only systems with the lowest enthalpies of elimination formed products.

The barrier heights for elimination in the first singlet electronic excited-state do not favour the observed product selectivity obtained experimentally. This observation also supports ground-state elimination over elimination in the first singlet electronic excited-state. The enthalpies for internal conversion and ground-state planarisation, which are both exothermic are both recorded in Appendix (B).

4.4.5 Conclusion

So far it has been shown that substituents play an essential role in controlling non-oxidative eliminative cyclisation. In this study, substituents have been found to have an essential role in lowering the barrier heights to elimination as well as in predicting regio-selectivities. Moreover, since the elimination step is likely to proceed via the ground state, it means that other organic reactivity predictors for thermal eliminative processes can also be applied in predicting the outcome of the elimination step in non-oxidative cyclisation.

Bibliography

[1] Z. Wei, J. Wei, B. Bai, H. Wang, and M. Li, "Anion response of dimeric hydrazide derivatives: Dependence on the nature of terminal substituents," *Journal of Molecular Liquids*, vol. 204, pp. 100 – 105, 2015.

[2] G. Bouchoux, "Gas phase acidity of substituted benzenes," *Chemical Physics Letters*, vol. 506, no. 4, pp. 167 – 174, 2011.

[3] H. Backer, N. Nibbering, D. Espinosa, F. Mongin, and M. Schlosser, "Additivity of substituent effects in the fluoroarene series: Equilibrium acidity in the gas phase and deprotonation rates in ethereal solution," *Tetrahedron Letters*, vol. 38, no. 49, pp. 8519 – 8522, 1997.

[4] B. E. Ziegler and T. B. McMahon, "Computational analysis of substituent effects and Hammett constants for the ionization of gas phase acids," *Computational and Theoretical Chemistry*, vol. 1008, pp. 46 – 51, 2013.

[5] H. B. Watson, "Relationships between dipole moments and reaction velocities," *Transactions of the Faraday Society*, vol. 34, pp. 165–171, 1938.

[6] V. M. Vlasov, "Substituent effects on the activation parameters of snar reactions," *Russian Journal of Organic Chemistry*, vol. 46, no. 1, pp. 73–81, 2010.

[7] H. Gilow, "Substituent effects in electrophilic aromatic substitution. A laboratory in organic chemistry," *Journal of Chemical Education*, vol. 54, no. 7, p. 450, 1977.

[8] T. M. Krygowski, K. Ejsmont, B. T. Stepie, M. K. CyraaÑski, J. Poater, and M. Sola†, "Relation between the substituent effect and aromaticity," *The Journal of Organic Chemistry*, vol. 69, no. 20, pp. 6634–6640, 2004.

[9] M. P. Ranaia, I. Stojiljkovia, M. Milo, N. Prlainovia, M. Jovanoviaá, M. K. Milia, and A. D. Marinkovia, "Solvent and substituent effect on intramolecular charge transfer in 5-arylidene-3-substituted-2,4-thiazolidinediones: Experimental and theoretical study," *Arabian Journal of Chemistry*, 2016.

[10] C. S. Meira, J. M. dos Santos Filho, C. C. Sousa, P. S. Anjos, J. V. Cerqueira, H. A. D. Neto, R. G. da Silveira, H. M. Russo, J.-L. Wolfender, E. F. Queiroz, D. R. Moreira, and M. B. Soares, "Structural design, synthesis and substituent effect of hydrazone-n-acylhydrazones reveal potent immunomodulatory agents," *Bioorganic an Medicinal Chemistry*, vol. 26, no. 8, pp. 1971 – 1985, 2018.

[11] K. S. Varaksin, H. Szatylowicz, and T. M. Krygowski, "Towards a physical interpretation of substituent effect: Quantum chemical interpretation of Hammett substituent constants," *Journal of Molecular Structure*, vol. 1137, pp. 581 – 588, 2017.

[12] O. O. Wahab, L. O. Olasunkanmi, K. K. Govender, and P. P. Govender, "Synergistic effect of opposite polar substituents on selected properties of disperse yellow 119 dye," *Chemical Physics Letters*, vol. 704, pp. 55 – 61, 2018.

[13] S. Cumsille, J. Morales, C. Sandoval-Altamirano, G. Gather, A. Vega, and N. Pizarro, "Substituent effect of side chains on the photochemical behavior of a new generation 1,4-dihydropyridine: Lercanidipine," *Journal of Photochemistry and Photobiology A: Chemistry*, vol. 353, pp. 1 – 9, 2018.

[14] A. Martos, R. M. Sebastian, and J. Marquet, "Studies on the ring-opening polymerization of benzoxazines: Understanding the effect of the substituents," *European Polymer Journal*, vol. 108, pp. 20 – 27, 2018.

[15] C. Verma, L. Olasunkanmi, E. E. Ebenso, and M. Quraishi, "Substituents effect on corrosion inhibition performance of organic compounds in aggressive ionic solutions: A review," *Journal of Molecular Liquids*, vol. 251, pp. 100 – 118, 2018.

[16] Z. Yang and J. Xu, "Substituent effect on the diastereoselectivity in the sulfa-staudinger cycloaddition," *Tetrahedron*, vol. 71, no. 19, pp. 2844 – 2852, 2015.

[17] F. Chen, T. Tian, C. Zhao, B. Bai, M. Li, and H. Wang, "Substituent effect on photophysical properties of bi-1,3,4-oxadiazole derivatives in solution," *Journal of Molecular Structure*, vol. 1109, pp. 239 – 246, 2016.

[18] Y. W. Yoon, S. Y. Chae, and S. K. Lee, "Substituent effect on electronic transition energy of dichlorobenzyl radicals," *Chemical Physics Letters*, vol. 644, pp. 167 – 170, 2016.

[19] G. Karpiaska, A. P. Mazurek, and J. C. Dobrowolski, "On substituent effect on the benzodiazepinone system," *Computational and Theoretical Chemistry*, vol. 993, pp. 13 – 19, 2012.

[20] G. J. Chuang and C.-C. Liao, "Substituent effect on di-methane reactions of benzopyrazinobarrelenes and benzoquinoxalinobarrelenes," *Tetrahedron*, vol. 72, no. 10, pp. 1301 – 1315, 2016.

[21] Q. Wei, W. Wang, E. Zhou, X.-P. Liu, M.-H. Liang, K. Deng, J.-K. Yang, and P. Jiang, "Positioned substituent effect on self-assembly behaviors of perylene diimide derivatives on graphite," *Journal of Colloid and Interface Science*, vol. 504, pp. 58 – 67, 2017.

[22] T. Moriuchi-Kawakami, K. Kawata, S. Nakamura, Y. Koyama, and Y. Shibutani, "Design of bisquinolinyl malonamides as zn2+ ion-selective fluoroionophores based on the substituent effect," *Tetrahedron*, vol. 70, no. 52, pp. 9805 – 9813, 2014.

[23] L. Cui, H. Zhang, G. Zhang, Y. Zhou, L. Fan, L. Shi, C. Zhang, S. Shuang, and C. Dong, "Substituent effect on the acid-induced isomerization of spiropyran compounds," *Spectrochimica Acta Part A: Molecular and Biomolecular Spectroscopy*, vol. 202, pp. 13 – 17, 2018.

[24] Y. Shi, L. Fang, X. Li, L. Qu, and H. Shao, "The observation of ion-pairing effect based on substituent effect of ferrocene derivatives," *Journal of Electroanalytical Chemistry*, vol. 757, pp. 258 – 262, 2015.

[25] E. Bozkurt, H. I. Gul, and E. Mete, "Solvent and substituent effect on the photophysical properties of pyrazoline derivatives: A spectroscopic study," *Journal of Photochemistry and Photobiology A: Chemistry*, vol. 352, pp. 35 – 42, 2018.

[26] J. Zhang, M. She, J. Li, C. Wang, S. Wang, P. Liu, S. Zhang, and J. Li, "Substituent effect on fluorescence signaling of the naphthalene carbohydrazone based chemosensor: Its implication in the detection of Zn(II) ions and

secondary sensing PPi," *Sensors and Actuators B: Chemical*, vol. 270, pp. 362 – 370, 2018.

[27] K. ichi Nihei and I. Kubo, "Substituent effect of benzaldehydes on tyrosinase inhibition," *Plant Physiology and Biochemistry*, vol. 112, pp. 278 – 282, 2017.

[28] P. Rempala, J. Kroulik, and B. T. King, "A slippery slope:Aâ mechanistic analysis of the intramolecular scholl reaction of hexaphenylbenzene," *Journal of the American Chemical Society*, vol. 126, no. 46, pp. 15002–15003, 2004.

[29] B. T. King, J. Kroulik, C. R. Robertson, P. Rempala, C. L. Hilton, J. D. Korinek, and L. M. Gortari, "Controlling the Scholl reaction," *The Journal of Organic Chemistry*, vol. 72, no. 7, pp. 2279–2288, 2007.

[30] J. L. Ormsby, T. D. Black, C. L. Hilton, Bharat, and B. T. King, "Rearrangements in the Scholl oxidation: implications for molecular architectures," *Tetrahedron*, vol. 64, no. 50, pp. 11370 – 11378, 2008.

[31] H.-W. Ip, H.-F. Chow, and D. Kuck, "Electronic and steric effects on the three-fold Scholl-type cycloheptatriene ring formation around a tribenzotriquinacene core," *Organic Chemistry Frontiers*, vol. 4, pp. 817–822, 2017.

[32] F. B. Mallory, C. S. Wood, and J. T. Gordon, "Photochemistry of stilbenes. III. Some aspects of the mechanism of photocyclization to phenanthrenes," *Journal of the American Chemical Society*, vol. 86, no. 15, pp. 3094–3102, 1964.

[33] M. F. Budyka, N. I. Potashova, T. N. Gavrishova, and V. M. Li, "Photoisomerization and photocyclization of 4-styrylquinoline derivatives," *High Energy Chemistry*, vol. 43, no. 5, pp. 370–376, 2009.

[34] M. F. Budyka, N. I. Potashova, T. N. Gavrishova, and V. M. Lee, "The effect of substituents in the styryl moiety on the photocyclization of 4-styrylquinoline derivatives," *High Energy Chemistry*, vol. 44, no. 5, pp. 404–411, 2010.

[35] L. W. H., "Aspects of the photochemistry of aryl ethylenes," *Pure and applied chemistry*, vol. 56, no. 9, pp. 1225–1240, 1984.

[36] M. Irie, K. Sakemura, M. Okinaka, and K. Uchida, "Photochromism of dithienylethenes with electron-donating substituents," *The Journal of Organic Chemistry*, vol. 60, no. 25, pp. 8305–8309, 1995.

[37] T. Michinori, O. Miwa, M. Keisuke, and Y. Takehiko, "Synthesis and photochromic reaction of 1,2-diphenylperfluorocyclopentenes," *Journal of Physical Organic Chemistry*, vol. 16, no. 2, pp. 148–151, 2003.

[38] O. A. Fedorova, E. N. Gulakova, Y. V. Fedorov, I. E. Lobazova, M. V. Alfimov, and G. Jonusauskas, "A photochemical electrocyclization of the benzothiazolylphenylethenes involving a CN bond formation," *Journal of Photochemistry and Photobiology A: Chemistry*, vol. 196, no. 2, pp. 239 – 245, 2008.

[39] C. Fan, S. Pu, G. Liu, and T. Yang, "Substituent position effect on the properties of isomeric photochromic diarylethenes bearing chlorine atoms," *Journal of Photochemistry and Photobiology A: Chemistry*, vol. 194, no. 2, pp. 333 – 343, 2008.

[40] S. Pu, C. Fan, W. Miao, and G. Liu, "The effect of substituent position upon unsymmetrical isomeric diarylethenes bearing a methoxy group," *Dyes and Pigments*, vol. 84, no. 1, pp. 25 – 35, 2010.

[41] Y.-Z. Chen, C.-W. Ni, F.-L. Teng, Y.-S. Ding, T.-H. Lee, and J.-H. Ho, "Construction of polyaromatics via photocyclization of 2-(fur-3-yl)ethenylarenes,

using a 3-furyl group as an isopropenyl equivalent synthon," *Tetrahedron*, vol. 70, no. 9, pp. 1748 – 1762, 2014.

[42] X. Zhao and J. D. Rainier, "Pyridone photoelectrocyclizations to pyridophenanthrenes," *Tetrahedron*, vol. 73, no. 32, pp. 4786 – 4789, 2017.

[43] W. Hao, X. Haodong, L. Yuan, Q. Yanjun, C. Yijing, and Z. Gang, "Electron donor and acceptor functionalized dithienylethenes: Effects of charge density on photochromic properties," *Physical Chemistry Chemical Physics.*, vol. 20, pp. 14348–14356, 2018.

[44] M. Austin, O. J. Egan, R. Tully, and A. C. Pratt, "Quinoline synthesis: Scope and regiochemistry of photocyclisation of substituted benzylidenecyclopentanone o-alkyl and o-acetyloximes," *Organic and Biomolecular Chemistry*, vol. 5, pp. 3778–3786, 2007.

[45] A. Behn, P. M. Zimmerman, A. T. Bell, and M. Head-Gordon, "Efficient exploration of reaction paths via a freezing string method," *The Journal of Chemical Physics*, vol. 135, no. 22, p. 224108, 2011.

[46] S. Mallikarjun Sharada, P. M. Zimmerman, A. T. Bell, and M. Head-Gordon, "Automated transition state searches without evaluating the hessian," *Journal of Chemical Theory and Computation*, vol. 8, no. 12, pp. 5166–5174, 2012.

[47] J. Baker, "An algorithm for the location of transition states," *Journal of Computational Chemistry*, vol. 7, no. 4, pp. 385–395, 1986.

[48] Y. Shao, Z. Gan, E. Epifanovsky, A. T. B. Gilbert, M. Wormit, J. Kussmann, A. W. Lange, A. Behn, J. Deng, X. Feng, D. Ghosh, M. Goldey, P. R. Horn, L. D. Jacobson, I. Kaliman, R. Z. Khaliullin, T. Kús, A. Landau, J. Liu, E. I. Proynov, Y. M. Rhee, R. M. Richard, M. A. Rohrdanz, R. P. Steele, E. J.

Sundstrom, H. L. Woodcock III, P. M. Zimmerman, D. Zuev, B. Albrecht, E. Alguire, B. Austin, G. J. O. Beran, Y. A. Bernard, E. Berquist, K. Brandhorst, K. B. Bravaya, S. T. Brown, D. Casanova, C.-M. Chang, Y. Chen, S. H. Chien, K. D. Closser, D. L. Crittenden, M. Diedenhofen, R. A. DiStasio Jr., H. Dop, A. D. Dutoi, R. G. Edgar, S. Fatehi, L. Fusti-Molnar, A. Ghysels, A. Golubeva-Zadorozhnaya, J. Gomes, M. W. D. Hanson-Heine, P. H. P. Harbach, A. W. Hauser, E. G. Hohenstein, Z. C. Holden, T.-C. Jagau, H. Ji, B. Kaduk, K. Khistyaev, J. Kim, J. Kim, R. A. King, P. Klunzinger, D. Kosenkov, T. Kowalczyk, C. M. Krauter, K. U. Lao, A. Laurent, K. V. Lawler, S. V. Levchenko, C. Y. Lin, F. Liu, E. Livshits, R. C. Lochan, A. Luenser, P. Manohar, S. F. Manzer, S.-P. Mao, N. Mardirossian, A. V. Marenich, S. A. Maurer, N. J. Mayhall, C. M. Oana, R. Olivares-Amaya, D. P. O'Neill, J. A. Parkhill, T. M. Perrine, R. Peverati, P. A. Pieniazek, A. Prociuk, D. R. Rehn, E. Rosta, N. J. Russ, N. Sergueev, S. M. Sharada, S. Sharmaa, D. W. Small, A. Sodt, T. Stein, D. Stück, Y.-C. Su, A. J. W. Thom, T. Tsuchimochi, L. Vogt, O. Vydrov, T. Wang, M. A. Watson, J. Wenzel, A. White, C. F. Williams, V. Vanovschi, S. Yeganeh, S. R. Yost, Z.-Q. You, I. Y. Zhang, X. Zhang, Y. Zhou, B. R. Brooks, G. K. L. Chan, D. M. Chipman, C. J. Cramer, W. A. Goddard III, M. S. Gordon, W. J. Hehre, A. Klamt, H. F. Schaefer III, M. W. Schmidt, C. D. Sherrill, D. G. Truhlar, A. Warshel, X. Xua, A. Aspuru-Guzik, R. Baer, A. T. Bell, N. A. Besley, J.-D. Chai, A. Dreuw, B. D. Dunietz, T. R. Furlani, S. R. Gwaltney, C.-P. Hsu, Y. Jung, J. Kong, D. S. Lambrecht, W. Liang, C. Ochsenfeld, V. A. Rassolov, L. V. Slipchenko, J. E. Subotnik, T. Van Voorhis, J. M. Herbert, A. I. Krylov, P. M. W. Gill, and M. Head-Gordon, "Advances in molecular quantum chemistry contained in the Q-Chem 4 program package," *Mol. Phys.*, vol. 113, pp. 184–215, 2015.

[49] K. E. Riley, B. T. Op't Holt, and K. M. Merz, "Critical assessment of the performance of density functional methods for several atomic and molecular properties," *Journal of Chemical Theory and Computation*, vol. 3, no. 2, pp. 407–433, 2007.

[50] J. Tirado-Rives and W. L. Jorgensen, "Performance of B3LYP density functional methods for a large set of organic molecules," *Journal of Chemical Theory and Computation*, vol. 4, no. 2, pp. 297–306, 2008.

CHAPTER 5

A New Photocyclisation Reactivity Predictor

5.1 Introduction

Before attempting chemical synthesis, synthetic chemists often perform thorough synthetic planning for the reaction under consideration. This might involve sampling of the most cost-effective reagents or building blocks that will lead to the desired product in high yield. Alternatively, this may involve an in-depth study of the primary reactants with critical consideration of all the possible outcomes that could result from the synthesis. Finally, it may involve making an educated guess of the reaction mechanism leading to the desired product to enable better control of the reaction. In most cases, this synthetic planning is often limited to performing a literature survey, which is followed by "trial-and-error" synthesis before arriving at the desired product. However, doing this is not always efficient and cost-effective, because it can lead to a significant wastage of chemical resources as well as time, and may even be physically risky for certain chemical reactions. [1]

One alternative to help guide synthetic planning is to couple literature survey with the application of computational chemistry techniques. Although there are many computational chemistry approaches, quantum computational chemistry has emerged as the best developed and most intuitive approach for synthetic planning. This is achieved by either mapping out stationary points along the potential-energy surface for the minimum energy path of a given reaction and/or through applying rule-based parameters known as reactivity predictors.

Mapping out stationary points along the potential-energy surface for a reaction involves a careful determination of energy and geometric coordinates of reactants, products, intermediates, and all possible transition states that define the minimum energy path of the reaction. Although this approach provides intuitive thermody-

namic and kinetic information about the reaction, synthetic chemists find it less appealing, [2] because it can be very time consuming, especially if results within chemical accuracy (1 kcal mol^{-1}) are desired. [3] Besides, this is not a black-box approach, meaning that a certain level of knowledge, skill, and understanding of quantum computational chemistry methods are required.

On the other hand, reactivity predictors involve computing some properties of the reactant and correlating them with observed chemical reactivities for a class of reaction. [4] Most frequently, reactivity predictors are based on the analysis of electronic properties of molecules (charge density, electrostatic potential, molecular orbitals) because chemistry is mostly concerned with the position and movement of electrons. [2] The computation of these properties is usually less computationally demanding in comparison to mapping out stationary points on the potential-energy surface for the minimum energy path of a reaction. Moreover, reactivity predictors are mostly implemented as black-box methods, which do not require any expertise in computational chemistry making them more appealing for synthetic planning.

A plethora of reactivity predictors have been implemented to determine reactive species or sites in molecules of nucleophilic/electrophile addition and substitution reactions. [5–21] However, not much has been done towards designing reactivity predictors for planarisation and elimination in eliminative cyclisation reactions despite their utility in synthesising polyaromatic compounds, which are building blocks for organic semiconductors. [22–25] Some old reactivity predictors do exist for predicting the propensity of a molecule to photoplanarise. However, these predictors are not broadly and widely applicable, so have fallen out of use.

This chapter is aimed at designing a more robust reactivity predictor specifically

for predicting photoplanarision. The focus is on photocyclisation reactions because they are easier and less sensitive to reaction conditions in comparison to thermal eliminative cyclisation, as shown in chapter 3. These reactions are more synthetically useful and widely applied in synthesis.

In the following sections that, existing reactivity predictors for photocyclisation will briefly be reviewed. This will be followed by implementation of a new reactivity predictor for photocyclisation.

5.2 Existing reactivity predictors for photocyclisation

The existing reactivity predictors for photocyclisation are all based on predicting the propensity of photo-induced 6-π electrocyclisation, otherwise known as photoplanarisation. For the rest of this thesis, reactivity predictors for photocyclisation will refer to predicting photoplanarisation except where otherwise stated. All the existing reactivity predictors were formulated from the Hückel molecular orbital theory. A summary of these reactivity predictors, including their basic tenets, is described below.

5.2.1 Localisation energy

Electron localisation energy and free valence index were first introduced by Scholz and co-workers. [26] Scholz defined the electron localisation energy, L^*, for a photocyclisation system as the difference in energy between the first singlet π electronic excited-state of the reactant molecule and the ground-state of the dihydrointermediate, whose structures are illustrated in Fig. 5.1 and calculated according to equation(5.1). [26]

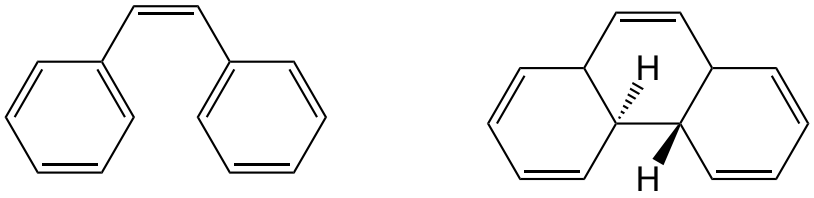

Fig. 5.1 Reactant (left) and dihydro-intermediate (right) whose energies are used in calculating the electron localisation energy.

$$L^* = R^* - I \tag{5.1}$$

Here R^* is the π-electron energy for the first singlet electronic excited-state of the reactant molecule, I is the ground-state π-electron energy for the dihydro-intermediate, all calculated from Hückel molecular orbital theory.

In the prediction of the outcome for a photochemical cyclisation reaction, Scholz hypothesised that cyclisation would most favourably proceed via the formation of the dihydro-intermediate with the lowest value of L^*. This results from the fact that R^* and I are both negative energies. However, I is less negative because the dihydro-intermediate has fewer π-electrons, which makes it less stable. Therefore, reactants or conformers forming a more stable dehydro-intermediate will be the most likely to give cyclisation products.

5.2.2 Free valence index

The free valence index, which was originally conceived by Coulson, the degree to which atoms in a molecule are bonded to other atoms relative to a theoretical maximum bonding power. The rationale here is that every atom in a molecule

has a valency that must be satisfied as it bonds to other atoms in a molecule. So, atoms whose valencies are not fully satisfied, or atoms with free valences, are active sites in the molecule that are most susceptible to form new chemical bonds. [27] Coulson defined the free valence index, V_r, of an atom r, as the difference between the sum of all bond orders of bonds formed by atom r to a theoretical maximum bond order empirically defined for the bond type. The formula for calculating the free valence index is given by equation (5.2).

$$V_r = N_{max} - N_r \tag{5.2}$$

Here N_r is the sum of π-bond orders for all the bonds joining atom r to the remainder of the system; N_{max} is the theoretical maximum π-bonding power that atom r can have in any chemical system.

The theoretical maximum bond order power, N_{max}, for an sp^2 hybridised carbon is $\sqrt{3}$. This value is calculated from trimethylene methane as described in Appendix (C). The π-bond order, $P_{r,s}$, between any two bonds, r and s, is calculated from the simple Hückel molecular orbitals using equation (5.3). [28]

$$P_{r,s} = \sum_{i=1}^{K} n_i a_{ri} a_{si} \tag{5.3}$$

n_i is the number of electrons in each occupied orbital, a_{ri} and a_{si} are the atomic orbital coefficients for atom r and s respectively, and the sum is taken over all the K occupied orbitals.

In order to use this concept in predicting photocyclisation, Scholz and co-workers calculated the free valence indices, V_r^*, in the first π-excited state for each cyclising atom as expressed in equation (5.4).

$$V_r^* = \sqrt{3} - \sum_i P_{r,i}^* \tag{5.4}$$

The second term in equation (5.4) represents the sum of all π-bond orders formed by r in the molecule for its first π-excited state. The authors reported from this calculation that the preferred mode for ring closure is between atoms with the largest value of V_r^*.

Case study - localisation energy and free valence index

One example of the use of free valence index, V_r^* in the first excited-state and the electron localisation energy, L^*, was in predicting the mode of cyclisation in 2-styryl naphthalene, 5.1, 1,2-di(2-naphthyl)ethyl, 5.2 and 1-(1-naphthyl)-2-(2-naphthyl)ethyl, 5.3. These molecules are illustrated in Fig. 5.2 and their free valence indices, V_r^*, in the first excited-state and their electron localisation energies, L^*, are presented in Table 5.1.

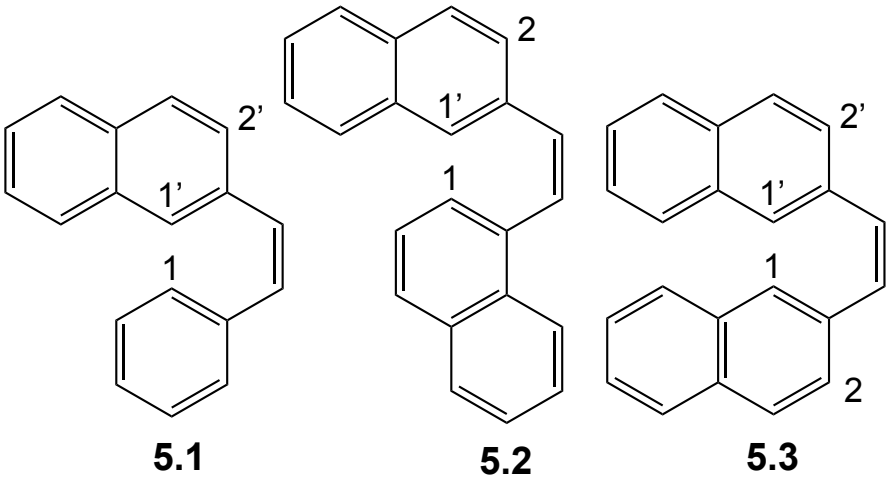

Fig. 5.2 Illustration of 2-styryl naphthalene, 5.1, 1,2-di(2-naphthyl)ethyl, 5.2 and 1-(1-naphthyl)-2-(2-naphthyl)ethyl, 5.3.

Table 5.1 An illustration of the use of free valence index, V_r^* in the first excited state and the localisation energy, L^*, in predicting the mode of cyclisation in 2-styryl naphthalene, 5.1, 1,2-di(2-naphthyl)ethyl, 5.2 and 1-(1-naphthyl)-2-(2-naphthyl)ethyl, 5.3, where p is indicates that a product is formed. [26]

Molecule	Atom position	V_r^*	Bond formed	L^*	Observed product %
5.1	1'	0.504	1, 1'	3.114	p
	1	0.667			
	2	0.450	1, 2	3.472	0
5.2	1'	0.610	1, 1'	3.106	p
	1	0.493			
	2	0.455	1, 2	3.472	0
5.3	1 = 1'	0.630	1, 1'	2.922	p
			1, 2'	3.281	p
	2 = 2'	0.452	2, 2'	3.622	0

For all molecules presented in Table 5.1, atom 1 and 1' have the largest V_r^* and the lowest L^* between them. This implies that these atoms have the smallest π character, which makes them more suitable for bond formation. Moreover, the lowest values of L^* show that the intermediates resulting from bonds formed between these atoms are the most stable. Therefore, the predicted mode of ring closure would be via bond formation between these two atoms. [26] However, this prediction is vague, given that it does not give any idea of how large V_r^* or how small L^* should be for a product to be formed.

5.2.3 Laarhoven rules for photocyclisation

In 1968, Laarhoven proposed a critical value for the free valence index, V_r^*, in the first excited-state and the localisation energy, L^* [29]. From a series of calculations on different photocyclisable systems, Laarhoven postulated that a system would photocyclise if L^* is less than $3.450(\beta)$, where β is an empirical value for the Coulombic interatomic electronic interaction, which has a commonly agreed value of -0.7 eV. From a conceptual standpoint, L^* values are more meaningful because they are easy to interpret and have an actual physical interpretation, since they represent an energy difference between two molecular electronic configurations. However, L^* values were less commonly used because, at the time of its development, there were limited computational resources and they were considered to be computationally very demanding since one computation had to be carried out for the reactant and another one for the dihydro-intermediate. [30]

V_r^* was more appealing since one calculation on a reactant molecule was sufficient to completely describe the free valencies for all atoms in the molecule.

In order to predict the susceptibility of a cyclisation that proceeds via bond formation between atom r and s, the sum of free valence indices in the first excited-state,$V_{r,s}^*$, is calculated for these atoms as shown in equation (5.5).

$$V_{r,s}^* = V_r^* + V_s^* \tag{5.5}$$

Here V_r^* and V_s^* are the first excited-state free valence indices of atoms r and s, respectively. After evaluating $V_{r,s}^*$ for a series of photocyclisable systems, the following rules for predicting photocyclisation were established, formally known as Laarhoven rules. [31]

1. A system will undergo photocyclisation via bond forming between atom r and s only when $V^*_{r,s}$ is greater than 1.0.

2. When two or more isomers can be formed from a given photocyclisation reaction, only one product will be formed if the difference in the first excited-state free valence indices, $\Delta V^*_{r,s}$ for both isomers, is greater than 0.1.
   Here $\Delta V^*_{r,s} = V^*_{r,s}(1)$ - $V^*_{r,s}(2)$ with (1) and (2) representing isomers one and two respectively.

3. When a planar and a non-planar product can arise from a given photocyclisation reaction, the planar aromatic compound will be the main product provided $V^*_{r,s} > 1$.

Case study - Laarhoven's rules

An example of the illustration of these rules is found in Scheme 5.1. Compound 5.4, with $V^*_{1,2} = 1.111$ photocyclises to 5.6 with 60% yield. However, no cyclisation product is obtained for 5.7 with $V^*_{1,2'} = 0.941$, as predicted by the first rule. On the other hand, compound 5.5 in which $V^*_{1,2} = 1.095$ and $V^*_{1,2'} = 1.188$, gives only one product. In this case, only the planar isomer, 5.7, is formed with a 75% yield. No product yield is recorded for the non-planar isomer, 5.6, which follows from the third rule that the planar compound will be the main cyclisation product in cases where both planar and non-planar compounds can be formed. [32]

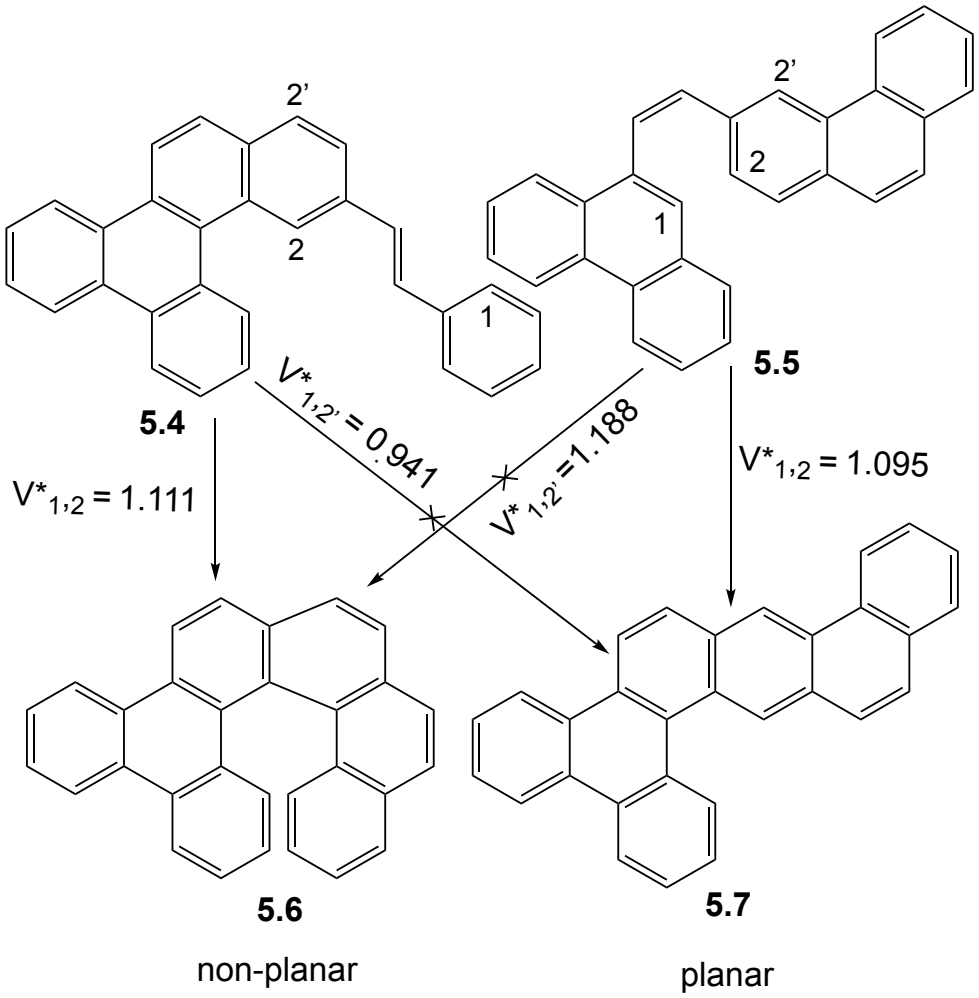

Scheme 5.1 Illustration of an application of Laarhoven's rules. $V^*_{1,2}$ represents the sum of first excited-state free valence index between atom 1 and 2. $V^*_{1,2'}$ presents those for atom 1 and 2'. [30]

5.2.4 Variation in electronic overlap population

Another approach for predicting photocyclisation is based on applying the Mulliken overlap populations $n_{r,s}$ calculated from the Hückel theory. [33, 34] The rationale in this approached was based on the fact that interactions between bonding centres can intuitively be deduced by calculating their electronic overlap population.

Muszkat *et al.*, calculated the electronic overlap between two cyclisation centres r and s in the ground and the first singlet excited-state for reactant molecules as a measure for predicting photocyclisation reaction. [35, 36] They used the difference in electronic overlap between both states, $\Delta n^*_{r,s}$, as a measure for evaluating how this interaction changes between both states. [37, 38]

$$\Delta n^*_{r,s} = n^*_{r,s} - n_{r,s} \tag{5.6}$$

Here $n^*_{r,s}$ is the electronic overlap between atom r and s in the excited-state; $n_{r,s}$ is the electronic overlap population between these atoms in the ground-state; and r and s represent the atoms forming the new σ-bond in the cyclisation reaction.

Positive values of $\Delta n^*_{r,s}$ are hypothesised to indicate a bonding interaction between atom r and s, consequently favouring the propensity for bond formation between these atoms during photocyclisation. Negative values of $\Delta n^*_{r,s}$ suggest antibonding interactions, thus disfavouring new bond formation, which is interpreted as disfavouring photocyclisation. [39]

Unlike Laarhoven's rules, this reactivity predictor was less successful in predicting photocyclisation, because Laarhoven's rules are more straightforward and easier to implement. The only times this was used as reactivity predictors were for syntheses authored by Muszkat. [39]

5.2.5 Variation in bond order

The final existing reactivity predictor for photocyclisation involved analysing the changes in Coulson bond order between the ground and the first singlet electronic excited state, again calculated from Hückel molecular orbital theory. [40–42] The rationale in this model was based on the fact that changes in bonding patterns

that result from the deactivation of an electronic excited-state correspond to the molecular rearrangements that lead to the formation of the photochemical product. A qualitatively easy way to evaluate these changes in bonding pattern is by evaluating how the bond orders in the molecule change in states.

Minot and co-workers suggested that the most critical changes in bonding pattern in the first singlet electronic excited-state for a photocyclisation system would correspond to the formation of a new σ-bond. Consequently, a large bond order in the first singlet excited-state between atoms forming the new bond will imply a high bonding interaction and therefore, a higher propensity for a σ- bond to be formed between both atoms, and vice versa. They evaluated this by calculating the variation in the bond order, $\Delta P^*_{r,s}$, for this centre in the ground and excited-state as shown in equation (5.7).

$$\Delta P^*_{r,s} = P^*_{r,s} - P^*_{r,s} \tag{5.7}$$

Here r and s, represent the two atoms between which the new σ-bond would formed during cyclisation. $P^*_{r,s}$ and $P_{r,s}$ are, respectively, the first singlet electronic excited-state and ground-state bond orders between both atoms. A positive value of $\Delta P^*_{r,s}$ implies a higher propensity to photocyclise, and vice versa. [43]

Similarly to the variation in electronic overlap population, these reactivity predictors have fallen short of use. Again, the only publications in which they were used are from papers authored by Minot *et al* and Laarhoven. [30]

5.2.6 Summary

A summary of key aspects of these existing reactivity predictor is presented in Table 5.2. Of all four existing reactivity predictors, $V^*_{r,s}$ is the most straightforward and preferentially used. Due to the limited computational resources at the time of creation, L^* was seldom used and, as a consequence, it is difficult to conclude on its predictive power. $\Delta n^*_{r,s}$ and $\Delta P^*_{r,s}$ are a little more complicated to implement, which significantly limited their application.

Table 5.2 Summary of the used of localisation energy, L^*, sum of excited-state free valence index, $V^*_{r,s}$, variation in atomic overlap, $\Delta n^*_{r,s}$, and variation in bond order, $\Delta n^*_{r,s}$ in predicting photocyclisation

Reactivity predictor	Definition	Prediction
L^*	Difference in excited-state energy of reactant and dihydro-intermediate	Molecule should photocyclise if $L^* < 3.450(\beta)$
$V^*_{r,s}$	Sum of excited-state free valence of atom r and s, which form the putative bond during photocyclisation	Molecule should photocyclise if $V^*_{r,s} > 1.0$
$\Delta n^*_{r,s}$	Change in electronic overlap between ground and excited-state for atom r and s that forms the σ-bond during cyclisation	Molecule photocyclises if $\Delta n^*_{r,s}$ is largely positive number

Continues on next page

Table 5.2 – *Continued from previous page*

Reactivity predictor	Definition	Prediction
$\Delta P^*_{r,s}$	Variation in bond order between ground and excited-state for atom r and s forming the new bond	Molecule photocyclises if $\Delta P^*_{r,s} > 0$

5.2.7 Limitations of existing reactivity predictors

The existing reactivity predictors for photocyclisation have fallen short of use in recent years. There are so far few or no publications where these reactivity predictors were used in synthetic planning. The only instances where these reactivity predictors were applied are from papers published in the 1980s and the early 1990s, mostly authored by the developers of these predictors and mostly applied to justify observed results rather than make accurate de novo predictions.

The main reason for this decline of reactivity predictors is that they are based on Hückel theory, which is no longer in used except as an introductory method in textbooks. Its inherent oversimplification on the wave function and the molecular Hamiltonian limits its application to π-conjugated hydrocarbons, and more advanced wave-function or density-functionals methods are required to enable the inclusion of a broader range of systems.

Apart from the localisation energy, all other reactivity predictors rely on analysing changes in electron distribution between the ground and the first singlet electronic

excited-state. The problem with this approach stems from the fact that electrons are delocalised over the entire molecular orbital of a molecule. Analysing changes in electron distribution will depend on the population analysis method that is being used to arbitrary distribute electrons to different atoms in the molecule; and there is no agreed standard for judging the correctness of a population analysis method since there are no corresponding experimental observables. [44]

5.3 Rationale for new reactivity predictor

Upon outlining the fundamental principles and reasons for the fall in use of existing reactivity predictors for photocyclisations, it is evident that a new generation of reactivity predictors is required. To do this, it is important to take a step back and reiterate the purpose and essence of a reactivity predictor. A reactivity predictor is a cheap, fast and easy-to-understand parameter that can be used to pull out qualitatively important information about the most important points on the PES of a reaction. In order to design a new reactivity predictor, it is important to give a careful thought what changes in molecular properties are important in gaining useful and reasonable qualitative insight about the rate-determining step of the reaction in question.

In principle, a PES is a plot of how the energy of a molecule changes along all possible degrees of freedoms for a given reaction. In this scheme, the rate-determining step is found by identifying the highest energy point on the PES corresponding to changes in the most important degree of freedom along which the reaction proceeds. Consequently, the rate-determining step is vertically linked to the energy and horizontally linked to a change in a particular set of molecular coordinates. We could resort to finding ways of predicting the patterns or directions along which these sets of coordinates will change rather than trying to estimate the energy of

the rate-determining step. The idea is first to make an educated guess on the most critical changes in the molecular coordinates that will correspond to the most significant changes in the degree of freedom at the rate-determining step and then devise an easy way to estimate these changes in a qualitative manner.

In a photochemical reaction, light absorption often leads to a change in the bonding pattern of the atoms that contribute to the HOMO and the LUMO, which correspond to the first singlet electronic excited-state. For a photocyclisation reaction, it could hypothesise that, if this region is located on the putative forming ring, then the most considerable changes in the bonding pattern will occur between the atoms that make up this ring.

Since photoplanarisation is a necessary precondition for photocyclisation that relies on a molecule's inherent ability to absorb light and undergo 6-π electrocyclisation, the necessity for predicting this step is of great importance. If the planarisation step can successfully be predicted, product formation will simply rely on optimising reaction conditions to favour the elimination. Based on this hypothesis, the remaining task is to devise a means to qualitatively predict or quantify the changes in bonding pattern within the putative forming ring in the first singlet electronic excited-state in a quick, easy and robust way without having to perform multiple time-consuming computations.

5.3.1 Induced atomic forces upon vertical excitation

When a molecule absorbs a photon of light and is excited to its first singlet electronic excited-state, the instantaneous changes in electron distributions resulting from this excitation induces forces on the atoms within the molecule. These forces act by driving the atoms in the molecule to reorganise from their initial ground-

state conformation towards the excited-state equilibrium geometry. If the directions of these forces are consistent with driving the atoms in the molecule towards becoming planar or more aromatic-like, then it is likely that the molecule will photoplanarise. Consequently, these induced forces can be used as a proxy for predicting whether an initial electronic excitation would lead to a 6-π electrocyclisation reaction.

This can be done either by: 1) evaluating the components of the induced forces along the torsional coordinate about which bond rotation occurs in the putative forming ring during planarisation and/or 2) evaluating the components of the induced forces along bond vectors within the putative forming ring. Evaluating the components of the induced forces along the torsional coordinates along which bond rotation occurs is more intuitive. This is because it directly points out whether the induced forces act by decreasing or increasing the torsional angle, which could favour or disfavour photoplanarisation. Since torsional barriers are usually quite low, [45, 46] these forces will be relatively small and might not be so easy to detect. On the other hand, evaluating the components of the induced forces along the bond vectors in the putative forming ring provides information on the changes in bonding patterns that would likely occur in the ring. Consequently, this can be used to predict whether the changes in bonding patterns would lead to the putative forming ring becoming more aromatic-like or not.

5.4 Methodology and computational details

5.4.1 Force projection on bond vector

Consider the scaffold for the putative forming ring of a hypothetical photocyclisation to be represented by Scheme 5.2. The atoms constituting the putative forming

ring are labelled 1 to 6.

Scheme 5.2 Scaffold for the putative forming ring of a hypothetical photocyclisation system. The numbers 1- 6 represent atom labelings for atoms found in the putative forming ring. R_1 and R_2 represent any ring substituents

For any two atoms in the putative forming ring represented by the position vectors $\boldsymbol{r_1}$ and $\boldsymbol{r_2}$, respectively, the atomic forces are $\boldsymbol{f_1}$ and $\boldsymbol{f_2}$, respectively. The bond vector between these two atoms can be represented by $\boldsymbol{r_{1,2}}$ and the force vector by $\boldsymbol{f_{1,2}}$. The component of the force, $F_{1,2}$, along the bond vector $\boldsymbol{r_{1,2}}$ can be evaluated from equation (5.8).

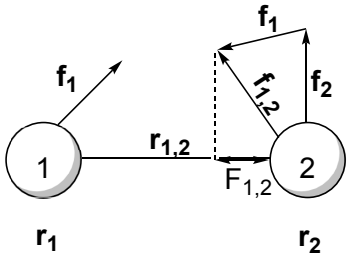

$$F_{1,2} = \frac{\boldsymbol{f_{1,2}}.\boldsymbol{r_{1,2}}}{||\boldsymbol{r_{1,2}}||} \tag{5.8}$$

To be consistent with 6-π electrocyclisation, the components of the induced forces along each π-bond vector should adopt a positive value, which is indicative of double-bond lengthening. The combine components of these induced forces, F^*_π, on the π-bonds vectors for atoms in the putative forming ring can be obtained by

summing up the components of the forces on each pair of atoms forming a double bond in the putative forming ring as given by equation (5.9).

$$F_{\pi}^{*} = F_{1,2} + F_{3,4} + F_{5,6} \tag{5.9}$$

The components of the forces along each single bond vector in the putative forming ring should adopt a negative value, which is indicative of σ-bond shortening. Moreover, the combine components of the induced forces on all σ-bond vectors, F_{σ}^{*}, is given as the sum of the components of the forces on each pair of atoms forming a single bond in the putative forming ring as shown in (5.10).

$$F_{\sigma}^{*} = F_{2,3} + F_{4,5} \tag{5.10}$$

Finally, the combine components of these forces on all bond vectors, $F_{\pi,\sigma}^{*}$, in the putative forming ring is the difference between F_{π}^{*} and F_{σ}^{*} as given by equation (5.11).

$$F_{\pi,\sigma}^{*} = F_{\pi}^{*} - F_{\sigma}^{*} \tag{5.11}$$

5.4.2 Data set

The dataset in this chapter is composed of 34 aromatic hydrocarbons with published free valence indices. [29,30,47,48] Their experimental yields are also selected from the same published literatures. The structures of these molecules and their free valence indices computed by Laarhoven *et al* are presented in Table 5.3 in the results section.

5.4.3 Procedure

For each reactant molecule, an approximate guess geometry was constructed using the Avogadro 1.2.0 molecular builder software. [49] Each starting geometry was constructed so that the atoms forming the new bond were in a cis-configuration

relative to each other. This was done for all possible conformers resulting in different isomeric products. The geometries of these guess structures were then optimised in the ground-state using the methods described in chapter 2. From these ground-state optimised geometries, the Cartesian position vector for each atom in the putative forming ring was selected, from which the bond vectors were calculated. The energy gradients, from which the force vectors were calculated from, were computed in the first singlet electronic excited-state at the ground-state optimised geometries for each reactant conformer. The components of the induced forces in the putative forming ring for all the conformers were then computed using an analysis script implemented in Python 2.7.10

5.5 Results and Discussion

The components of the forces, F^*_π, F^*_σ, $F^*_{\pi,\sigma}$, along π-bond vectors, σ-bonds and for all the bond vector of atoms constituting the putative forming ring are presented in Table 5.3. These results are presented alongside Laarhoven free valence indices, $V^*_{r,s}$, where r and s correspond to the atoms that are susceptible to form the new bond in the planarisation step.

Table 5.3 Molecules, sums of free valence indices, $V^*_{r,s}$, components of induced forces along π-bond vectors, F^*_π, σ-bond vectors, F^*_σ, both π and σ-vectors along the putative forming. All components of induced forces along the putative forming are given in E_h/a_0. r and s correspond to atoms between which the new bond is formed during planarisation.

Molecule	r, s	$V^*_{r,s}$	F^*_π	F^*_σ	$F^*_{\pi,\sigma}$	Yields %
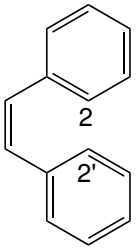 **5.13**	a = 2,2'	1.050 [x]	0.257	-0.214	0.471	P
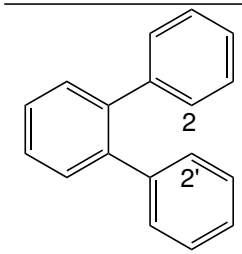 **5.14**	a = 2,2'	1.028 [x]	0.184	-0.172	0.356	P

Continues on next page

Table 5.3 – *Continued from previous page*

Molecule	r, s	$V^*_{r,s}$	F^*_π	F^*_σ	$F^*_{\pi,\sigma}$	Yields %
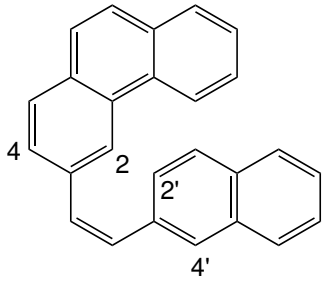 **5.15**	a = 2',4	0.916 [y]	0.118	-0.144	0.262	0
	b = 2,2'	1.020 [y]	0.167	-0.155	0.322	0
	c = 4,4'	1.083 [y]	0.190	-0.154	0.344	50
	d = 2,4'	1.183 [y]	0.224	-0.161	0.389	22
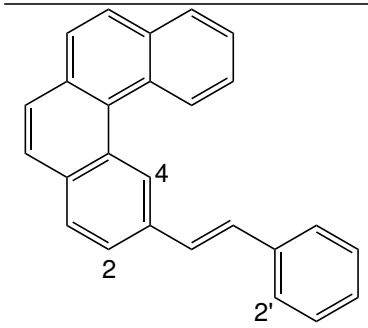 **5.16**	a = 2,2'	0.955 [y]	0.15	-0.109	0.259	0
	b = 4,2'	1.117 [y]	0.085	-0.105	0.190	80

Continues on next page

Table 5.3 – *Continued from previous page*

Molecule	r, s	$V^*_{r,s}$	F^*_π	F^*_σ	$F^*_{\pi,\sigma}$	Yields %
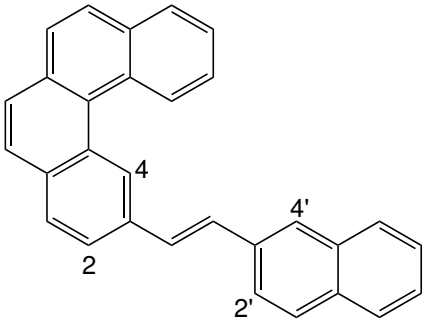	a = 2,2'	0.916 ^{y}	0.077	-0.122	0.199	0
	b = 4,2'	1.046 ^{y}	0.146	-0.124	0.270	0
	c = 2,4'	1.080 ^{y}	0.157	-0.142	0.299	65
	d = 4,4'	1.0216 ^{y}	0.138	-0.127	0.265	20
5.17						
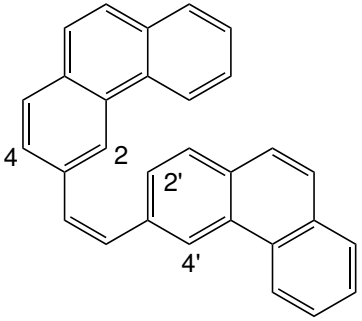	a = 4,2'	0.927 ^{y}	0.142	-0.150	0.292	0
	b= 4,4'	1.027 ^{y}	0.174	-0.153	0.327	0
	c = 2,4'	1.126 ^{y}	0.171	-0.152	0.323	50
5.18						

Continues on next page

Table 5.3 – *Continued from previous page*

Molecule	r, s	$V^*_{r,s}$	F^*_π	F^*_σ	$F^*_{\pi,\sigma}$	Yields %
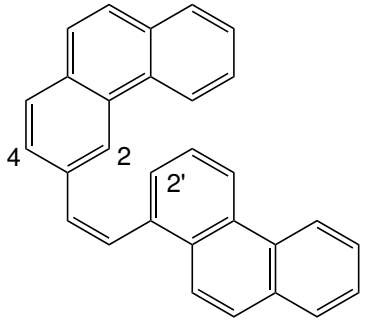 **5.19**	a = 4,2'	0.972 [y]	0.157	-0.145	0.302	0
	b = 2,2'	1.069 [y]	0.195	-0.150	0.345	80
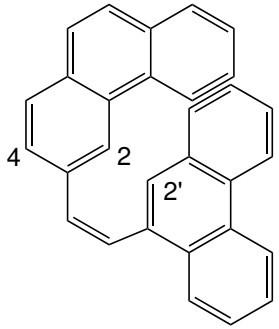 **5.20**	a = 4,2'	1.095 [y]	0.201	-0.148	0.349	75
	b = 2,2'	1.188 [y]	0.230	-0.150	0.380	0

Continues on next page

Table 5.3 – *Continued from previous page*

Molecule	r, s	$V^*_{r,s}$	F^*_π	F^*_σ	$F^*_{\pi,\sigma}$	Yields %
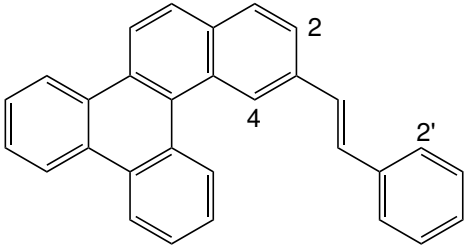 **5.21**	a = 2,2'	0.941 [y]	0.076	-0.087	0.163	0
	b = 4,2'	1.111 [y]	0.121	-0.087	0.208	60
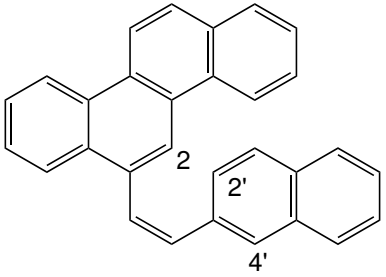 **5.22**	a = 2,2'	1.032 [y]	0.158	-0.126	0.284	0
	b = 2,4'	1.164 [y]	0.212	-0.136	0.348	90

Continues on next page

Table 5.3 – *Continued from previous page*

Molecule	r, s	$V^*_{r,s}$	F^*_π	F^*_σ	$F^*_{\pi,\sigma}$	Yields %
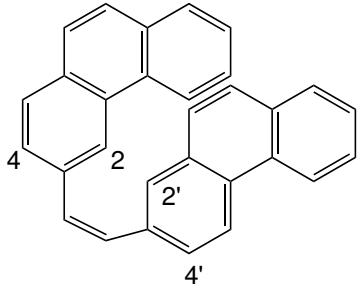	a = 4,4'	0.938 [y]	0.145	-0.154	0.299	0
	b = 4,2'	1.048 [y]	0.186	-0.161	0.347	75
	c = 2,4'	1.049 [y]	0.192	-0.164	0.356	0
	d = 2,2'	1.160 [y]	0.225	-0.169	0.394	0
5.23						
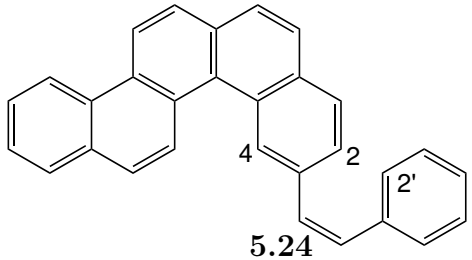	a = 2,2'	0.959 [y]	0.099	-0.1	0.198	0
	b = 4,2'	1.083 [y]	0.156	-0.121	0.277	65
5.24						

Continues on next page

Table 5.3 – *Continued from previous page*

Molecule	r, s	$V^*_{r,s}$	F^*_π	F^*_σ	$F^*_{\pi,\sigma}$	Yields %
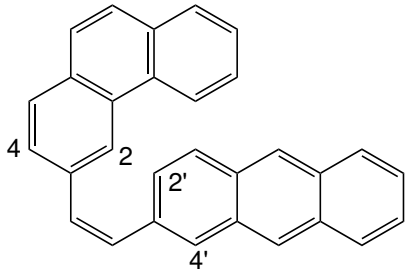	a = 4,2'	0.911 [y]	0.085	-0.085	0.17	0
	b = 2,2'	0.983 [y]	0.121	-0.09	0.211	0
	c = 4,4'	1.074 [y]	0.149	-0.111	0.260	60
	d = 2,4'	1.146 [y]	0.184	-0.118	0.302	22
5.25						
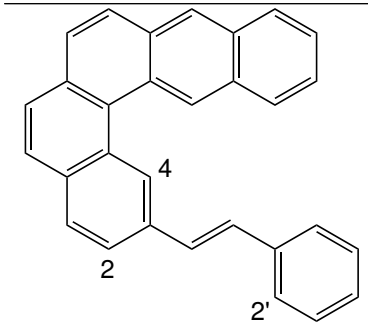	a = 2, 2'	0.915 [y]	0.099	-0.097	0.196	0
	b = 4, 2'	1.035 [y]	0.092	-0.062	0.154	10
5.26						

Continues on next page

Table 5.3 – *Continued from previous page*

Molecule	r, s	$V^*_{r,s}$	F^*_π	F^*_σ	$F^*_{\pi,\sigma}$	Yields %
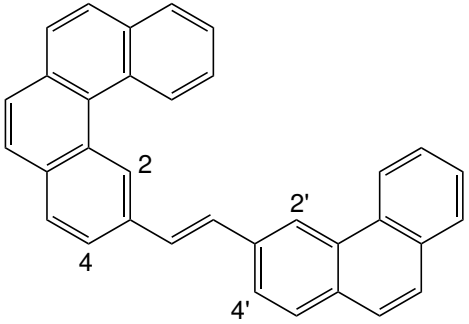	a = 4, 4'	0.922 [y]	0.068	-0.086	0.154	0
	b = 4, 2'	1.023 [y]	0.101	-0.106	0.207	0
	c = 2, 4'	1.053 [y]	0.146	-0.123	0.269	0
	d = 2, 2'	1.146 [y]	0.208	-0.152	0.360	62
5.27						
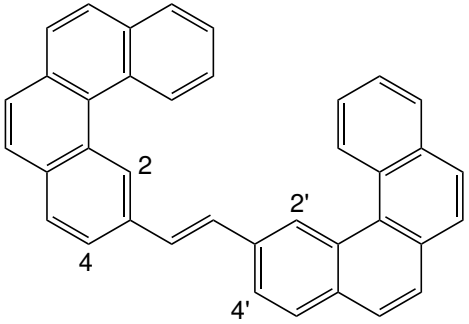	a = 4, 4'	0.916 [y]	0.075	-0.092	0.167	0
	b = 2, 4'	1.046 [y]	0.106	-0.102	0.208	0
	c = 2, 2'	1.126 [y]	0.192	-0.131	0.323	70
5.28						

Continues on next page

Table 5.3 – *Continued from previous page*

Molecule	r, s	$V^*_{r,s}$	F^*_π	F^*_σ	$F^*_{\pi,\sigma}$	Yields %
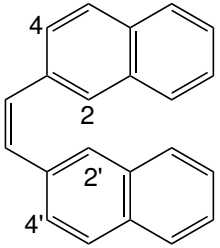 **5.29**	a = 4, 4'	0.904 [y]	0.083	-0.134	0.217	0
	b = 4, 2'	1.082 [y]	0.141	-0.125	0.266	0
	c = 2, 2'	1.260 [y]	0.245	-0.156	0.401	80
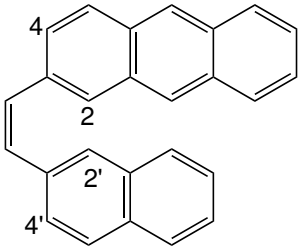 **5.30**	a = 4, 4'	0.907 [y]	0.074	-0.076	0.150	0
	b = 4, 2'	1.012 [y]	0.113	-0.104	0.217	0
	c = 2, 4'	1.071 [y]	0.139	-0.092	0.231	5
	d = 2, 2'	1.176 [y]	0.181	-0.105	0.286	0
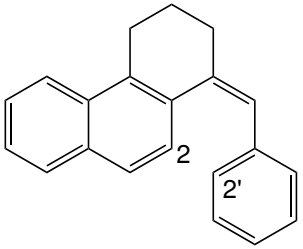 **5.31**	a = 2, 2'	1.170 [t]	0.130	-0.117	0.247	P

Continues on next page

Table 5.3 – *Continued from previous page*

Molecule	r, s	$V^*_{r,s}$	F^*_π	F^*_σ	$F^*_{\pi,\sigma}$	Yields %
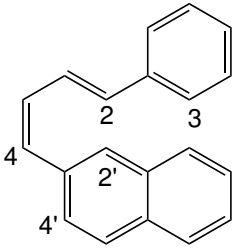 **5.32**	a = 2, 2'	1.240 [z]	0.269	-0.166	0.435	7
	b = 2, 4'	1.092 [z]	0.199	-0.158	0.357	0
	c = 3, 4'	1.1133 [z]	0.233	-0.165	0.398	0
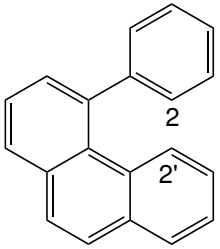 **5.33**	a = 2, 2'	0.934 [z]	0.029	-0.07	0.088	46
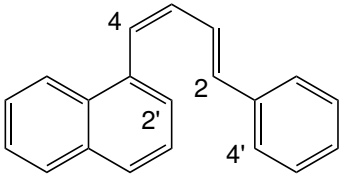 **5.34**	a = 2, 2'	1.149 [z]	0.254	-0.159	0.413	8.5
	b = 4, 4'	1.070 [z]	0.216	-0.152	0.368	0

Continues on next page

Table 5.3 – *Continued from previous page*

Molecule	r, s	$V^*_{r,s}$	F^*_π	F^*_σ	$F^*_{\pi,\sigma}$	Yields %
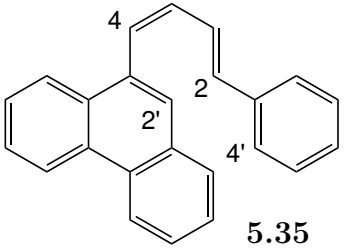 **5.35**	a = 2, 2'	1.238 [z]	0.276	-0.158	0.434	13.5
	b = 4, 4'	1.067 [z]	0.213	-0.149	0.362	0
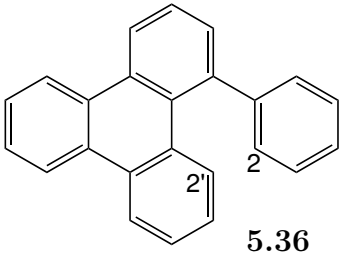 **5.36**	a = 2, 2'	0.949 [z]	0.032	-0.089	0.121	0
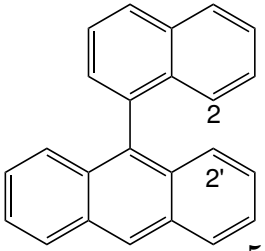 **5.37**	a = 2, 2'	0.934 [z]	0.082	-0.008	0.090	0

Continues on next page

Table 5.3 – *Continued from previous page*

Molecule	r, s	$V^*_{r,s}$	F^*_π	F^*_σ	$F^*_{\pi,\sigma}$	Yields %
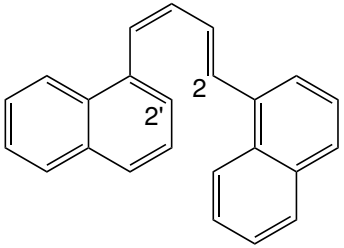 **5.38**	a = 2, 2'	1.091 [z]	0.226	-0.143	0.369	10
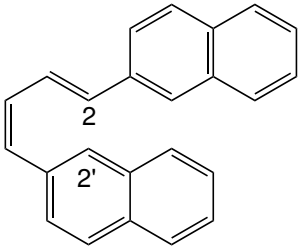 **5.39**	a = 2, 2'	1.124 [z]	0.253	-0.161	0.414	2
	b = 2, 4'	0.988 [z]	0.190	-0.153	0.343	0

Continues on next page

Table 5.3 – *Continued from previous page*

Molecule	r, s	$V^*_{r,s}$	F^*_π	F^*_σ	$F^*_{\pi,\sigma}$	Yields %
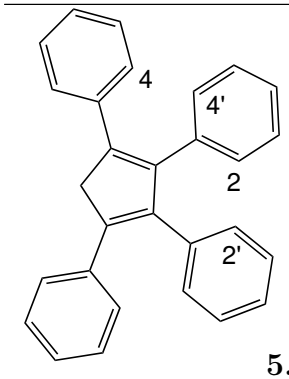 **5.40**	a = 2, 2'	0.912[x]	0.083	-0.071	0.154	0
	b = 4, 4'	0.948 [x]	0.130	-0.098	0.228	p
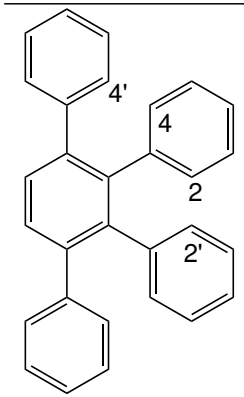 **5.41**	a = 2, 2'	0.908[x]	0.086	-0.090	0.176	0
	b = 4, 4'	0.955 [x]	0.095	-0.106	0.201	p

Continues on next page

Table 5.3 – *Continued from previous page*

Molecule	r, s	$V^*_{r,s}$	F^*_π	F^*_σ	$F^*_{\pi,\sigma}$	Yields %
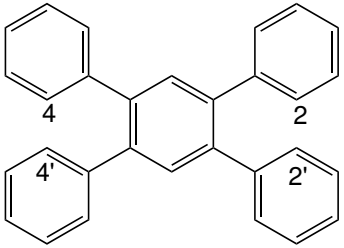 **5.42**	a = 2, 2' = 4,4'	0.955[x]	0.133	-0.133	0.246	p
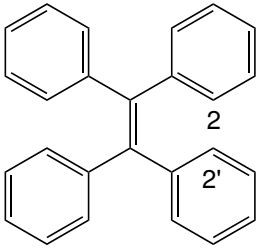 **5.43**	a = 2, 2'	0.965 [x]	0.187	-0.127	0.314	p
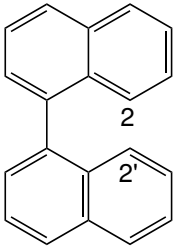 **5.44**	a = 2, 2'	0.972 [x]	0.076	-0.012	0.088	0

Continues on next page

Table 5.3 – *Continued from previous page*

Molecule	r, s	$V^*_{r,s}$	F^*_π	F^*_σ	$F^*_{\pi,\sigma}$	Yields %
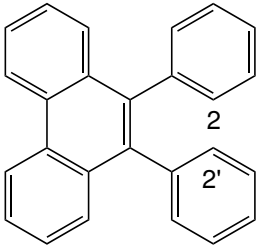 **5.45**	a = 2, 2'	0.976 ^{x}	0.084	-0.032	0.116	0
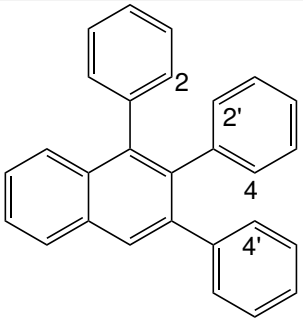 **5.46**	a = 2, 2'	0.961^x	0.048	-0.09	0.138	0
	b = 4, 4'	0.914 ^{x}	0.08	-0.065	0.145	0

Abbreviations:

p : product formed with no recorded yield from refercence

t : see ref [30]

x : see ref [29]

y : see ref [47]

z : see ref [48]

5.5.1 Predictive power

A close look at Table 5.3 shows, that experimentally, products are mostly observed for molecules with $F_{\pi}^{*} \geq 0.1$ E_h/a_0 and $F_{\pi,\sigma}^{*} \geq 0.20$ E_h/a_0 . For molecules with many rotamers, isomeric products are consistently observed for rotamers with the largest F_{π}^{*} and F_{π}^{*}, provided they are above or equal to 0.1 and 0.2 E_h/a_0, respectively. These observations are summarised in Table 5.4 and Table 5.5, where experimental results are compared for each molecule as a whole and not the individual rotamers based on the hypothesis that the formation of the preferred isomer precludes the formation of others. For systems with many rotamers, only the rotamers with the largest F_{π}^{*} and $F_{\pi,\sigma}^{*}$ are considered, since the experimental results reported for each isomer are not independent. Predictions obtained from applying Laarhoven's rules to these molecules are also summarised in Table 5.6.

Table 5.4 Summary of cross-correlation of the predictive power of F_{π}^{*} with experimental results for which 30 molecules formed products and 4 molecules did not. Each column represents experimental observations while each row represents predictions from F_{π}^{*}

Prediction	Products/30	No product/4
$F_{\pi}^{*} \geq 0.1$	28	0
$F_{\pi}^{*} < 0.1$	2	4

Table 5.5 Summary of cross-correlation of the predictive power of $F_{\pi,\sigma}^{*}$ with experimental results for which 30 molecules formed products and 4 molecules did not. Each column represents experimental observations while each row represents predictions from $F_{\pi,\sigma}^{*}$.

Prediction	Products/30	No product/4
$F_{\pi,\sigma}^{*} \geq 0.20$	28	0
$F_{\pi,\sigma}^{*} < 0.20$	2	4

Table 5.6 Summary of cross-correlation of the predictive power of V^{*} with experimental results for which 30 and 4 molecules did not. Each column represent experimental observation while each row represent predictions from V^{*}.

Prediction	Products/30	No product/4
$V^{*} \geq 1.0$	25	0
$V^{*} < 1.0$	5	4

Performance of force base reactivity predictor for molecules that are experimentally observed to photocyclise

From Table 5.4 and Table 5.5 it can be observed that 28 out of the 30 molecules that were experimentally observed to yield cyclisation products had $F_{\pi}^{*} \geq 0.1$ $\mathrm{E}_h/\mathrm{a}_0$ and $F_{\pi,\sigma}^{*} \geq 0.2$ $\mathrm{E}_h/\mathrm{a}_0$. A typical example is cis-stilbene, 5.13, whose induced forces are illustrated in Fig. 5.3.

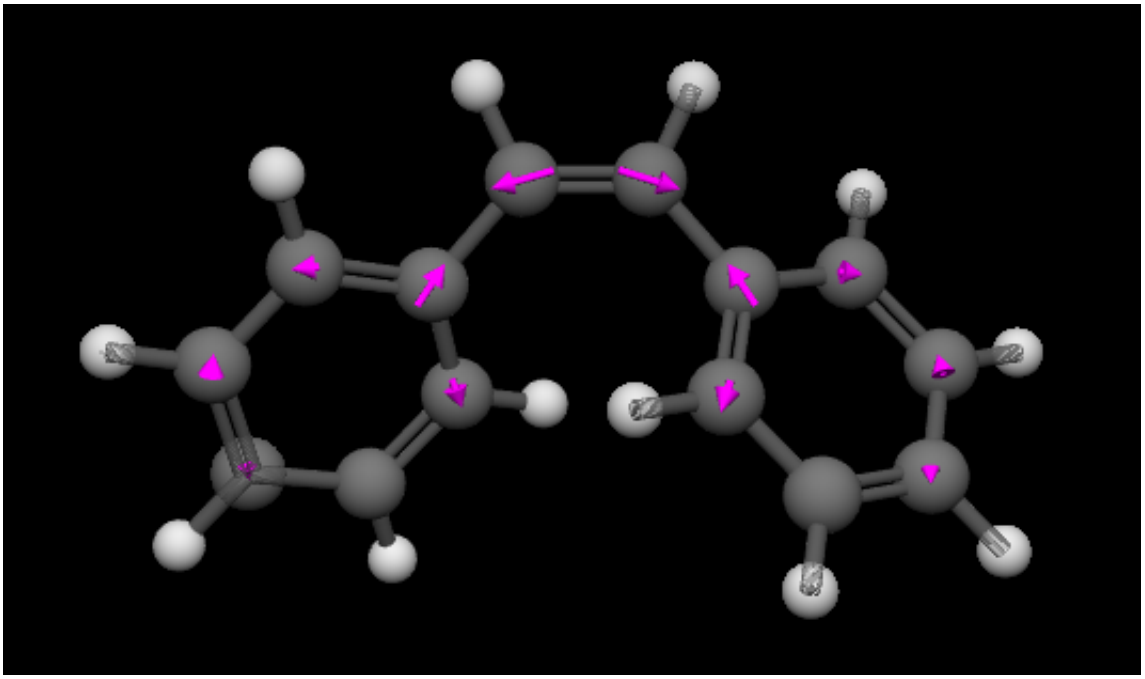

Fig. 5.3 Illustration of induced forces atomic forces in cis-stilbene, 5.13. The pink arrows indicate the direction and position of the forces within the molecule, and the lengths of the arrows correspond to the magnitude of the induced forces. The dark grey balls represent carbon atoms and the light grey balls represent hydrogen atoms.

It can be observed from Fig. 5.3 that the induced forces are highly localised along the region of the putative forming ring, which is indicative of the fact that the

electronic transition occurs in this region and promotes aromatisation of the ring. This is evident from the fact that forces on atoms forming σ-bonds point in the direction corresponding to σ-bonds shortening. Meanwhile, forces on atoms forming π-bonds point directions corresponding to π-bonds lengthening. Overall, this effect is consistent with bond equilibration along the putative forming ring, which is indicative of aromatisation of this ring, thus leading to a high propensity for 6-π electrocyclisation or photoplanarisation.

Two molecules, 5.26, 5.33, with $F_{\pi}^{*} < 0.1$ $\mathrm{E}_h/\mathrm{a}_0$ and $F_{\pi,\sigma}^{*} < 0.2$ $\mathrm{E}_h/\mathrm{a}_0$, which are predicted not to photoplanarise were actually observed to yield cyclisation products. The induced forces in these molecules are illustrated in Fig. 5.4 and Fig. 5.5 respectively.

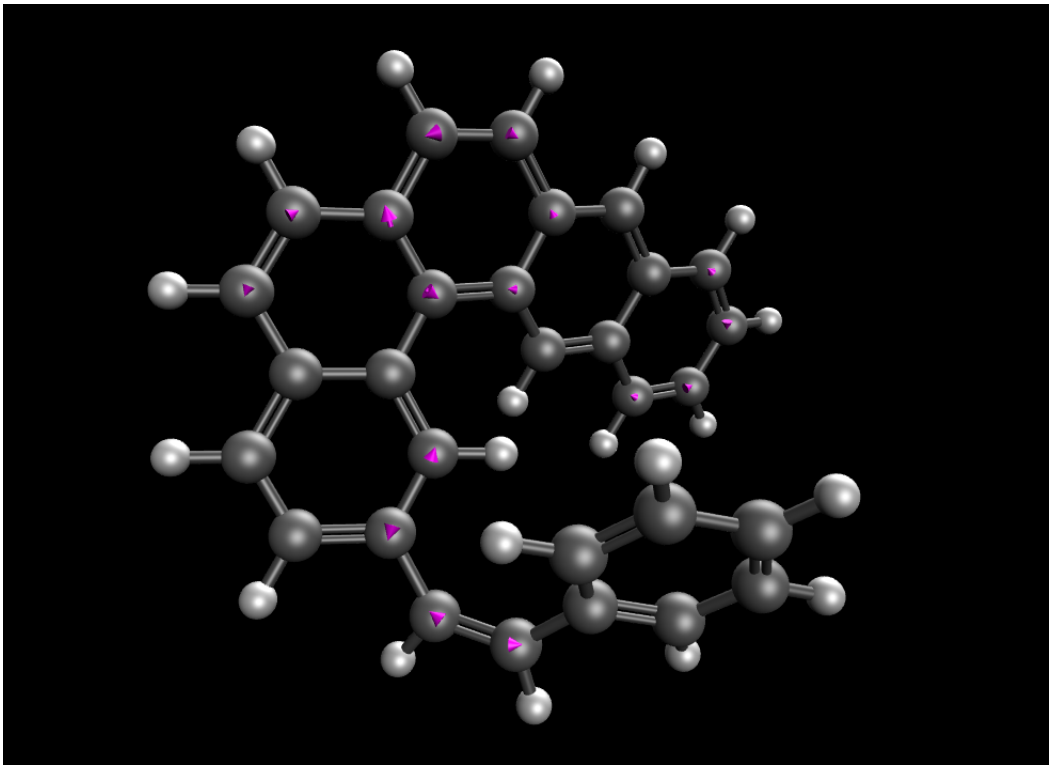

Fig. 5.4 Illustration of induced forces in compound 5.26b. The pink arrows indicate the direction of the induced forces while the lengths of the arrows correspond to the magnitude of the induced forces. The dark grey balls represent carbon atoms and the light grey balls represent hydrogen atoms.

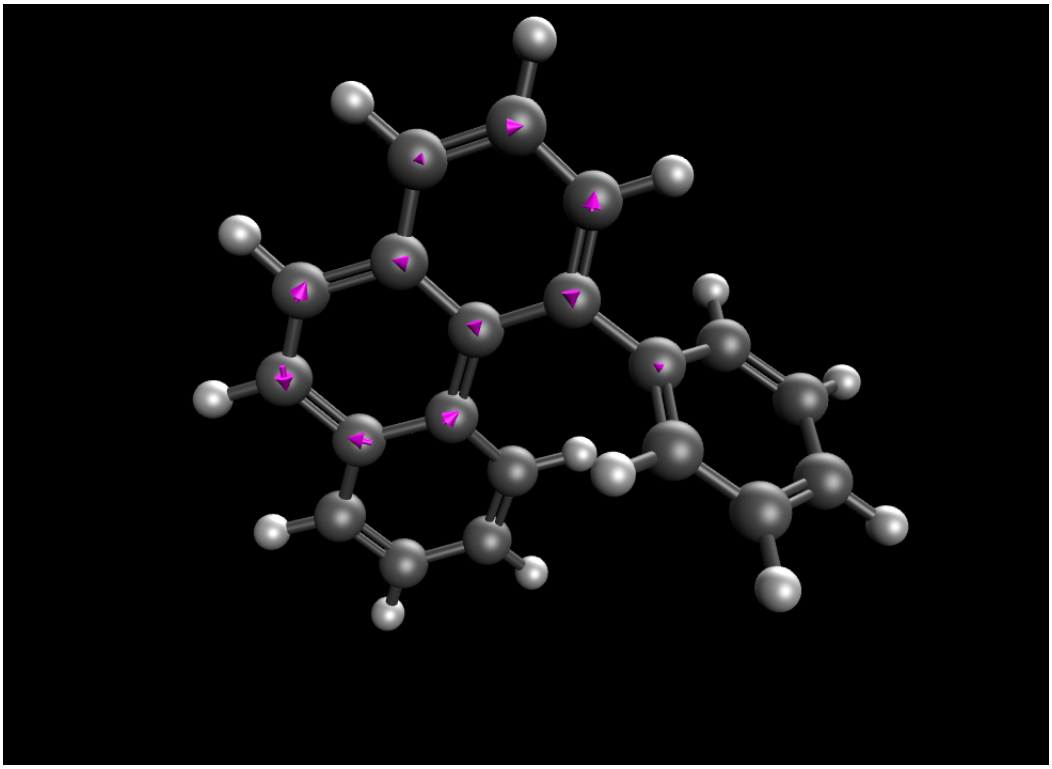

Fig. 5.5 Illustration of induced forces in compound 5.33. The pink arrows indicate the direction of the induced forces while the length of the arrows correspond to the magnitude of the induced forces. The dark grey balls represent carbon atoms and the light grey balls represent hydrogen atoms.

From close inspection of Fig. 5.4 and Fig. 5.5 it can be observed that the induced forces are only sparsely localised on few atoms in the putative forming ring and highly delocalised on the large aromatic fragment. This is indicative of the fact that the electronic transition does not readily occur in the region of the putative forming, hence does not promote aromatisation or drive photoplanarisation.

The fact that these molecules are experimentally observed to photocyclise means that predictions from the force analysis for these systems are wrong. One pecu-

liarity about these molecules is that they all possess a terminal aryl ring connected to a large aromatic fragment. Hence, it is likely that rotation about the bond connecting the two aromatic units breaks π-conjugation and prevents aromatisation. But the equilibrium torsional angles in these systems do not differ much from other molecules in the dataset that are predicted to photoplanarise, which makes this explanation unlikely. In addition, if all the thermally accessible bond rotations are taken into account, it will substantially increase the computational cost as well as complexity of this model, thus would prevent it from being routinely applied.

Tt is possible that the electronic structure model, TD-B3LYP/6-31G*, used in computing the induced excited-state forces is not consistent with aromatisation of the putative forming ring within these systems. In order to confirm this hypothesis, future studies will be performed using the Coulomb-attenuating version of the B3LYP (CAM-B3LYP) functional, which is suitable for describing long-range interactions in electronically excited states. [50]

Overall, this model correlates well with experimental results and provides useful qualitative insights at a modest computational cost across a diverse set of molecules, even if it should be interpreted with caution for this type of molecules.

Perfomance of reactivity predictor for molecules that are not experimentally observed to photocyclise

It follows from Table 5.4 and Table 5.5 that all the 4 molecules with no recorded experimental products are those with $F^*_\pi < 0.1$ $\mathrm{E}_h/\mathrm{a}_0$ and $F^*_{\pi,\sigma} < 0.2$ $\mathrm{E}_h/\mathrm{a}_0$. Two representatives of these molecules are illustrated in Fig. 5.6 and Fig. 5.7.

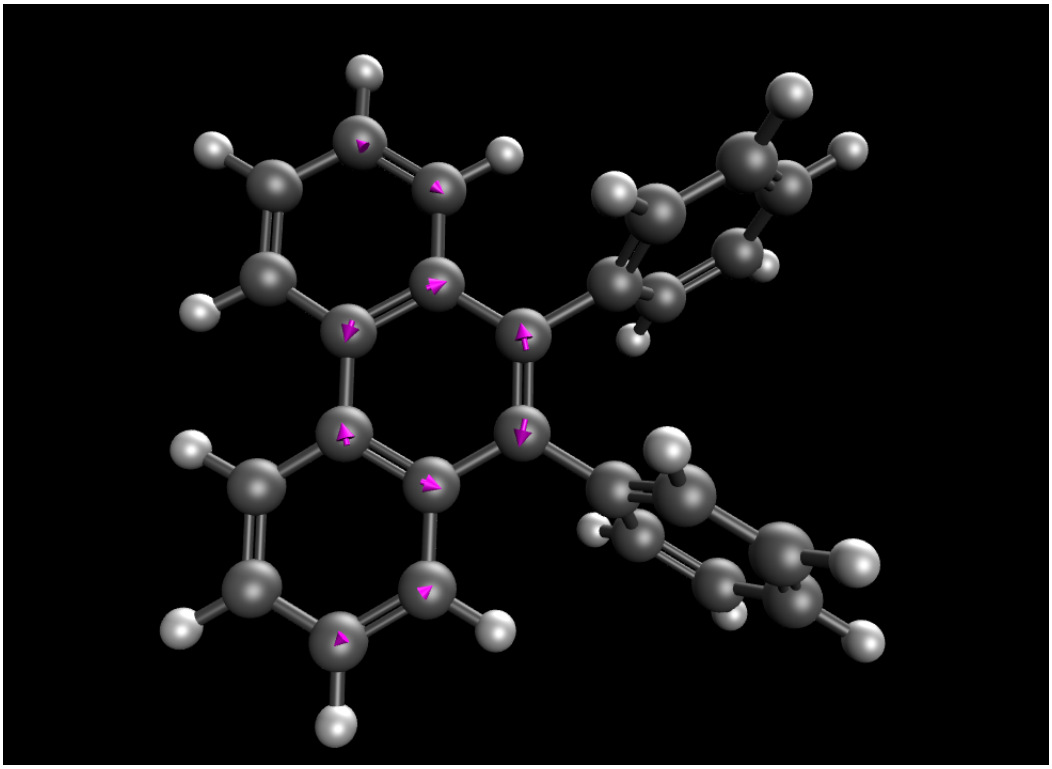

Fig. 5.6 Illustration of the delocalisation of induced forces on the phenathryl fragment in compound 5.45. The pink arrows indicate the direction and position of the forces within the molecule and the lengths of the arrows correspond to the magnitude of the induced force. The dark grey balls represent carbon atoms while the light grey balls represent hydrogen atoms

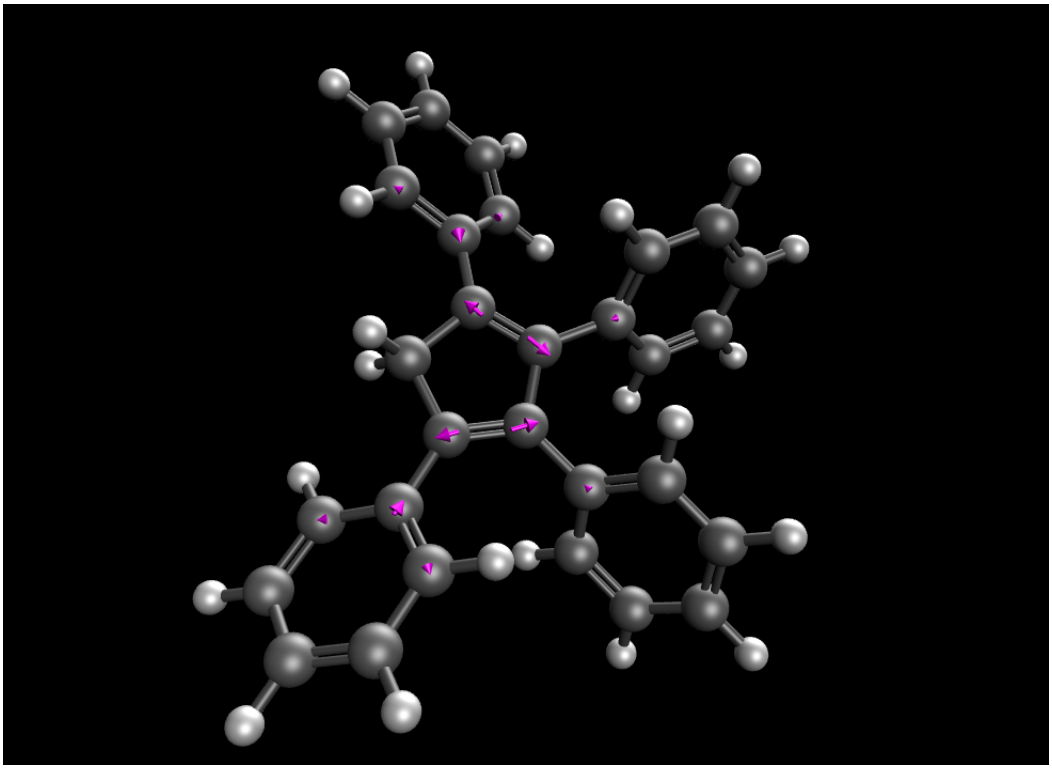

Fig. 5.7 Illustration of the delocalised induced forces in compound 5.40. The pink arrows indicate the direction and position of the forces within the molecule and the lengths of the arrows correspond to the magnitude of the induced force while the light grey balls represent hydrogen atoms

It can be observed from Fig. 5.6 that the induced forces in compound 5.45 are delocalised on the phenanthryl fragment away from the putative forming ring. This implyies that the electronic transition occurs on the phenanthryl fragment and so does not promote aromatisation of the putative forming ring.

In contradistinction to compound 5.45, the induced forces in compound 5.40 are highly delocalised across the entire molecule, as illustrated in Fig. 5.7. This leads to small induced forces along the putative forming ring, which are insufficient to

promote aromatisation of the putative forming ring .

Since the electronic transition in these molecules does not promote the aromatisation of the putative forming ring, it is unlikely that any cyclisation product would be obtained, regardless of the solvent and oxidising agent used to optimised experimental conditions.

Prediction of isomeric products

In as much as this analysis is capable of predicting whether photoplanarisation will proceed or not, it can also be useful in predicting preferred photoplanarisation pathways in cases where isomeric products can be formed. From results presented in Table 5.3, it is observed that isomerisation products are obtained from rotamers with the largest F_{π}^{*} and $F_{\pi,\sigma}^{*}$. Nonetheless, no observed products were obtained for certain rotamers with $F_{\pi}^{*} \geq 0.1$ $\mathrm{E}_h/\mathrm{a}_0$ and $F_{\pi,\sigma}^{*} \geq 0.2$ $\mathrm{E}_h/\mathrm{a}_0$. The fact that no experimental products were observed for these rotamers does not mean that they could not absolutely photoplanarise, but rather that they were relatively disfavoured since the experimental yields reported for each isomer are not independent.

5.5.2 Comparison with Laarhoven's rules

Based on Table 5.4, Table 5.5, and Table 5.6, a comparison between this new force analysis model and Laarhoven's free valence index can be made. This comparison based on the number of times both models correctly and falsely predict the formation or non-formation of products relative to experimental results are recorded in Table 5.7

Table 5.7 Comparison between V^* and F_π^* /$F_{\pi,\sigma}^*$ based on the percentages by which they correctly and falsely predict the formation and non-formation of products relative to experimental results. CP: Correct prediction of product formation, CN: Correct prediction of no product formation, FP: False prediction of product formation and FN: False prediction of no product

Methods	CP (/30)	CN (/4)	FN (/30)	FP(/4)
V^*	25	4	5	0
F_π^* /$F_{\pi,\sigma}^*$	28	4	2	0

According to Table 5.7, it can be observed that our model and Laarhoven's free valence indices correlate quite well in predicting conformers for which experimental products were observed. However, our model is slightly better, for instance, our model correctly predict the formation of products for 28 out of the 30 molecules yielding experimental products, whereas, Laarhoven's free valence index correctly predict products for 25 of these molecules.

Moreover, both methods are good at correctly predicting conformers that do not yield experimental products. For these systems, both methods correctly predict the non-formation of products for all the 4 molecules with no observed experimental products.

For cases in which both predictors failed to correctly predict the formation products, our model is slightly better than Laarhoven's. Our model falsely predict the non-formation of products for two molecules, whereas, Laarhoven's free valence index falsely predict the non-formation of products for 5 molecules.

Although Laarhoven's free valence index and our force-based reactivity predictor are conceptually different, they are still capable of capturing the same essential changes in electronic structure that result from photo-excitation. This shows that simple models based on Hückel molecular orbital theory are sometimes valuable in qualitatively explaining the electronic structures of molecular systems in a clear and neat way like our more complex model, which is based on time-dependent density functional theory.

Overall, apart from having a better predictive power, our model is superior to Laarhoven's rules because the Hückel molecular orbital theory on which Laarhoven's indices are calculated cannot be easily applied to non-conjugated hydrocarbons or systems possessing one or more heteroatoms. Previous attempts to extend Laarhoven's free valence index to heteroatom containing rings by generalising the Hückel molecular orbital theory to include heteroatom containing systems have failed. [30] Since our model is designed from time-dependent density functional theory, it will work equally well for heteroatom containing systems as for hydrocarbons.

5.5.3 Practical application

Our force-based reactivity predictor predicts the outcome of the photo-planarisation step, which is an essential precondition for photocyclisation. Molecules with $F_{\pi}^{*} \geq 0.1$ $\mathrm{E}_h/\mathrm{a}_0$ and $F_{\pi,\sigma}^{*} \geq 0.2$ $\mathrm{E}_h/\mathrm{a}_0$ are most likely to yield photocyclisation products provided experimental conditions are optimised to favour elimination. Since F_{π}^{*}, F_{σ}^{*}, $F_{\pi,\sigma}^{*}$ values all give us the same information, it will be more comfortable and more practical for synthetic chemists to deduce only $F_{\pi,\sigma}^{*}$ values for any precursor molecule. This is because it will be easier to state the atoms present in the puta-

tive forming ring contrary to stating their bond types (i.e. whether they form σ or π-bonds). All subsequent excited-state force analysis in this thesis will be based on calculating only $F^*_{\pi,\sigma}$.

5.6 Summary

In this chapter, we aimed to design a novel reactivity predictor for the outcome of photocyclisation reaction. This predictor is based on the components of induced forces along the bond vectors in the putative forming ring. Results show that molecules in which induced forces are localised along the putative forming are more susceptible to photo-planarisation, which in most cases leads to cyclisation products. Comparing this model to Laarhoven's free valence index shows that both models capture the same essential changes in electronic structure that result from photo-excitation. However, our dataset was selected only for systems in which Laarhoven's free valence indices could be found in the literature. This dataset is not considered extensive enough to explore the generalisability of our force-based reactivity predictor. In the next chapter, our model will be applied to a more extensive dataset in order to fully assess its strengths and limitations.

Bibliography

[1] O. Engkvist, P.-O. Norrby, N. Selmi, Y. hong Lam, Z. Peng, E. C. Sherer, W. Amberg, T. Erhard, and L. A. Smyth, "Computational prediction of chemical reactions: current status and outlook," *Drug Discovery Today*, vol. 23, no. 6, pp. 1203 – 1218, 2018.

[2] Q. Peng, F. Duarte, and R. S. Paton, "Computing organic stereoselectivity ,Äì from concepts to quantitative calculations and predictions," *Chem. Soc. Rev.*, vol. 45, pp. 6093–6107, 2016.

[3] K. N. Houk and P. H.-Y. Cheong, "Computational prediction of small-molecule catalysts," *Nature*, vol. 455, pp. 309–313, 2008.

[4] P. Klan and J. Wirz, "Quantum mechanical models of electronic excitation and photochemical reactivity," in *Photochemistry of Organic Compounds*, pp. 137–182, John Wiley and Sons, Ltd, 2009.

[5] F. Kenichi, Y. Teijiro, and N. Chikayoshi, "Theory of substitution in conjugated molecules," *Bulletin of the Chemical Society of Japan*, vol. 27, no. 7, pp. 423–427, 1954.

[6] F. Kenichi, M. Keiji, and Y. Teijiro, "LCAO SCF calculation on anthracene and reactivity indexes in SCF method," *Bulletin of the Chemical Society of Japan*, vol. 32, no. 8, pp. 853–857, 1959.

[7] F. Kenichi, Y. Teijiro, and N. Chikayoshi, "Molecular orbital theory of reactivity in non-alternant hydrocarbons," *Bulletin of the Chemical Society of Japan*, vol. 34, no. 1, pp. 37–40, 1961.

[8] F. Kenichi, N. Chikayoshi, Y. Teijiro, and M. Keiji, "Theoretical reactivity index of addition in the frontier electron theory," *Bulletin of the Chemical Society of Japan*, vol. 34, no. 2, pp. 230–232, 1961.

[9] F. Kenichi, K. Hiroshi, and Y. Teijiro, "A molecular orbital theory of saturated compounds. I. Ionization potential and bond dissociation energy," *Bulletin of the Chemical Society of Japan*, vol. 33, no. 9, pp. 1197–1200, 1960.

[10] F. Kenichi, M. Keiji, and Y. Teijiro, "Localization energy with electronic interaction," *Bulletin of the Chemical Society of Japan*, vol. 32, no. 10, pp. 1015–1019, 1959.

[11] H. Chermette, "Chemical reactivity indexes in density functional theory," *Journal of Computational Chemistry*, vol. 20, no. 1, pp. 129–154, 1999.

[12] R. Vijayaraj, V. Subramanian, and P. K. Chattaraj, "Comparison of global reactivity descriptors calculated using various density functionals: A QSAR perspective," *Journal of Chemical Theory and Computation*, vol. 5, no. 10, pp. 2744–2753, 2009.

[13] C. Morell, A. Grand, S. Gutierrez-Oliva, , and A. Toro-Labbe, "Using the reactivity-selectivity descriptor f(r) in organic chemistry," in *Theoretical Aspects of Chemical Reactivity* (A. Toro-Labbe, ed.), vol. 19, pp. 101 – 117, Elsevier, 2007.

[14] P. Johnson, L. J. Bartolotti, P. W. Ayers, T. Fievez, and P. Geerlings, *Charge Density and Chemical Reactions: A Unified View from Conceptual DFT*, pp. 715–764. Dordrecht: Springer Netherlands, 2012.

[15] L. R. Domingo, M. Rios-Gutierrez, and P. Perez, "Applications of the conceptual density functional theory indices to organic chemistry reactivity," *Molecules*, vol. 21, no. 6, 2016.

[16] P. Geerlings and F. De Proft, "Conceptual DFT: The chemical relevance of higher response functions," *Physical Chemistry Chemical Physics*, vol. 10, pp. 3028–3042, 2008.

[17] R. K. Roy, "Nucleophilic substitution reaction of alkyl halides: A case study on density functional theory (DFT) based local reactivity descriptors," *The Journal of Physical Chemistry A*, vol. 107, no. 3, pp. 397–404, 2003.

[18] P.-R. Ricardo, Y. Osvaldo, I. Diego, R. Lina, C. Carlos, F. Patricio, and T. William, "Proposal of a simple and effective local reactivity descriptor through a topological analysis of an orbital-weighted fukui function," *Journal of Computational Chemistry*, vol. 38, no. 8, pp. 481–488, 2017.

[19] T. I. Gorbunova, J. O. Subbotina, V. I. Saloutin, and O. N. Chupakhin, "Reactivity of polychlorinated biphenyls in nucleophilic and electrophilic substitutions," *Journal of Hazardous Materials*, vol. 278, pp. 491 – 499, 2014.

[20] T. I. Madzhidov, A. V. Bodrov, T. R. Gimadiev, R. I. Nugmanov, I. S. Antipin, and A. A. Varnek, "Structure–reactivity relationship in bimolecular

elimination reactions based on the condensed graph of a reaction," *Journal of Structural Chemistry*, vol. 56, no. 7, pp. 1227–1234, 2015.

[21] J. Cao, Q. Ren, F. Chen, and T. Lu, "Comparative study on the methods for predicting the reactive site of nucleophilic reaction," *Science China Chemistry*, vol. 58, no. 12, pp. 1845–1852, 2015.

[22] H. T. Black, S. Liu, and V. Sheares Ashby, "Synthesis, crystal structures, and electronic properties of nonlinear fused thienoacene semiconductors," *Organic Letters*, vol. 13, no. 24, pp. 6492–6495, 2011.

[23] M.-L. Sun, F. Zhang, Y. Qian, C.-J. Ou, B. Liu, L.-H. Xie, Y. Wei, B.-Y. Ren, and W. Huang, "Catalyst-free photocyclization for the synthesis of spiro-fused aromatic organic semiconductor based on SFX," *Tetrahedron*, vol. 74, no. 16, pp. 2063 – 2067, 2018.

[24] Y. Zhang, Z. Zhao, X. Huang, Y. Xie, C. Liu, J. Li, X. Guan, K. Zhang, C. Cheng, and Y. Xiao, "N-type organic semiconductor bisazacoronene diimides efficiently synthesized by a new type of photocyclization involving a Schiff base," *RSC Adv.*, vol. 2, pp. 12644–12647, 2012.

[25] L. M. S., Y. S. G., A. A. A., H. K. W. J., R. James, E. A. C., P. A. V. S., and Q. Peter, "Insights into the Scholl coupling reaction: A key transformation of relevance to the synthesis of graphenes and related systems," *European Journal of Organic Chemistry*, vol. 2017, no. 13, pp. 1694–1703, 2017.

[26] M. Scholz, M. Muhlstadt, and F. Dietz, "Die richtung der photocyclisierung naphthalinsubstituierter athylene," *Tetrahedron Letters*, vol. 8, no. 7, pp. 665 – 668, 1967.

[27] F. H. Burkitt, C. A. Coulson, and H. C. Longuet-Higgins, "Free valence in unsaturated hydrocarbons," *Transactions of the Faraday Society*, vol. 47, pp. 553–564, 1951.

[28] M. Tamres, "Valence (Coulson, C. A.)," *Journal of Chemical Education*, vol. 40, no. 3, p. 169, 1963.

[29] W. H. Laarhoven, T. J. R. M. Cuppen, and R. J. F. Nivard, "Photodehydrocyclization in stilben-like compound," *Recueil des Travaux Chimiques des Pays-Bas*, vol. 87, pp. 686–698, 1968.

[30] W. H. Laarhoven, "Photochemical cyclizations and intramolecular cycloadditions of conjugated arylolefins. Part I: Photocyclization with dehydrogenation," *Recueil des Travaux Chimiques des Pays-Bas*, vol. 102, no. 4, pp. 185–204, 1983.

[31] W. Laarhoven, T. Cuppen, and R. Nivard, "Photodehydrocyclizations of stilbene-like compounds-XI : Synthesis and racemization of the double helicene diphenanthro[4.3-a; 3'.4'-o]picene," *Tetrahedron*, vol. 30, no. 18, pp. 3343 – 3347, 1974.

[32] W. Laarhoven and T. Cuppen, "The formation of stilbenes and phenanthrenes by irradiation of dibenzyl sulfides," *Tetrahedron Letters*, vol. 7, no. 41, pp. 5003 – 5007, 1966.

[33] R. S. Mulliken, "Electronic population analysis on LCAO-MO molecular wave functions. I," *The Journal of Chemical Physics*, vol. 23, no. 10, pp. 1833–1840, 1955.

[34] R. Mulliken, "Electronic population analysis on LCAO-MO molecular wave functions. II. Overlap populations, bond orders, and covalent bond energies," *The Journal of Chemical Physics*, vol. 23, no. 10, pp. 1841–1846, 1955.

[35] E. Heilbronner and K. A. Muszkat, "Applications of photoelectron spectroscopy. X. Relative importance of through-space vs. through-bond interaction between the lone pairs in 1,4-diazabicyclo[2.2.2]octane," *Journal of the American Chemical Society*, vol. 92, no. 12, pp. 3818–3821, 1970.

[36] K. A. Muszkat, "Correlation between photoelectron ionization bands and electronic levels in pyrazine," *Chemical Physics Letters*, vol. 13, no. 3, pp. 301–303, 1972.

[37] K. A. Muszkat, G. Seger, and S. Sharafi-Ozeri, "Electronic overlap population as a measure of reactivity in electrocyclic reactions. Part 2.-photocyclization and photodimerization reactions," *Journal of the Chemical Society, Faraday Transactions 2: Molecular and Chemical Physics*, vol. 71, pp. 1529–1544, 1975.

[38] K. B. Wiberg, "A scheme for strain energy minimization. Application to the cycloalkanes1," *Journal of the American Chemical Society*, vol. 87, no. 5, pp. 1070–1078, 1965.

[39] K. Muzkat and S. Sharafi-Ozeri, "Electronic overlap population as measure of reactivity in electrocyclic reactions, stilbenes and analogs," *Chemical Physics Letters*, vol. 20, no. 4, pp. 397 – 400, 1973.

[40] J. P. Malrieu, "Electronic properties and photochemical monomolecular reactions in organic conjugated compounds: Photocyclizations, photoisomerizations and photochemical rearrangements," *Photochemistry and Photobiology*, vol. 5, no. 4, pp. 291– 299, 1966.

[41] J. P. Malrieu, "Electronic properties and photochemical monomolecular reactions in organic conjugated compounds: Photocyclizations, photoisomeriza-

tions and photochemical rearrangements II," *Photochemistry and Photobiology*, vol. 5, no. 4, pp. 301–313, 1966.

[42] G. Feler, "Indices de liaison et isomérie de valence," *Theoretica Chimica Acta*, vol. 10, no. 1, pp. 33–42, 1968.

[43] P. R.-G. C. Minot and C. Thal, "Photocyclisation de stilbènes,et de composès indoliques apparentès: Contribution à l'utilisation des indices de réactivitè," *Tetrahedron*, vol. 36, no. 9, pp. 1209–1214, 1980.

[44] R. F. W. Bader and H. Essen, "The characterization of atomic interactions," *The Journal of Chemical Physics*, vol. 80, no. 5, pp. 1943–1960, 1984.

[45] M. P. Johansson and J. Olsen, "Torsional barriers and equilibrium angle of biphenyl: Reconciling theory with experiment," *Journal of Chemical Theory and Computation*, vol. 4, no. 9, pp. 1460–1471, 2008.

[46] F. D. Lewis and X. Zuo, "Torsional barriers for planar versus twisted singlet styrenes," *Journal of the American Chemical Society*, vol. 125, no. 8, pp. 2046–2047, 2003.

[47] W. Laarhoven, T. Cuppen, and R. Nivard, "Photodehydrocyclizations in stilbene-like compounds III : Effect of steric factors.," *Tetrahedron*, vol. 26, no. 20, pp. 4865 – 4881, 1970.

[48] A. R.J.Hayward and C.C.Leznoff, "Photocyclization reactions of aryl polyenes VI: The photocyclization of 1,4-diaryl-1,3-butadienes," *Tetrahedron*, vol. 28, no. 3, pp. 439–447, 1972.

[49] M. D. Hanwell, D. E. Curtis, D. C. Lonie, T. Vandermeersch, E. Zurek, and G. R. Hutchison, "Avogadro: an advanced semantic chemical editor, visualiza-

tion, and analysis platform," *Journal of Cheminformatics*, vol. 4, no. 1, p. 17, 2012.

[50] T. Yanai, D. P. Tew, and N. C. Handy, "A new hybrid exchange-correlation functional using the coulomb-attenuating method (cam-b3lyp)," *Chemical Physics Letters*, vol. 393, no. 1, pp. 51 – 57, 2004.

CHAPTER 6

Photocyclisation Reactivity Predictor: Generalised Case Studies and Testing

6.1 Introduction

In chapter 3, reaction coordinate profiles were mapped out for a series of photocyclisation systems. It was concluded from this study that the barrier for elimination was highly sensitive to the reaction conditions. Meanwhile, the planarisation step was found to be photoactivated, meaning that it depends on the inherent ability of a molecule to absorb light and undergo 6-π electrocyclisation. To predict photocyclisation, one can resort to determining whether a reactant molecule possesses the inherent ability to photoplanarise. This can be done on the basis that if a molecule photoplanarises, product formation will rely on optimising the reaction conditions -solvents and oxidising agent- to favour elimination.

In chapter 5, a novel reactivity predictor for predicting photoplanarisation was established, based on the components of the induced forces from the first singlet electronic excited-states along the bond vectors of the putative forming ring. The power of this reactivity predictor was assessed by evaluating how well it could be used to predict product formation in photocyclisation. It was observed that systems in which $F_{\sigma,\pi} \geq 0.2$ $\mathrm{E}_h/\mathrm{a}_0$ were the most likely to photocyclise.

In order to enable comparison with Laarhoven's free valence index, the dataset was restricted only to molecules with published free valence indices. [1–4] But since Laarhoven's free valence index can only be applied to conjugated hydrocarbons, the dataset was not sufficiently extensive to assess the generalisability of this new force-based reactivity predictor.

In this chapter, the force-based reactivity predictor will be applied to structurally and chemically diverse range of photocyclisable systems to investigate how predict-

ing the ability of a molecule to photoplanarise correlates with product formation. The aim is not to predict product yields, which depend on other experimental variables such as purifications, but to determine if one can discriminate whether a product will form or not based on analysing induced forces from the first singlet electronic excited-state.

6.2 Dataset and Methodology

All molecules used were selected from published experimental literature and have structures presented in the results section. The dataset is divided into three categories to enable a more critical assessment of the strengths and weaknesses of this predictor.

- The first class of molecules is composed of systems possessing one or more heteroatoms with a single cyclisation centre.
- The second class of systems is heteroatom-containing molecules with multiple potential photocyclisation centres.
- The last class of molecules involves systems that undergo non-oxidative or purely eliminative photocyclisation.

The methodology and computational details used in Chapter 5 are replicated in this chapter.

6.3 Results and discussion

For each putative forming ring, only the results $F_{\sigma,\pi}$, are presented. This is mainly for simplicity since it is easier to specify atoms found in the putative forming ring

rather than also having to identify their bond types. The results are accompanied by experimental yields as well as the literature references from which they were obtained.

6.3.1 Class one: Heteroatom-containing systems with a single cyclisation centre

The heteroatom-containing systems with a single cyclisation considered here constitute a series of (6.1) acryloyl, [5] (6.2) indolyl, [6] and (6.3) dibenzo[e,g]indolyl [6] systems. Scaffolds for these systems are presented in Fig. 6.1. The components of the forces along the putative forming ring in these systems are presented in Table 6.1.

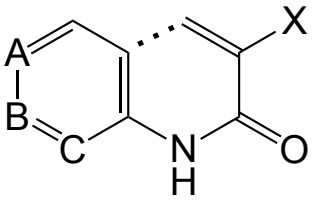

6.1. Acryloyl

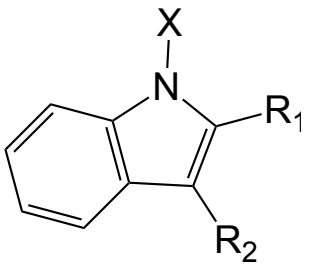

6.2. Indolyl

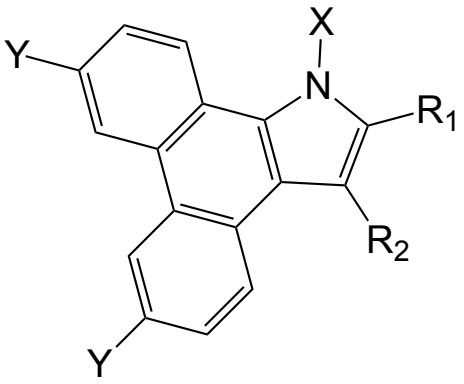

6.3. Dibenzo[e,g]indolyl

Fig. 6.1 Scaffolds for the heteroatom containing systems with a single cyclisation centre. A, B, and C represent ring constituents, R represents ring substituents that are potentially involved in photocyclisation. X and Y represent electronically active substituents, and the identity of these groups are defined in Table 6.1. For each of these molecules, photocyclisation can occur between ring substituents or between the scaffold atoms illustrated by (. . .).

Table 6.1 Component of bond aromatisation forces, $F^*_{\pi,\sigma}$, along all the putative forming rings in (**6.1**) Acryloyl, [5] (**6.2**) indolyl, [6] and (**6.3**) dibenzo[e,g]indolyl [6]. A, B, and C represent ring constituents, X and Y represent different electronically active substituents. Rs and (...) represent bonding centres Fig. 6.1. Experimental yields are presented in order to verify whether a product was formed or not.

	Molecules	Forming ring	$F^*_{\pi,\sigma}$ (E_h/a_0)	Yield %
	6.1. Acryloyl			
a	A = B = CH, C = N, X = H	...	0.29	17
b	A = B = CH, C = N, X = Me	...	0.29	78
c	A = C = CH, B = N, X = Me	...	0.28	53
d	A = CH, B = N, C = CCl, X = Me	...	0.27	25
e	A = N, B = C = CH, X = Me	...	0.26	72
	6.2. Indolyl			
a	R_1 = R_2 = phenyl, X = Et	R_1–R_2	0.30	64
b	R_1 = R_2 = 4-methoxyphenyl, X = Et	R_1–R_2	0.35	60
c	R_1 = R_2 = 4-methylphenyl, X = Et	R_1–R_2	0.31	87
d	R_1 = R_2 = 4-*tert*-butylphenyl, X = Et	R_1–R_2	0.33	89
e	R_1 = R_2 = phenyl, X = Bz	R_1–R_2	0.30	84
f	R_1 = R_2 = 4-methoxyphenyl, X = Bz	R_1–R_2	0.33	62
g	R_1 = R_2 = 4-methylphenyl, X = Bz	R_1–R_2	0.32	56
h	R_1 = R_2 = 4-*tert*-butylphenyl, X = Bz	R_1–R_2	0.33	78
	6.3. Dibenzo[e,g]indole			
a	R_1 = R_2 = phenyl, X = Et, Y = H	R_1–R_2	0.04	–
b	R_1 = R_2 = 4-methylphenyl, X = Et, Y = H	R_1–R_2	0.04	–

Continues on next page

Table 6.1 – *Continued from previous page*

	Molecules	Forming ring	$F^*_{\pi,\sigma}$ (E_h/a_0)	Yield %
c	$R_1 = R_2$ = 4-*tert*-butylphenyl, X = Et, Y = H	R_1–R_2	0.04	–

It can be observed from Table 6.1 that the components of the induced forces in the putative forming ring, of both the acryloyls and indolyls, are above 0.2 E_h/a_0. This implies that both systems should photoplanarise. Experimental results confirm that these systems do photocyclise into their corresponding acrylamides and dibenzo[a,c]carbazoles compounds as illustrated in Scheme 6.1 and Scheme 6.2 respectively.

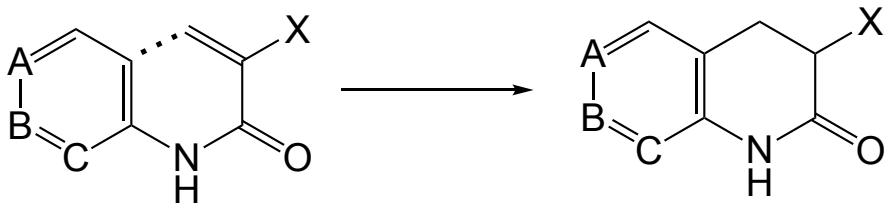

Scheme 6.1 Scaffold for the photocyclisation of acryoly into acrylamide. A, B, and C represent ring constituents, X represents the different electronically active substituents and (. . .) represents the cyclisation centres.

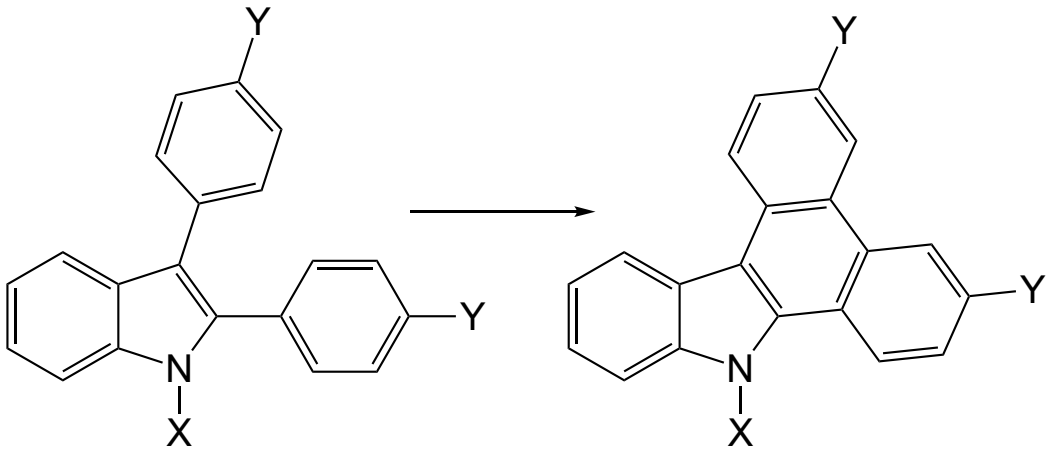

Scheme 6.2 Scaffold for the photocyclisation of indolyl into dibenzo[a,c]carbazoles. X and Y represent different electronically active substituents.

The putative forming ring in the acryolyl systems does not cyclise into an aromatic ring system. Nonetheless, the induced forces in putative forming ring in these systems correctly predict that these systems should photoplanarise. This can be attributed to the fact that the putative forming ring in the acryolyl systems form an extended conjugated system involving the π-electrons in the terminal olefinic bond, carbonyl group, the lone pair of electron on the nitrogen atom, and the aromatic π-electron system. This extended conjugation surely results in the delocalisation of π-electrons within their putative forming rings, which enables the electronic transition to occur along their putative forming ring. Consequently, it can be hypothesise that these systems photoplanarise in a similar manner to the 6-π electrocyclisation of 1,3,5-hexatriene.

It can also be observed from Table 6.1 that the components of the induced forces, $F^*_{\pi,\sigma}$, along the putative forming ring of the dibenzo[e,g]indole systems are very low,

having a value of 0.04 E_h/a_0. Consequently, these systems are predicted not to photoplanarise. Experimental results for the photocyclisation of these systems show that they failed to cyclised into the corresponding tetrabenzo[a,c,g,i]carbazoles Scheme 6.3. [6]

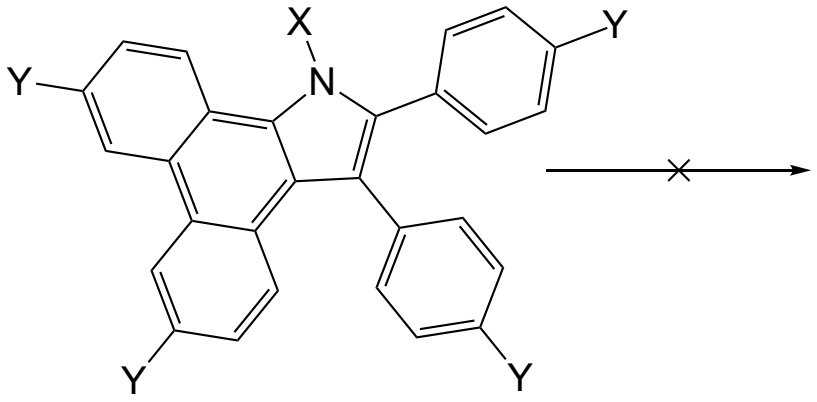

Scheme 6.3 Scaffold for the cyclisation of dibenzo[e,g]indolel. X and Y represent different electronically active substituents.

The induced forces for a prototypical dibenzo[e,g]indole system, 6.3a, are illustrated in Fig. 6.2. It can be observed from this figure that the induced forces are localised solely on the dibenzo[e,g]indole scaffold. This implies that the electronic transition occurs solely in this region, and so does not promote aromatisation of the putative forming ring. Consequently, these systems do not photoplanarise, and if the photoplanarised intermediate does not form, so it is unlikely that elimination would proceed, which is consistent with experimental results obtained for these systems. [6]

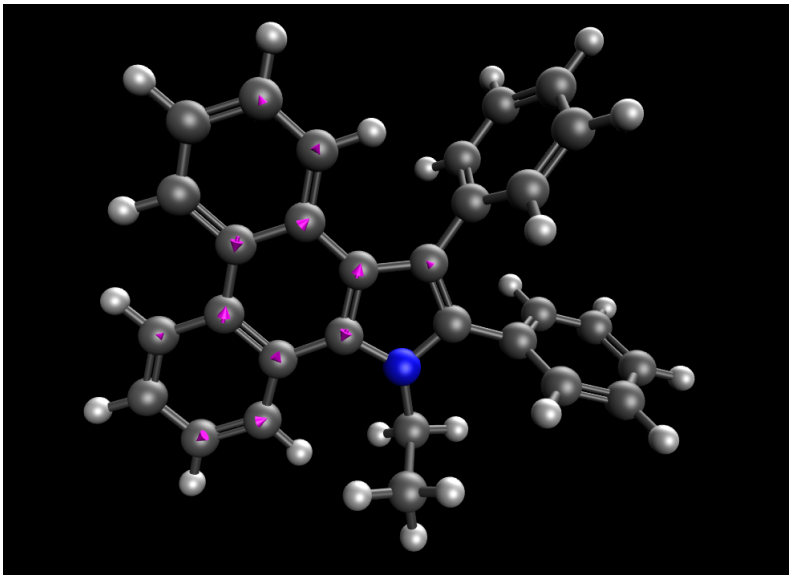

Fig. 6.2 Illustration of induced forces in N-ethyl-2,3-diaryl-dibenzo[e,g]indole, (**6.3a**). The pink arrows indicate the direction and position of the forces within the molecule. The dark grey balls represent carbon atoms and the light grey balls represent hydrogen atoms.

6.3.2 Class two: Heteroatom-containing molecules with multiple potential photocyclisation centres

Results obtained from computing the components of the induced forces along the putative forming rings of heteroatom containing systems with multiple cyclisation centres are presented in Table 6.3.

Table 6.2 Components of induced forces along each putative ring for systems with two or more putative forming rings. Results are presented in terms of sequential photocyclisation. The components of the forces $F_{\sigma,\pi}$ in $\mathrm{E}_h/\mathrm{a}_0$ are found in each putative forming ring.

	Reactant	Product1/Reactant2	Product2	Reference
6.4	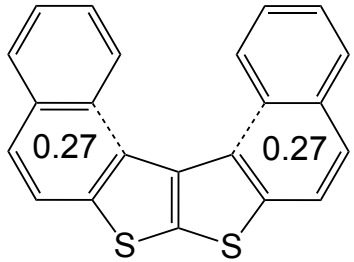	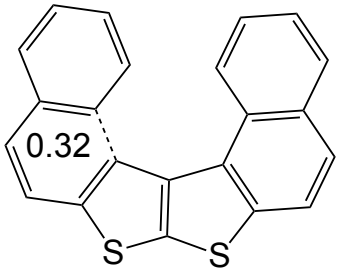	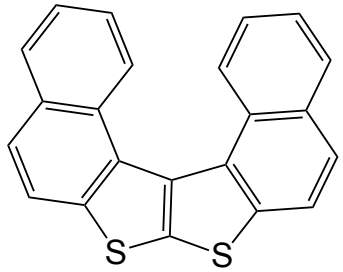	[7]
6.5	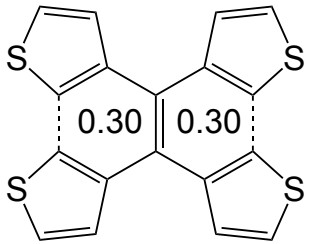	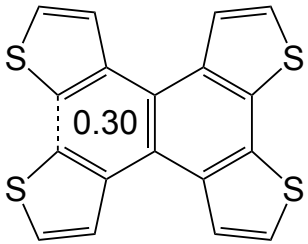	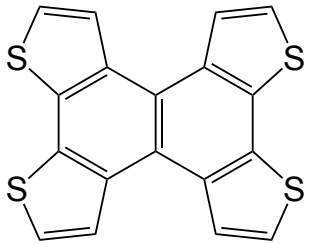	[8, 9]

	Reactant	Product1/Reactant2	Reference
6.6	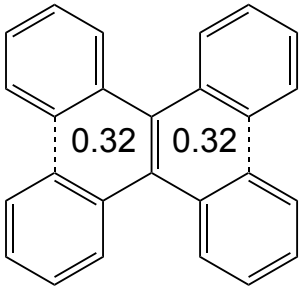	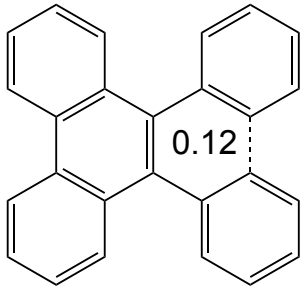	[8, 9]
6.7	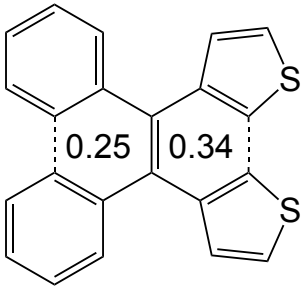	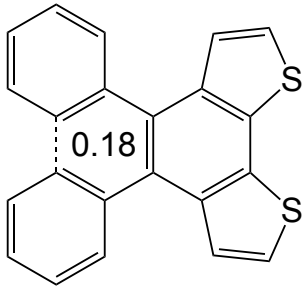	[8, 9]
6.8	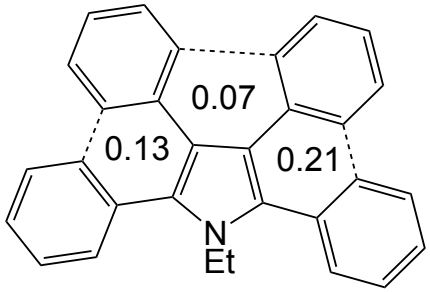	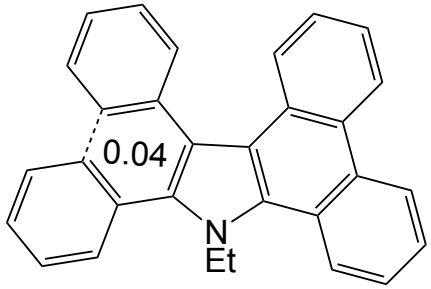	[10]

Continues on next page

Table 6.3 – *Continued from previous page*

Reactant	Product1/Reactant2	Reference
6.9 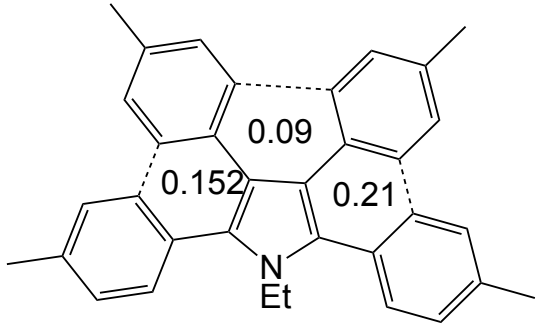	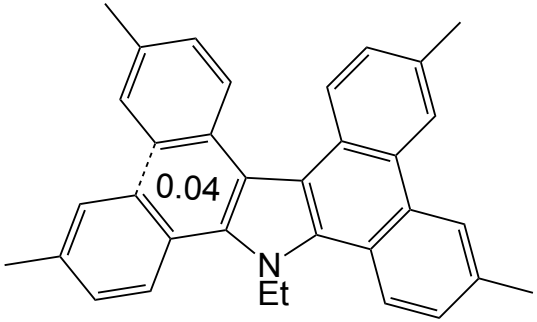	[10]
6.10 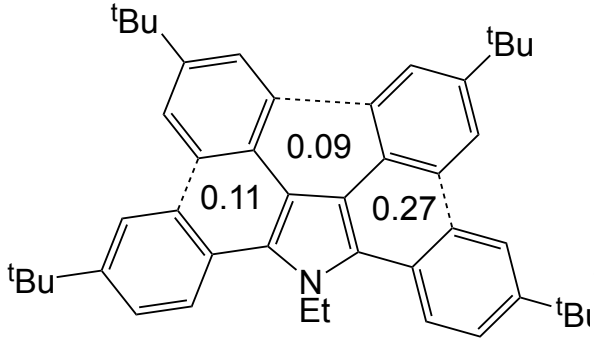	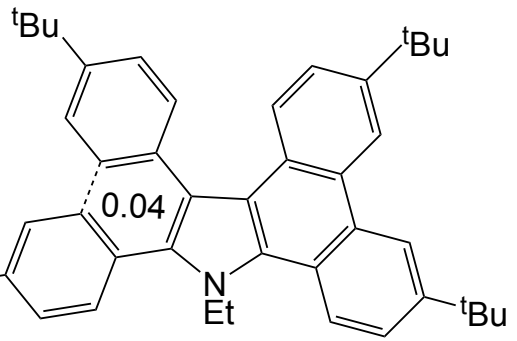	[10]

Continues on next page

Table 6.3 – *Continued from previous page*

Reactant	Product1/Reactant2	Reference
6.11	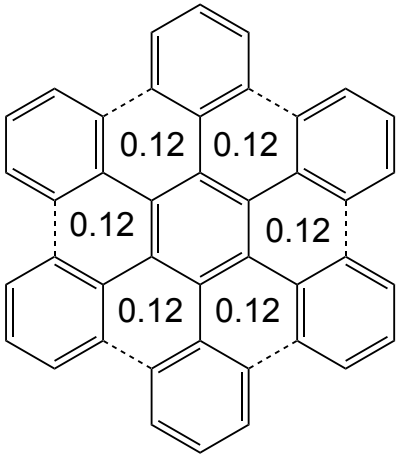	[1]

For systems involving two symmetric putative forming rings, where the induced forces along both rings are equal, a cyclisation product can be formed for any of the rings, provided $F_{\sigma,\pi}$ is greater than or equal to 0.2 E_h/a_0. For instance in 6.4-6.6, it is not possible to discriminate between the two putative forming rings.

In asymmetric systems with different $F_{\sigma,\pi}$ for the putative forming rings, a cyclisation product is formed via cyclisation of the ring with the largest $F_{\sigma,\pi}$, provided it is greater than or equal to 0.2 E_h/a_0. For instance in 6.7 cyclisation products are observed only for putative the forming ring containing the thiophene groups, which has a $F_{\sigma,\pi} = 0.34$ E_h/a_0. Similarly, the cyclisation of tetraphenyl pyrrolyl compounds 6.8-6.10, involves the cyclisation of only one putative forming ring, which is suggested to be the ring with the largest $F_{\sigma,\pi}$.

In hexaphenylbenzene 6.11, where $F_{\sigma,\pi}$ for all the putative forming rings are symmetric and have the same value of 0.12 E_h/a_0, it experimentally observed that no cyclisation product results from any of the putative forming rings. The induced atomic forces in this system are illustrated in Fig. 6.3. It can be observed from this figure that the induced forces are highly delocalised across the whole system, meaning that the electronic transition is delocalised and does not promote aromatisation in any of the putative forming rings. Consequently, the resulting forces are too weak to drive the system to photoplanarise. This could be a possible reason why hexabenzocoronene [11] has never been synthesised from hexaphenylbenzene via photocyclisation reaction.

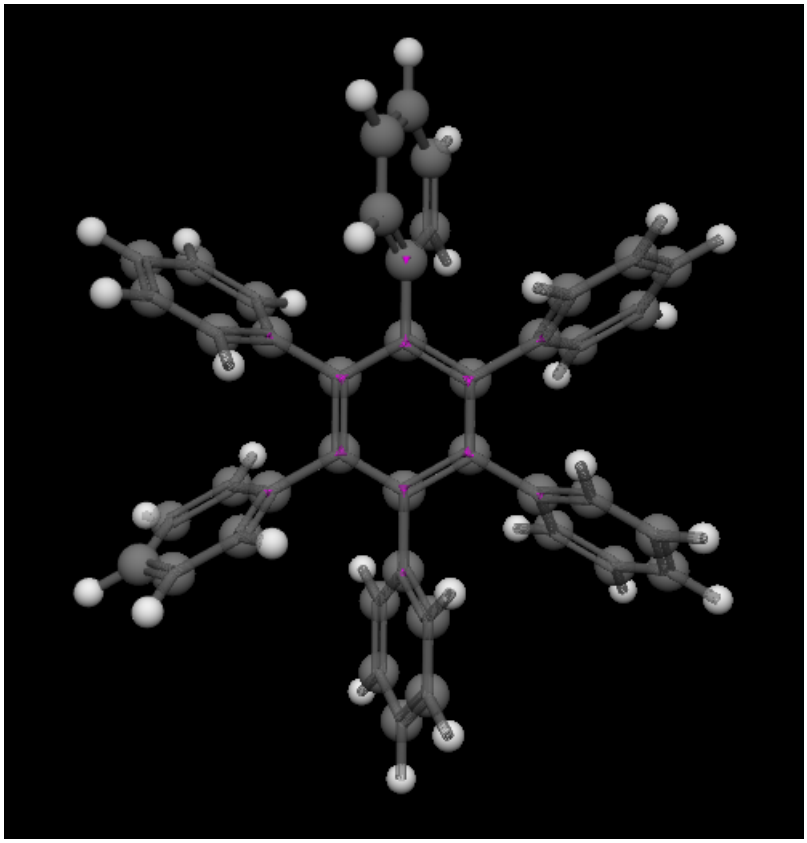

Fig. 6.3 Illustration of induced forces in hexaphenylbenzne, (**6.11**). The pink arrows indicate the direction and position of the forces within the molecule. The dark grey balls represent carbon atoms and the light grey balls represent hydrogen atoms.

The complete photocyclisation pathway for tetrakis(thiophene-2-yl)ethene, (6.5), 1,1,2,2-tetraphenylethene, (6.6) and N-ethyl- 2,3,4,5-tetraarylpyrrole (6.8) are illustrated in Scheme 6.4, Scheme 6.5, and Scheme 6.6 respectively.

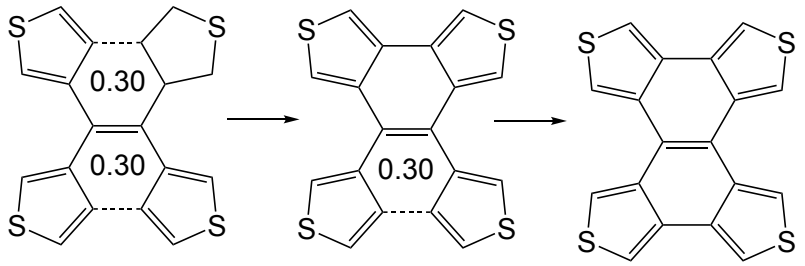

Scheme 6.4 Consecutive photocyclisation pathway for tetrakis(thiophene-2-yl)ethene, (6.5). The component of the forces, $F_{\sigma,\pi}$, for each putative forming ring is presented in $\mathrm{E}_h/\mathrm{a}_0$.

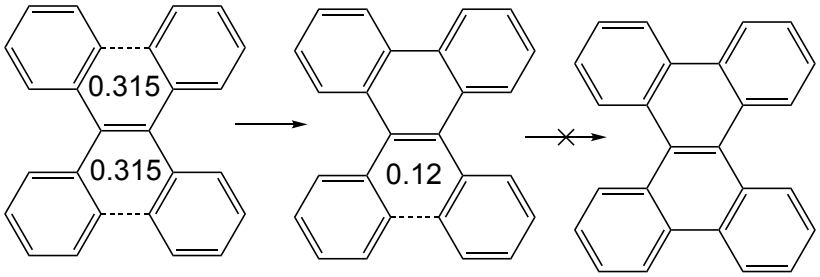

Scheme 6.5 Consecutive photocyclisation pathway for 1,1,2,2-tetraphenylethene, (6.6). The component of the forces, $F_{\sigma,\pi}$, for each putative forming ring is presented in $\mathrm{E}_h/\mathrm{a}_0$.

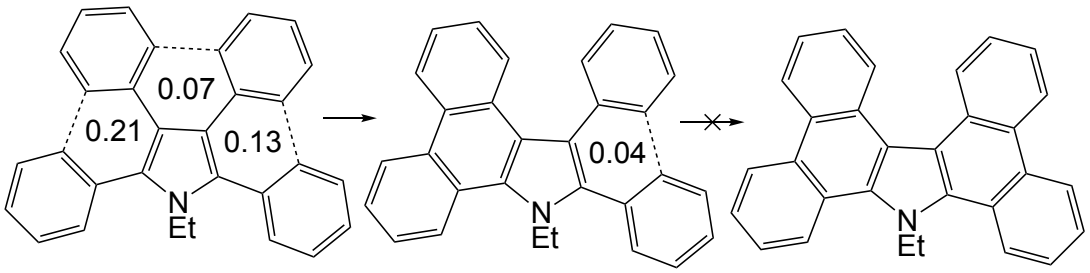

Scheme 6.6 Consecutive photocyclisation pathway for N-ethyl- 2,3,4,5-tetraarylpyrrole, (6.5). The component of the forces, $F_{\sigma,\pi}$, for each putative forming ring is presented in $\mathrm{E}_h/\mathrm{a}_0$.

It can be observed from Scheme 6.4, Scheme 6.5, and Scheme 6.6 that, apart from the photocyclisation of tetrakis(thiophene-2-yl)ethene, 6.5, the second photoplanarisation step is less facile than the first. In the second photocyclisation of tetrakis(thiophene-2-yl)ethene, it can be observed that the component of the forces along the putative forming has a value of 0.30 E_h/a_0, which is sufficiently large to drive the photoplanarisation. A possible explanation for this observation is the presence of the heteroatoms in the thiophenyl groups. Since these heteroatoms are highly electronegative, they cause the electronic cloud to be localised along the putative forming ring, thereby causing the electronic transition to occur in this region, which promotes the aromatisation of the ring.

The components of the forces in the second photocyclisation of both 6.6 and 6.8 are small and are consequently insufficient to drive the photoplanarisation process to completion in order to form the pro-aromatic intermediate. This suggests that photocyclisation is not well suited for systems with multiple cyclisation centres.

6.3.3 Case study 3: Systems that undergo non-oxidative elimination

For systems that undergo non-oxidative eliminative cyclisation reactions, the propensity of obtaining a cyclisation product depends on two things; the inherent ability of a molecule to photoplanarise, as well as, the ease with which the leaving group can break off from the cyclised intermediate. Although planarisation is still a necessary precondition for the reaction to proceed, the leaving groups ability to exit should be the most controlling factor. In order to confirm this hypothesis, the

components of the forces along the putative forming rings in various substituted benzylidenecyclopentanone O-methyl oximes [12] were computed. A scaffold for this system is illustrated in Scheme 6.7 and the calculated $F_{\sigma,\pi}$ are reported in Table 6.4.

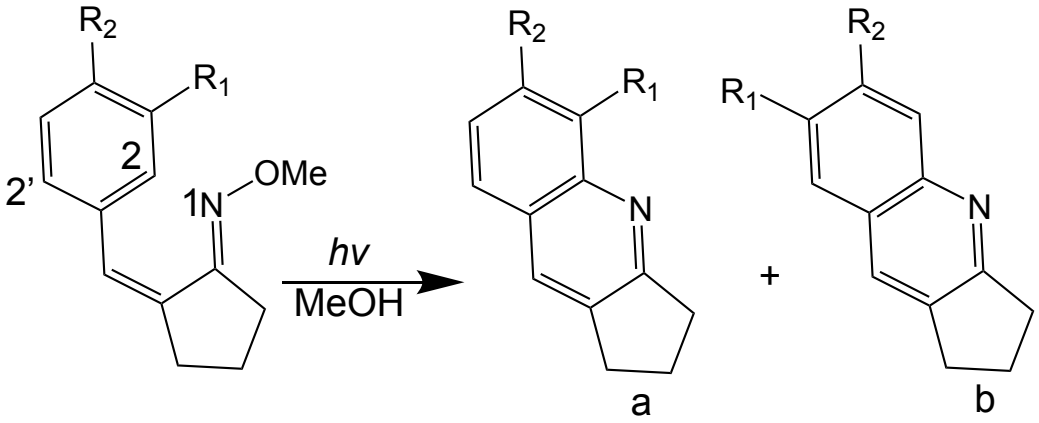

Scheme 6.7 Illustration of the two possible isomers **a** and **b** that can be formed from the photocyclisation of R-substitutedbenzylidenecyclopentanone O-methyloxime.

Table 6.4 Components of induced forces, $F_{\sigma,\pi}$, along the putative forming ring of R-substitutedbenzylidenecyclopentanone O-methyloxime for the two rotamers that potentially photocyclises into isomer (a) and (b). [12]

		(isomer **a**)		(isomer **b**)	
R_1	R_1	$F_{\sigma,\pi}(1, 2)$E $_h/a_0$	Yields %	$F_{\sigma,\pi}(1, 2')$ E $_h/a_0$	Yields %
Me	H	0.378	32	0.397	-
Me	Me	0.360	17	0.377	-
Me	OMe	0.279	15	0.303	-

Continues on next page

Table 6.4 – *Continued from previous page*

R_1	R_2	$F_{\sigma,\pi}(1, 2)$ E $_h/a_0$	Yields %	$F_{\sigma,\pi}(1, 2')$E $_h/a_0$	Yields %
^{t}Bu	H	0.405	13	0.404	-
OMe	H	0.320	-	0.360	63
OMe	OMe	0.268	-	0.317	21
OMe	Me	0.310	-	0.348	57
OH	H	0.321	-	0.365	30
NMe_2	H	0.332	-	0.347	6
NH_2	H	0.365	-	0.404	26
OAc	H	0.365	17	0.404	20
NO_2	H	0.280	-	0.301	-
Cl	H	0.372	-	0.401	-
CN	H	0.316	-	0.349	-
F	H	0.353	-	0.402	-

In Table 6.4, it can be observed that the components of the forces along the putative forming ring for all the rotamers are above 0.2 E $_h/a_0$. This implies that these systems should readily photoplanarise. If planarisation were the rate-determining step, then the results in Table 6.4 would imply that; products will always be formed, and prediction of preferential isomer formation with higher $F_{\sigma,\pi}$ would not be consistent with the experimentally observed product distribution. However, it was observed in Chapter 4 that elimination is the rate-determining step for this reaction. Therefore, the non-formation of products in certain molecules is not due to the lack of photoplanarisation, but it is rather due to high barriers for elimination.

This dependency on the barrier for elimination in this class of systems raises the need for a reactivity predictor for the eliminative step. However, in Chapter 4, it was hypothesised that elimination would likely proceed in the ground state. If this hypothesis is valid, this means that routine reactivity predictors for ground states thermal elimination reactions may be applicable to these reactions.

6.4 Summary

This chapter aimed to apply $F_{\sigma,\pi}$ to a range of potentially photocyclisable systems with different molecular and structural diversity. It was found that molecules with $F_{\sigma,\pi} > 0.2$ E $_h/\mathrm{a}_0$ generally formed cyclisation products. Moreover, $F_{\sigma,\pi}$ is not suitable for predicting reactions in which elimination is the rate-determining step. However, it is likely that if $F_{\sigma,\pi}$ is coupled with a reactivity predictor for elimination, then a complete prediction for non-oxidative cyclisation reactions would be achieved. Nonetheless, if the planarisation step is the rate-determining step or if the barrier to elimination is the same regardless of the isomer, $F_{\sigma,\pi}$ will be able to predict preferred isomers.

Bibliography

[1] W. H. Laarhoven, "Photochemical cyclizations and intramolecular cycloadditions of conjugated arylolefins. Part I: Photocyclization with dehydrogenation," *Recueil des Travaux Chimiques des Pays-Bas*, vol. 102, no. 4, pp. 185–204, 1983.

[2] W. Laarhoven, T. Cuppen, and R. Nivard, "Photodehydrocyclizations in stilbene-like compounds III : Effect of steric factors.," *Tetrahedron*, vol. 26, no. 20, pp. 4865 – 4881, 1970.

[3] A. R.J.Hayward and C.C.Leznoff, "Photocyclization reactions of aryl polyenes VI: The photocyclization of 1,4-diaryl-1,3-butadienes," *Tetrahedron*, vol. 28, no. 3, pp. 439–447, 1972.

[4] W. H. Laarhoven, T. J. R. M. Cuppen, and R. J. F. Nivard, "Photodehydrocyclization in stilben-like compound," *Recueil des Travaux Chimiques des Pays-Bas*, vol. 87, pp. 686–698, 1968.

[5] M. Ogata and H. Matsumoto, "Organic photochemical reactions. VIII. Photocyclization of n-acryloyl heteroaromatic amines," *Chemical and Pharmaceutical Bulletin*, vol. 20, no. 10, pp. 2264–2268, 1972.

[6] J. L. Ferguson, M. A. Squire, and C. M. Fitchett, "Photochemical and oxidative cyclisation of tetraphenylpyrroles," *Organic and Biomolecular Chemistry*, vol. 15, pp. 9293–9296, 2017.

[7] N. Hoffmann, "Photochemical reactions applied to the synthesis of helicenes and helicene-like compounds," *Journal of Photochemistry and Photobiology C: Photochemistry Reviews*, vol. 19, pp. 1 – 19, 2014.

[8] Y. Cai, L. Du, K. Samedov, X. Gu, F. Qi, H. H. Y. Sung, B. O. Patrick, Z. Yan, X. Jiang, H. Zhang, J. W. Y. Lam, I. D. Williams, D. Lee Phillips, A. Qin, and B. Z. Tang, "Deciphering the working mechanism of aggregation-induced emission of tetraphenylethylene derivatives by ultrafast spectroscopy," *Chemical Science*, pp. –, 2018.

[9] E. Fischer, J. Larsen, J. B. Christensen, M. Fourmigue, H. G. Madsen, and N. Harrit, "Synthesis of new sulfur heteroaromatics isoelectronic with dibenzo[g,p]chrysene by photocyclization of thienyl- and phenyl-substituted ethenes," *The Journal of Organic Chemistry*, vol. 61, no. 20, pp. 6997–7005, 1996. PMID: 11667599.

[10] J. L. Ferguson, *Colossal Aromatic Molecules*. PhD dissertation, University of Canterbury, 2013.

[11] R. Rathore and C. L. Burns, "A practical one-pot synthesis of soluble hexaperi-hexabenzocoronene and isolation of its cation-radical salt," *The Journal of Organic Chemistry*, vol. 68, no. 10, pp. 4071–4074, 2003.

[12] M. Austin, O. J. Egan, R. Tully, and A. C. Pratt, "Quinoline synthesis: Scope and regiochemistry of photocyclisation of substituted benzylidenecyclopentanone o-alkyl and o-acetyloximes," *Organic and Biomolecular Chemistry*, vol. 5, pp. 3778–3786, 2007.

CHAPTER 7

Conclusion and Future Work

7.1 Conclusion

The aim of this thesis was to design a reliable computational model to cheaply and efficiently predict the outcome of eliminative cyclisation reactions. The introduction set up the importance and need for such a reliable predictor. After this, the computational methods that were relevant for this modelling were summarised in chapter 2. The rest of the chapters were devoted to the computational modelling.

In chapter 3, reaction coordinate profiles were mapped out for both thermal and photochemical cyclisation reactions for a range of heteroatom containing systems. The minimum energy reaction path for thermal cyclisation was found to be sensitive to the reaction conditions, which include the presence and position of the heteroatoms as well as the oxidation potential of the reactants. Meanwhile, the minimum energy path in photochemical reaction was found to be less sensitive to reaction conditions, because the planarisation step, which is often the rate determining step is photoactivated. Computational evidence suggests that oxidative elimination in photochemical cyclisation reaction is most likely to proceed in the ground state following internal conversion after the formation of the planar intermediate. This process may be mediated by vibrionic coupling with the oxidant.

In Chapter 4, ground and excited-state reaction coordinate profiles were mapped out for a series of ortho and para-substituted benzylidene O-methyloximes that undergo non-oxidative eliminative cyclisation. For these systems, it was observed that the rate determining step of the reaction is no longer the planarisation step, which is photoactivated. Instead, the reaction was found to be controlled by the ability of the leaving group to leave. This elimination was also found to favourably proceed in the ground state with a strong dependence on the nature and position

of the substituent to the elimination site.

In Chapter 5, a new force based reactivity predictor for predicting photoplanarisation was designed. This was based on evaluating the components of the induced atomic forces, resulting from photo-excitation, along the bond vectors of the atoms constituting the putative forming ring. This was used as a proxy for predicting photoplanarisation based on analysing whether the electronic transition resulted in a more aromatic-like putative forming ring. Molecules with more aromatic-like putative forming ring in the first excited-state were predicted to have a high propensity to photoplanarise.

Finally in Chapter 6, this force based reactivity predictor was applied to a range of systems with varied structural and molecular diversity. It was observed that this reactivity predictor is more suitable for systems undergoing oxidative photocyclisation wherein the rate-determining is the six π-electrocyclisation step.

7.2 Recommendation for synthetic chemists

Based on the results, understanding and experienced acquired from this studies, the following recommendations can be made to synthetic chemists who are involved with these reactions.

- When performing thermal eliminative cyclisation reaction, a good balance should be made between the oxidising potential of the oxidant and the reducing potential of the precursor molecule. Since both the planarisation and elimination step in this reaction require an oxidative transfer of electron from the precursor to the oxidant. Hence, it is advisable to use oxidants that have a stronger oxidation potential than the precursor.

- Based on the hypothesis that elimination in non-oxidative photocyclisation is a ground-state process, such reactions can be controlled by correctly selecting the substituents and leaving group. For this purpose, electron donating substituents will be more effective to help stabilise the enthalpy of elimination. However, apart from the purpose of regioselectivity and ease of not having to seperate oxidants, there seem to be no real synthetic benefit in choosing non-oxidative cyclisation over oxidative cyclisation.

- It also advisable to apply the force analysis before any oxidative photocyclisation reaction. This will help to avoid time wastage on trying to synthesise a compound that cannot be synthesised from the initial reactant molecules.

- Finally, I highly encourage synthetic chemists to be more upfront in publishing molecules that fail to cyclised because such systems are desirable to enable a more complete representation of molecules for benchmarking new reactivity predictors.

The purpose of this thesis was to design a full reactivity predictor that predicts both the elimination and photo-planarisation step of photocyclisation reaction. A reactivity predictor for predicting photo-planarisation was successfully designed. It is clear that photo-planarisation is a necessary pre-condition for photocyclisation, but just because a molecule can photo-planarise does not necessarily mean that it will photocyclise, because it must subsequently undergo an elimination step. Fortunately, for molecules undergoing oxidative elimination reaction, this can be controlled by the choice of the experimental conditions, which include the strength of the oxidant, solvent and temperature. [1–3] On the other hand, for non-oxidative photocyclisation, elimination is dependent on both distal substituent effects, as shown in Chapter4 and, more importantly, on the nature of the leaving group.

Nonetheless, the need for a full reactivity predictor that is capable of capturing both steps in the reaction is still a necessity. In the future, it will be important to perform a computational study to analyse how different solvents and oxidising agents control the barrier for elimination. This will hopefully enable a careful prescription of an adequate cocktail for the most suitable reaction conditions for a diverse range of molecules. This will be done with the intention of hopefully establishing a machine learning reactivity predictor for eliminative cyclisation.

Finally, a similar approach of using induced excited-state forces, known as judgement of energy distribution index (JEDI) was recently published. This method uses both excited-state gradients and Hessian to analyse the energy distributed on atoms as they are excited on the Franck-Condon point on the excited-state potential energy surface [4–7] However, this method was used on only a single representative photochemical system to explain the photo-isomerisation of stilbene. In the future, it will be important to implement and apply this model to all reactants in the dataset used in this thesis in order to compare this model with the newly developed force-base reactivity predictor.

Bibliography

[1] F. D. Lewis, P. C. Karagiannis, M. C. Sajimon, K. S. Lovejoy, X. Zuo, M. Rubin, and V. Gevorgyan, "Solvent dependent photocyclization and photophysics of some 2-ethynylbiphenyls," *Photochemical and Photobiological Sciences*, vol. 5, pp. 369–375, 2006.

[2] J. Claret, I. Fernandez, C. Galvez, and R. Lapouyade, "Role of dichloromethane in the photocyclization-oxidation of vinylheterocyclic systems," *Journal of Photochemistry and Photobiology A: Chemistry*, vol. 55, no. 3, pp. 347 – 359, 1991.

[3] A. G. Neo, C. Lapez, V. Romero, B. Antelo, J. Delamano, A. Perez, D. Fernandez, J. F. Almeida, L. Castedo, and G. Tojo, "Preparation of phenanthrenes by photocyclization of stilbenes containing a tosyl group on the central double bond. a versatile approach to the synthesis of phenanthrenes and phenanthrenoids," *The Journal of Organic Chemistry*, vol. 75, no. 20, pp. 6764–6770, 2010.

[4] T. Stauch and A. Dreuw, “Predicting the efficiency of photoswitches using force analysis,” *The Journal of Physical Chemistry Letters*, vol. 7, no. 7, pp. 1298–1302, 2016.

[5] T. Stauch and A. Dreuw, “On the use of different coordinate systems in mechanochemical force analyses,” *The Journal of Chemical Physics*, vol. 143, no. 7, p. 074118, 2015.

[6] T. Stauch and A. Dreuw, “A quantitative quantum-chemical analysis tool for the distribution of mechanical force in molecules,” *The Journal of Chemical Physics*, vol. 140, no. 13, p. 134107, 2014.

[7] T. Stauch and A. Dreuw, “Response to comment on T. Stauch, A. Dreuw, "Stiff-stilbene photoswitch ruptures bonds not by pulling but by local heating", Phys. Chem. Chem. Phys., 2016, 18, 15848,” *Physical Chemistry Chemical Physics*, vol. 18, pp. 26994–26997, 2016.

APPENDIX A

Complete details of all species involved in reaction pathway and full details of thermochemical data

A.0.1 Detailed mechanism for Scholl reaction

(S_1)	- e^- $\rightarrow$	(S_2)	via TS (S_3) $\rightarrow$	(S_4)	+ Cl^- $\rightarrow$	(S_5)	via TS (S_6) $\rightarrow$	(S_7)	- e^- $\rightarrow$	(S_8)	+ Cl^- $\rightarrow$	(S_9)
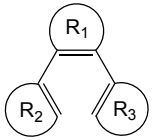		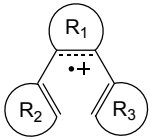		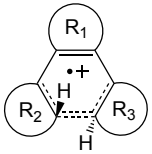		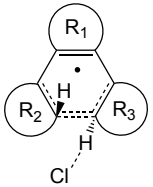		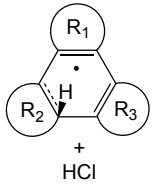		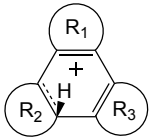		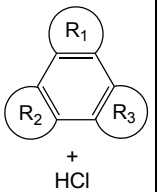
$[Fe(III)Cl_3(H_2O)_3]$ $+H_2O$	+ e^- $\rightarrow$	$[Fe(II)Cl_3(H_2O)_3]^-$ $+H_2O$		$[Fe(II)Cl_3(H_2O)_3]^-$ $+H_2O$	- Cl^- $\rightarrow$	$[Fe(II)Cl_2(H_2O)_4]$		$[Fe(II)Cl_2(H_2O)_4]$		$[Fe(II)Cl_2(H_2O)_4]$		$[Fe(II)Cl_2(H_2O)_4]$
$[Fe(III)Cl_3(H_2O)_3]$ $+H_2O$		$[Fe(III)Cl_3(H_2O)_3]$ $+H_2O$		$[Fe(III)Cl_3(H_2O)_3]$ $+H_2O$		$[Fe(III)Cl_3(H_2O)_3]$ $+H_2O$		$[Fe(III)Cl_3(H_2O)_3]$ $+H_2O$	+ e^- $\rightarrow$	$[Fe(II)Cl_3(H_2O)_3]^-$ $+H_2O$	- Cl^- $\rightarrow$	$[Fe(II)Cl_2(H_2O)_4]$

F_1: $[Fe(III)Cl_3(H_2O)_3]$

F_2: $[Fe(II)Cl_3(H_2O)_3]^-$

F_3: $[Fe(II)Cl_2(H_2O)_4]$

Small molecules: H_2O, HCl

A.0.2 Detailed mechanism for Mallory reaction (oxidative pathway)

Using Iodine as catalyst

$(M_1 = S_1)$	via TS (M_2) →	(M_3)	- e^- →	$(M_4 = S_4)$	+ I^- →	(M_5)	via TS (M_6) →	$(M_7 = S_7)$	- e^- →	$(M_8 = S_8)$	+ I^- →	$(M_9 = S_9)$
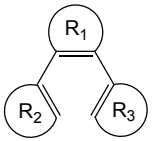		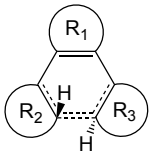		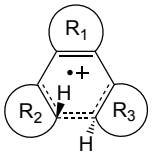		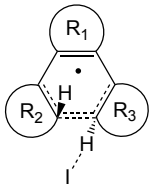		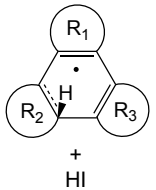		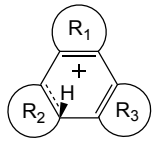		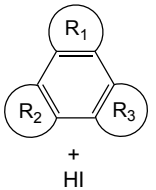
I_2		I_2	+ e^- →	$I + I^-$	- I^- →	I		I	+ e^- →	I^-	- I^- →	

Using $Fe(III)Cl_3(H2O)_3$ as catalyst

$(M_1 = S_1)$	via TS (M_2) →	(M_3)	- e^- →	$(M_4 = S_4)$	+ Cl^- →	(M_5)	via TS (M_6) →	$(M_7 = S_7)$	- e^- →	$(M_8 = S_8)$	+ Cl^- →	$(M_9 = S_9)$
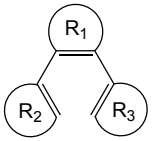		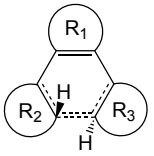		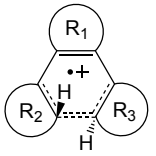		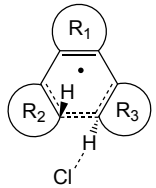		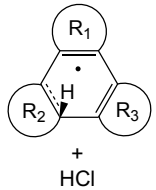		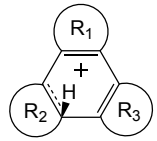		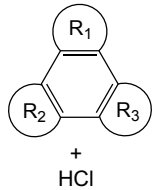
$[Fe(III)Cl_3(H_2O)_3] + H_2O$	+ e^- →	$[Fe(II)Cl_3(H_2O)_3]^- + H_2O$		$[Fe(II)Cl_3(H_2O)_3]^- + H_2O$	- Cl^- →	$[Fe(II)Cl_2(H_2O)_4]$		$[Fe(II)Cl_2(H_2O)_4]$		$[Fe(II)Cl_2(H_2O)_4]$		$[Fe(II)Cl_2(H_2O)_4]$
$[Fe(III)Cl_3(H_2O)_3] + H_2O$		$[Fe(III)Cl_3(H_2O)_3] + H_2O$		$[Fe(III)Cl_3(H_2O)_3] + H_2O$		$[Fe(III)Cl_3(H_2O)_3] + H_2O$		$[Fe(III)Cl_3(H_2O)_3] + H_2O$	+ e^- →	$[Fe(II)Cl_3(H_2O)_3]^- + H_2O$	- Cl^- →	$[Fe(II)Cl_2(H_2O)_4]$

A.0.3 Detailed mechanism for Mallory reaction (eliminative pathway)

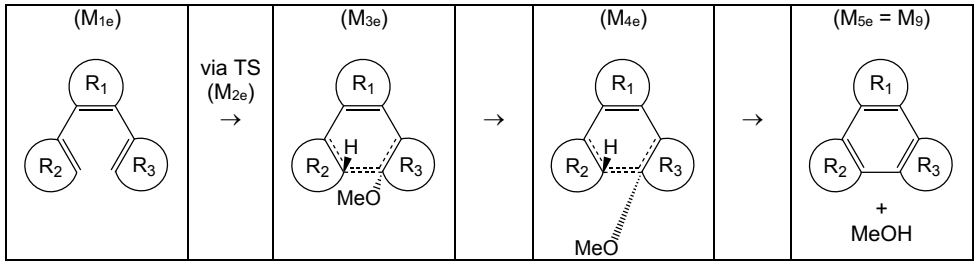

Small molecules: MeOH

A.0.4 Geometries, energies and thermochemical data for reaction pathway minima, transition states and intermediates

Compound	E (Hartree)	ZPVE (kcal/mol)	H (kcal/mol)	-TS (kcal/mol)	Gsol (Hartree)
[FeCl3(H2O)3]	-1732.641787	49.987	9.338	-34.7058526	-0.03890442
[FeCl3(H2O)3]-	-1732.738749	49.601	8.982	-35.00907115	-0.11881448
[FeCl2(H2O)4]	-1348.858737	64.27	10.411	-37.35849315	-0.04264669
HCL	-460.7997862	4.273	2.074	-13.2992789	-0.006443977
H2O	-76.4188287	13.411	2.371	-13.4513354	-0.010888571

S_1

Energies & thermochemical data:

R1	R2=R3	E (Hartree)	ZPVE (kcal/mol)	H (kcal/mol)	-TS (kcal/mol)	Gsol (Hartree)
ethene	phenyl	-540.7210023	135.187	7.524	-31.68589125	-0.006222913
pyrrole	phenyl	-672.2832085	153.689	8.791	-34.27919995	-0.033129726
thiophene	phenyl	-1015.078583	143.59	8.95	-34.8435979	-0.063181801
benzene	phenyl	-694.3760609	164.632	9.135	-35.0242768	-0.010489987
benzene	3-pyridine	-726.4291731	149.907	8.992	-34.84151085	-0.031780496
benzene	2-thiophene	-1335.883339	122.473	8.775	-34.29649265	-0.007340811
benzene	2-pyrrole	-649.9825591	142.531	8.421	-33.2884475	-0.254414051
benzene	3-pyridine	-726.4291731	149.907	8.992	-34.84151085	-0.031780496
benzene	3-thiophene	-1335.882225	122.246	8.809	-34.686771	-0.007871462
benzene	3-pyrrole	-650.2184884	142.34	8.522	-33.7225539	-0.015690785
benzene	phenyl/2-methoxyphenyl	-808.9016287	185.113	10.8	-39.10326695	-0.01014625

S_2

Energies & thermochemical data:

R1	R2=R3	E (Hartree)	ZPVE (kcal/mol)	H (kcal/mol)	-TS (kcal/mol)	Gsol (Hartree)
ethene	phenyl	-540.4607245	135.382	7.542	-31.38893385	-0.062665404
pyrrole	phenyl	-672.045994	152.475	8.534	-33.3099143	-0.069288739
thiophene	phenyl	-1014.864398	143.148	9.032	-34.8519461	-0.060290762
benzene	phenyl	-694.1140343	164.863	9.125	-34.633104	-0.059109131
benzene	3-pyridine	-726.1503721	149.687	9.034	-34.5126514	-0.08703688
benzene	2-thiophene	-1335.62935	122.597	8.694	-33.59882165	-0.061049978
benzene	2-pyrrole	-649.9918036	142.927	8.323	-32.4613794	-0.067792689
benzene	3-pyridine	-726.1503721	149.687	9.034	-34.5126514	-0.08703688
benzene	3-thiophene	-1335.624801	122.51	8.657	-33.54694355	-0.062601505
benzene	3-pyrrole	-649.9881672	143.001	8.293	-32.32572115	-0.068102815
benzene	phenyl/2-methoxyphenyl	-808.6456339	185.318	10.792	-38.4213979	-0.05833202

S_7

Energies & thermochemical data:

R1	R2=R3	E (Hartree)	ZPVE (kcal/mol)	H (kcal/mol)	-TS (kcal/mol)	Gsol (Hartree)
ethene	phenyl	-1000.876749	132.536	9.014	-36.1220651	-0.008995311
pyrrole	phenyl	-1132.44545	151.207	10.34	-38.9729754	-0.015051395
thiophene	phenyl	-1475.2751	141.308	10.468	-39.4207967	-0.010762293
benzene	phenyl	-1154.524429	162.584	10.591	-39.05138885	-0.010564946
benzene	3-pyridine	-1186.573451	148.003	9.965	-37.6014854	-0.052802241
benzene	2-thiophene	-1796.037352	120.394	10.356	-38.8578895	-0.011221123
benzene	2-pyrrole	-1110.375878	140.531	9.729	-36.93512015	-0.016911855
benzene	3-pyridine	-1186.573451	148.003	9.965	-37.6014854	-0.052802241
benzene	3-thiophene	-1796.049448	120.567	10.376	-39.12234855	-0.011560372
benzene	3-pyrrole	-1110.382154	140.636	9.764	-36.9318405	-0.018220966
benzene	phenyl/2-methoxyphenyl	-1269.043731	183.055	12.198	-42.58744785	-0.01192554

S_8

Energies & thermochemical data:

R1	R2=R3	E (Hartree)	ZPVE (kcal/mol)	H (kcal/mol)	-TS (kcal/mol)	Gsol (Hartree)
ethene	phenyl	-539.8273506	128.807	6.781	-28.986143	-0.10888675
pyrrole	phenyl	-671.4469804	147.688	8.031	-31.925902	-0.075976981
thiophene	phenyl	-1014.265753	137.261	8.267	-32.66441955	-0.072216431
benzene	phenyl	-693.4892257	158.534	8.487	-33.0374052	-0.095338482
benzene	3-pyridine	-725.5528965	143.128	8.383	-32.91784705	-0.093608564
benzene	2-thiophene	-1335.041975	116.308	8.023	-32.0517213	-0.064585008
benzene	2-pyrrole	-649.3927529	136.892	7.56	-30.64117365	-0.082010725
benzene	3-pyridine	-725.5528965	143.128	8.383	-32.91784705	-0.093608564
benzene	3-thiophene	-1335.049329	116.816	7.999	-32.0892882	-0.065906014
benzene	3-pyrrole	-649.3925838	137.064	7.623	-30.79442275	-0.082873261
benzene	phenyl/2-methoxyphenyl	-808.038175	178.956	10.098	-36.55289185	-0.06763671

S_9

Energies & thermochemical data:

R1	R2=R3	E (Hartree)	ZPVE (kcal/mol)	H (kcal/mol)	-TS (kcal/mol)	Gsol (Hartree)
ethene	phenyl	-539.5545665	122.099	6.517	-28.3755318	-0.006467846
pyrrole	phenyl	-671.1214265	140.498	7.87	-31.42530815	-0.013200534
thiophene	phenyl	-1013.951808	130.449	8.056	-32.12476805	-0.008354125
benzene	phenyl	-693.2002024	151.342	8.363	-33.0719906	-0.00813524
benzene	3-pyridine	-725.2483137	136.621	8.104	-32.34003235	-0.036781617
benzene	2-thiophene	-1334.717814	109.551	7.834	-31.5615627	-0.007858693
benzene	2-pyrrole	-649.0517601	129.262	7.567	-30.4923968	-0.016106302
benzene	3-pyridine	-725.2483137	136.621	8.104	-32.34003235	-0.036781617
benzene	3-thiophene	-1334.716315	109.538	7.846	-31.60717965	-0.008068084
benzene	3-pyrrole	-649.0483365	129.081	7.681	-30.7297242	-0.018239623
benzene	phenyl/2-methoxyphenyl	-807.6653005	172.019	9.997	-37.1846717	-0.06173623

M_3

Energies & thermochemical data:

R1	R2=R3	E_X (Hartree)	E_G (Hartree)	ZPVE (kcal/mol)	H (kcal/mol)	-TS (kcal/mol)	Gsol_X (Hartree)	Gsol_G (Hartree)
ethene	phenyl	-540.558798	-540.6578209	134.785	7.074	-29.70080855	-0.00969612	-0.005826782
pyrrole	phenyl	-672.1158017	-672.1928594	152.417	8.372	-32.456609	-0.02199998	-0.012801238
thiophene	phenyl	-1014.944966	-1015.018655	142.165	8.59	-33.21957485	-0.01512718	-0.007524966
benzene	phenyl	-694.1977628	-694.282947	164.027	8.807	-33.73120025	-0.01339075	-0.007482271
benzene	3-pyridine	-726.2708269	-726.3386618	149.37	8.597	-33.2753289	-0.020435601	-0.034882262
benzene	2-thiophene	-1335.733579	-1335.826769	122.582	8.374	-32.33228045	-0.01220785	-0.008460893
benzene	2-pyrrole	-650.0663899	-650.1513359	141.876	8.053	-31.04725395	-0.01763243	-0.013651042
benzene	3-pyridine	-726.2708269	-726.3386618	149.37	8.597	-33.2753289	-0.020435601	-0.034882262
benzene	3-thiophene	-1335.760321	-1335.84832	123.022	8.278	-32.2079519	-0.01348783	-0.008921109
benzene	3-pyrrole	-650.0694087	-650.158884	142.207	7.95	-31.3379502	-0.01955899	-0.012663841
benzene	phenyl/2-methoxyphenyl	-808.7163664	-808.7051832	184.605	10.394	-37.22372935	-0.014605255	-0.106791514

M_4

Energies & thermochemical data:

R1	R2=R3	E_X (Hartree)	E_G (Hartree)	ZPVE (kcal/mol)	H (kcal/mol)	-TS (kcal/mol)	Gsol_X (Hartree)	Gsol_G (Hartree)
ethene	phenyl	-540.3825427	-540.4330424	135.431	7	-29.04845635	-0.065062568	-0.064439138
pyrrole	phenyl	-671.962611	-672.0049572	153.469	8.338	-32.5949506	-0.068745184	-0.068764161
thiophene	phenyl	-1014.782757	-1014.820521	143.189	8.564	-33.2872549	-0.066544802	-0.06673107
benzene	phenyl	-694.0292552	-694.0566796	164.794	8.776	-33.7487911	-0.06374212	-0.082231703
benzene	3-pyridine	-726.0906785	-726.110944	149.461	8.696	-33.8913068	-0.071693622	-0.091367281
benzene	2-thiophene	-1335.544469	-1335.612718	123.177	8.264	-32.1626331	-0.064749294	-0.063432807
benzene	2-pyrrole	-649.9050798	-649.9703343	143.394	7.79	-30.614042	-0.071527153	-0.069596639
benzene	3-pyridine	-726.0906785	-726.110944	149.461	8.696	-33.8913068	-0.071693622	-0.091367281
benzene	3-thiophene	-1335.575165	-1335.636226	123.741	8.179	-32.0582806	-0.066922445	-0.064864903
benzene	3-pyrrole	-649.9247249	-649.9826145	143.661	7.769	-30.58094735	-0.072232918	-0.069811544
benzene	phenyl/2-methoxyphenyl	-808.5693877	-808.6018609	185.286	10.379	-37.256824	-0.060974154	-0.059355449

M_5=M_6

Energies & thermochemical data:

R1	R2=R3	E_X (Hartree)	E_G (Hartree)	ZPVE (kcal/mol)	H (kcal/mol)	-TS (kcal/mol)	Gsol_X (Hartree)	Gsol_G (Hartree)
ethene	phenyl	-1000.78806	-1000.839361	132.516	7.922	-32.22912055	-0.026670742	-0.025624889
pyrrole	phenyl	-1132.368325	-1132.40018	151.904	9.255	-35.16351285	-0.039428648	-0.036438373
thiophene	phenyl	-1475.185839	-1475.236956	140.636	9.277	-35.15218315	-0.024476093	-0.022423046
benzene	phenyl	-1154.438821	-1154.468756	163.128	9.703	-36.08897045	-0.034010137	-0.032435024
benzene	3-pyridine	-1186.476436	-1186.512179	146.827	9.302	-35.169774	-0.04194948	-0.063011468
benzene	2-thiophene	-1795.955462	-1796.009139	119.908	9.204	-35.4393016	-0.024782256	-0.022958386
benzene	2-pyrrole	-1110.300054	-1110.358426	139.336	8.964	-34.2562424	-0.032299832	-0.030096307
benzene	3-pyridine	-1186.476436	-1186.512179	146.827	9.302	-35.169774	-0.04194948	-0.063011468
benzene	3-thiophene	-1795.982273	-1796.026784	120.146	9.25	-35.4691166	-0.027477662	-0.026091699
benzene	3-pyrrole	-1110.322539	-1110.369466	140.02	8.901	-34.32034465	-0.038440439	-0.034886653
benzene	phenyl/2-methoxyphenyl	-1268.957213	-1268.994954	183.344	11.218	-39.5245529	-0.032036083	-0.02931753

M_7

Energies & thermochemical data:

R1	R2=R3	E_X (Hartree)	E_G (Hartree)	ZPVE (kcal/mol)	H (kcal/mol)	-TS (kcal/mol)	Gsol_X (Hartree)	Gsol_X (Hartree)
ethene	phenyl	-1000.79817	-1000.876749	132.536	9.014	-36.1220651	-0.009183712	-0.008995311
pyrrole	phenyl	-1132.353944	-1132.44545	151.207	10.34	-38.9729754	-0.015518894	-0.015051395
thiophene	phenyl	-1475.187142	-1475.2751	141.308	10.468	-39.4207967	-0.010850388	-0.010762293
benzene	phenyl	-1154.436471	-1154.524429	162.584	10.591	-39.05138885	-0.0104366	-0.010564946
benzene	3-pyridine	-1186.522043	-1186.573451	148.003	9.965	-37.6014854	-0.014371403	-0.052802401
benzene	2-thiophene	-1795.95585	-1796.037352	120.394	10.356	-38.8578895	-0.011302854	-0.011221123
benzene	2-pyrrole	-1110.293668	-1110.375878	140.531	9.729	-36.93512015	-0.017302715	-0.016911855
benzene	3-pyridine	-1186.522043	-1186.573451	148.003	9.965	-37.6014854	-0.014371403	-0.052802401
benzene	3-thiophene	-1795.963565	-1796.049448	120.567	10.376	-39.12234855	-0.011419743	-0.011560372
benzene	3-pyrrole	-1110.289261	-1110.382154	140.636	9.764	-36.9318405	-0.019320571	-0.018220966
benzene	phenyl/2-methoxyphenyl	-1268.955854	-1269.043731	183.055	12.198	-42.58744785	-0.011865153	-0.01192554

M_8

Energies & thermochemical data:

R1	R2=R3	E_X (Hartree)	E_G (Hartree)	ZPVE (kcal/mol)	H (kcal/mol)	-TS (kcal/mol)	Gsol_X (Hartree)	Gsol (Hartree)
ethene	phenyl	-539.7622939	-539.8273811	128.807	6.781	-28.986143	-0.066198452	-0.108856224
pyrrole	phenyl	-671.3782944	-671.4469804	147.688	8.031	-31.925902	-0.06139385	-0.075976981
thiophene	phenyl	-1014.200703	-1014.265753	137.261	8.267	-32.66441955	-0.05705109	-0.072216431
benzene	phenyl	-693.4387426	-693.4892257	158.534	8.487	-33.0374052	-0.058117368	-0.095338482
benzene	3-pyridine	-725.5022572	-725.5528965	143.128	8.383	-32.91784705	-0.058709591	-0.093608564
benzene	2-thiophene	-1334.952103	-1335.041975	116.308	8.023	-32.0517213	-0.06358869	-0.064585008
benzene	2-pyrrole	-649.3114406	-649.3927529	136.892	7.56	-30.64117365	-0.06850342	-0.082010725
benzene	3-pyridine	-725.5022572	-725.5528965	143.128	8.383	-32.91784705	-0.058709591	-0.093608564
benzene	3-thiophene	-1334.971126	-1335.049329	116.816	7.999	-32.0892882	-0.06171559	-0.065904164
benzene	3-pyrrole	-649.3232056	-649.3925838	137.064	7.623	-30.79442275	-0.0677067	-0.082873261
benzene	phenyl/2-methoxyphenyl	-807.9625478	-808.0399689	179.108	10.104	-36.6158015	-0.055308356	-0.06719489

M_9

Energies & thermochemical data:

R1	R2=R3	E_X (Hartree)	E_G (Hartree)	ZPVE (kcal/mol)	H (kcal/mol)	-TS (kcal/mol)	Gsol_X (Hartree)	Gsol_G (Hartree)
ethene	phenyl	-539.4061658	-539.5545665	122.099	6.517	-28.3755318	-0.006270942	-0.006467846
pyrrole	phenyl	-670.9758164	-671.1214265	140.498	7.87	-31.42530815	-0.01796811	-0.013200534
thiophene	phenyl	-1013.800507	-1013.951808	130.449	8.056	-32.12476805	-0.00968114	-0.008354125
benzene	phenyl	-693.0522621	-693.2002024	151.342	8.363	-33.0719906	-0.00782665	-0.00813524
benzene	3-pyridine	-725.1230569	-725.2483137	136.621	8.104	-32.34003235	-0.011854589	-0.036781507
benzene	2-thiophene	-1334.576175	-1334.717814	109.551	7.834	-31.5615627	-0.00795307	-0.007858693
benzene	2-pyrrole	-648.9079798	-649.0517601	129.262	7.567	-30.4923968	-0.01509626	-0.016106302
benzene	3-pyridine	-725.1230569	-725.2483137	136.621	8.104	-32.34003235	-0.011854589	-0.036781507
benzene	3-thiophene	-1334.567945	-1334.716315	109.538	7.846	-31.60717965	-0.01019549	-0.008068084
benzene	3-pyrrole	-648.8953924	-649.0483365	129.081	7.681	-30.7297242	-0.02322568	-0.018239623
benzene	phenyl/2-methoxyphenyl	-807.5726194	-807.7173566	172.026	10.013	-37.5382776	-0.010024728	-0.009754335

Energies & thermochemical data for 1-(2-methoxyphenyl)-2-phenylbenzene:

Geometry	E_X (Hartree)	E_G (Hartree)	ZPVE (kcal/mol)	H (kcal/mol)	-TS (kcal/mol)	Gsol_X (Hartree)	Gsol_G (Hartree)
M_{1e}	-808.7377264	-808.9021119	185.129	10.736	-38.4273609	-0.011370762	-0.00972967
M_{2e}	-808.7202076	-808.7832959	183.873	10.02	-35.9580826	-0.012359474	-0.009604674
M_{3e}	-808.7170554	-808.7043539	183.857	10.579	-37.6891415	-0.01569891	-0.103429943
M_{4e}	-808.7104584	-808.7799225	182.572	10.505	-37.232972	-0.017348284	-0.01397875
M_{5e}	-808.7804884	-808.9281102	184.22	11.186	-41.41154425	-0.011987689	-0.012433589

APPENDIX B

Complete Thermochemical Data for benzylidene O-methyloximes

Table B.1 Electronic energy + solvation correction (kJ/mol) for para-substituted benzylidene O-methyloximes. For every molecule, row1 =excited and row2= ground state energy

Molecule	Reactant	TS1	Intermediate	TS2	Product	Yield(%)
NMe2	358.85	-	305.46	394.518	270.781	26
	0.0	154.578	130.175	187.939	-230.694	
NH2	383.989	-	299.519	399.342	166.596	36
	0.0	146.71	126.795	185.706	-234.962	
OMe	388.847	-	299.503	403.578	169.61	53
	0.0	144.911	121.96	182.884	-233.229	
OH	403.789	-	302.067	409.54	168.053	36
	0.0	148.956	130.41	191.501	-230.127	
H	403.598	-	297.926	406.513	202.617	29
	0.0	149.234	124.915	181.484	-232.261	
Cl	394.85	-	297.177	408.497	161.659	-
	0.0	145.29	124.567	186.884	-229.077	
CN	394.882	-	296.351	409.782	145.682	-
	0.0	147.116	128.275	190.744	-226.343	
NO2	386.628	-	294.713	432.757	208.997	-
	0.0	147.281	128.829	191.895	-224.638	

Table B.2 Electronic energy + solvation correction (kJ/mol) for ortho-substituted benzylidene O-methyloximes. For every molecule, row1 =excited and row2= ground state energy: Rotamer A

Molecule	Reactant	TS1	Intermediate	TS2	Product	Yield(%)
NMe2	327.361	-	315.459	414.051	138.214	-
	0.0	147.252	114.729	156.067	-221.931	
NH2	367.319	-	300.194	392.175	174.843	-
	0.0	150.265	112.332	142.367	-241.401	
OMe	381.468	-	292.636	393.803	181.095	-
	0.0	156.078	130.477	184.111	-228.014	
OH	406.31	-	305.409	396.051	181.798	-
	0.0	146.717	119.249	168.357	-227.731	
F	402.504	-	296.102	405.289	183.372	-
	0.0	143.708	122.451	179.373	-225.448	
Cl	402.838	-	307.758	432.047	168.743	-
	0.0	149.339	129.519	188.829	-221.376	
CN	411.752	-	296.166	413.463	143.294	-
	0.0	133.428	119.802	182.271	-225.076	
NO2	336.099	-	306.939	475.602	63.743	-
	0.0	116.985	109.479	189.248	-202.173	

Table B.3 Electronic energy + solvation correction (kJ/mol) for ortho-substituted benzylidene O-methyloximes. For every molecule, row1 =excited and row2= ground state energy: Rotamer B

Molecule	Reactant	TS1	Intermediate	TS2	Product	Yield(%)
NMe2	340.873	-	297.772	385.212	166.87	6
	0.0	155.297	115.771	145.441	-236.671	
NH2	372.745	-	294.444	389.104	167.741	26
	0.0	157.099	116.379	149.161	-235.978	
OMe	388.585	-	296.33	402.921	167.591	63
	0.0	151.814	115.825	161.751	-235.522	
OH	402.784	-	295.312	400.602	166.568	30
	0.0	157.784	123.425	166.37	-232.52	
F	401.995	-	298.888	409.515	165.345	-
	0.0	152.476	124.268	177.765	-230.564	
Cl	403.222	-	295.682	405.781	160.886	-
	0.0	145.995	122.666	181.822	-229.955	
CN	414.167	-	288.264	395.939	145.517	-
	0.0	127.82	112.841	183.721	-229.848	
NO2	347.571	-	283.78	447.16	105.475	-
	0.0	116.829	102.722	182.378	-229.313	

APPENDIX C

Simple Hückel molecular orbital theory calculation of bond order of trimethylene methane

Apart from the Born-Oppenheimer approximation and the independent particle approximation, the Hückel molecular orbital theory also include π-electron seperation approximation. In this approximation, it is assumed that the reactivity of π-conjugated hydrocarbon is completely controlled by the π-electron system. Hence the Schrodinger's equation can further be separated to obtain an equation for the π-electron system in which the Hamiltonian for all electrons is replaced by the Hamiltonian for π-electrons only. Consequently the trial wavefunction can also be approximated as a linear combination of p atomic orbitals.

The trial wave function of trimethylene methane can therefore be approximated as shown in equation(C.1):

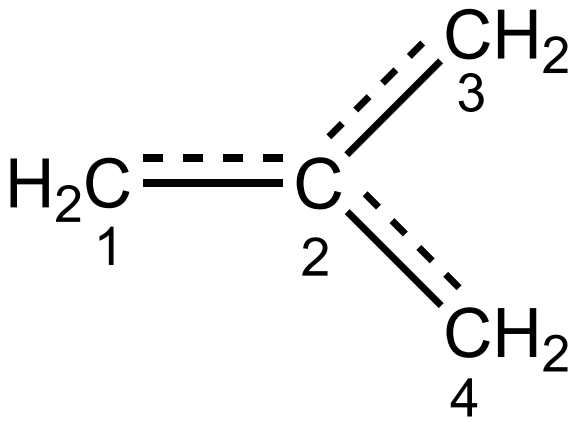

Fig. C.1 structure of trimethylene methane, with the number 1-4 representing the numbering of the carbon atomic orbitals used in constructing the molecular wave function. The dotted lines represent the delocalisation of π-electrons on the molecule

$$\Psi = c_1\phi_1 + c_2\phi_2 + c_3\phi_3 + c_4\phi_4 \tag{C.1}$$

where ϕ represent unhybridized p atomic orbitals of the double-bonded carbon atoms and c(s) represent the atomic orbital coefficient. Substituting this wave function to the π-only Schrödinger's gives the equation (C.2).

$$H\Psi = E\Psi \tag{C.2}$$

H here represents the one electron Hamiltonian for the π electron. Multiplying both sides of the equation (C.2) by Ψ and integrating over all over π electrons (τ) leads to the determination of the energy spectrum E.

$$E = \frac{\int \Psi H \Psi d\tau}{\int \Psi \Psi d\tau} \tag{C.3}$$

Substituting equation (C.1) in (C.4) results in

$$E = \frac{\int (c_1\phi_1 + c_2\phi_2 + c_3\phi_3 + c_4\phi_4) H (c_1\phi_1 + c_2\phi_2 + c_3\phi_3 + c_4\phi_4) d\tau}{(c_1\phi_1 + c_2\phi_2 + c_3\phi_3 + c_4\phi_4)^2 d\tau} \qquad \text{(C.4)}$$

setting:

$\int \phi_i \text{ H } \phi_i \text{ d}\tau = H_{ii}$

$\int \phi_i \text{ H } \phi_j \text{ d}\tau = H_{ij}$

$\int \phi_i \ \phi_i \text{ d}\tau = S_{ii}$

$\int \phi_i \ \phi_j \text{ d}\tau = S_{ij}$

Where i and j run from 1-4. Minimising the energy with respect to each of the coefficients and setting the value to zero leads to 4 set of secular equations that can be represented as a secular matrix.

$$\begin{bmatrix} H_{11} - ES_{11} & H_{12} - ES_{12} & H_{13} - ES_{13} & H_{14} - ES_{14} \\ H_{21} - ES_{21} & H_{22} - ES_{22} & H_{23} - ES_{23} & H_{24} - ES_{24} \\ H_{31} - ES_{31} & H_{32} - ES_{32} & H_{33} - ES_{33} & H_{34} - ES_{34} \\ H_{41} - ES_{41} & H_{42} - ES_{42} & H_{43} - ES_{43} & H_{44} - ES_{44} \end{bmatrix} \begin{bmatrix} c_1 \\ c_2 \\ c_3 \\ c_4 \end{bmatrix} = 0 \qquad \text{(C.5)}$$

The simple Hückel theory makes the following assumptions in order to solve the secular equation (C.5).

1) Firstly, Hückel assumes that all the carbon atoms are equivalent hence:

- The coulomb integrals H_{ii} which describes the energy of interaction of an electron in a free carbon $2p_z$ atomic orbital in the molecule α

- The resonant integral H_{ij}, which describes the energy of interaction of an electron in a smear out of all the nuclei takes a value of β if the carbon atoms are directly linked together or takes a value of zero if the are separated by two or more bonds.

2) Secondly, Hückel assumes that $2p_x$ atomic orbitals constituting the molecular wave-functions are orthonormal. Therefore, the overlap integrals are:

$S_{ii} = 1$

$S_{ij} = 0$

Applying this approximation to equation (C.5) simplifies it into equation (C.6)

$$\begin{bmatrix} \alpha - E & \beta & 0 & 0 \\ \beta & \alpha - E & \beta & \beta \\ 0 & \beta & \alpha - E & 0 \\ 0 & \beta & 0 & \alpha - E \end{bmatrix} \begin{bmatrix} c_1 \\ c_2 \\ c_3 \\ c_4 \end{bmatrix} = 0 \tag{C.6}$$

Setting $x = (\alpha$ - $E)/\beta$ and dividing every entry in the first matrix in equation (C.6) by β leads to equation (C.7)

$$\begin{bmatrix} x & 1 & 0 & 0 \\ 1 & x & 1 & 1 \\ 0 & 1 & x & 0 \\ 0 & 1 & 0 & x \end{bmatrix} \begin{bmatrix} c_1 \\ c_2 \\ c_3 \\ c_4 \end{bmatrix} = 0 \tag{C.7}$$

Calculation of the energy spectrum

The energy spectrum can easily be from equation (C.7) by determining the value of x. This can be done by equating the determinant of the matrix containing x to zero. Therefore

$$det(\begin{bmatrix} x & 1 & 0 & 0 \\ 1 & x & 1 & 1 \\ 0 & 1 & x & 0 \\ 0 & 1 & 0 & x \end{bmatrix}) = 0 \tag{C.8}$$

$$x\begin{bmatrix} x & 1 & 1 \\ 1 & x & 0 \\ 1 & 0 & x \end{bmatrix} - \begin{bmatrix} 1 & 1 & 1 \\ 0 & x & 0 \\ 0 & 0 & x \end{bmatrix} + 0 \begin{bmatrix} 1 & x & 1 \\ 0 & 1 & 0 \\ 0 & 1 & x \end{bmatrix} - 0 \begin{bmatrix} 1 & x & 1 \\ 0 & 1 & x \\ 0 & 1 & 0 \end{bmatrix} = 0$$

$$x\ [\ x\ \begin{bmatrix} x & 0 \\ 0 & x \end{bmatrix} - \begin{bmatrix} 1 & 0 \\ 1 & x \end{bmatrix} + \begin{bmatrix} 1 & x \\ 1 & 0 \end{bmatrix}\ ] - [\ \begin{bmatrix} x & 0 \\ 0 & x \end{bmatrix} - \begin{bmatrix} 0 & 0 \\ 0 & x \end{bmatrix} + \begin{bmatrix} 0 & x \\ 0 & 0 \end{bmatrix}\ ] = 0$$

$$x[x(x^2 - 0) - (x - 0) + (-x)] - x^2 = 0$$

$$x^4 - 3x^2 = 0$$

$$x^2(x^2 - 3) = 0$$

Hence $x = -\sqrt{3}, 0, 0, \sqrt{3}$

Substituting for x in $x = (\alpha$ - $E)/\beta$ results in the energy spectrum that is represent in Fig. C.2

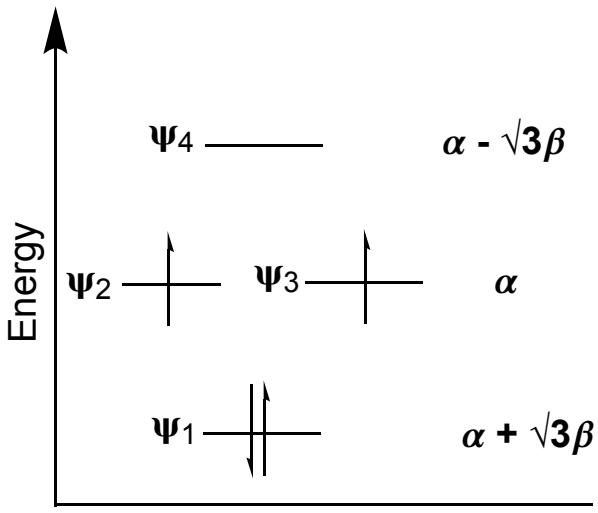

Fig. C.2 Energy level diagram of trimethyl methane showing the energy of each molecular orbital and their occupancy

Determination of the atomic orbital coefficient

Expanding equation C.7 leads to four simultaneous equations

$$c_1 x + c_2 = 0 \tag{C.9}$$

$$c_1 + c_2 x + c_3 + c_4 = 0 \tag{C.10}$$

$$c_2 + c_3 x = 0 \tag{C.11}$$

$$c_2 + c_4 x = 0 \tag{C.12}$$

From equation (C.9)

$$c_2 = -c_1 x \tag{C.13}$$

Hence substituting equation (C.13) in equation (C.11) and (C.12) results in $c_3 = c_1$ and $c_4 = c_1$ Since the wave function in equation (C.1) is orthonormal, this

implies that

$$c_1^2 + c_2^2 + c_3^2 + c_4^2 = 1 \tag{C.14}$$

substituting the values of c_2, c_3 and c_4 by their new values in equation (C.15) leads to

$$c_1^2 + c_1 x^2 + c_1^2 + c_1^2 = 1 \tag{C.15}$$

$=> c_1 = \frac{1}{\sqrt{3+x^2}}$

Thus

$c_1 = c_3 = c_4 = \frac{1}{\sqrt{3+x^2}}$

and

$c_2 = \frac{-x}{\sqrt{3+x^2}}$

When $x = 0$

$c_1 = c_3 = c_4 = \frac{\sqrt{3}}{3}$ and $c_2 = 0$

When $x = +\sqrt{3}$

$c_1 = c_3 = c_4 = \frac{\sqrt{6}}{6}$ and $c_2 = -\frac{\sqrt{3}}{\sqrt{6}}$

When $x = -\sqrt{3}$

$c_1 = c_3 = c_4 = \frac{\sqrt{6}}{6}$ and $c_2 = \frac{\sqrt{3}}{\sqrt{6}}$

Substituting these coefficients in equation (C.1) for the different energy levels leads to following wave functions

$\Psi_1 = \frac{\sqrt{6}}{6}\phi_1 + \frac{\sqrt{3}}{\sqrt{6}}\phi_2 + \frac{\sqrt{6}}{6}\phi_3 + \frac{\sqrt{6}}{6}\phi_4$

$\Psi_2 = \Psi_3 = \frac{\sqrt{3}}{3}\phi_1 + \frac{\sqrt{3}}{3}\phi_3 + \frac{\sqrt{3}}{3}\phi_4$

$\Psi_4 = \frac{\sqrt{6}}{6}\phi_1 - \frac{\sqrt{3}}{\sqrt{6}}\phi_2 + \frac{\sqrt{6}}{6}\phi_3 + \frac{\sqrt{6}}{6}\phi_4$

Determination of the bond order

According to Coulson, the bond order between any pair of atoms, r and s, can be calculated according to equation (C.16)

$$P_{rs} = \sum_{i=1}^{K} N_i c_{ri} c_{si} \tag{C.16}$$

Where N is the number of π- electrons in the orbital and the sum runs only over all the k occupied molecular orbitals. Hence the bond order for between carbon 1 and 2 is calculated as follows

$P_{1,2} = P_{2,3} = P_{2,4} = 2[\frac{\sqrt{6}}{6}$ x $\frac{\sqrt{3}}{\sqrt{6}}] + \frac{\sqrt{3}}{3} + \frac{\sqrt{3}}{3} = \sqrt{3}$

Therefore the π-bond order for all the carbon-carbon bond is equal to $\sqrt{3}$. Since each of the carbon atoms independently form 3 σ bonds, the total bond order formed by each of the carbon atoms will be equal to $3 + \sqrt{3}$.